UNIVERSITY OF CALIFORNIA
RIVERSIDE

Strategies for Development of Chronic Wounds Using the LIGHT$^{-/-}$ Mouse and a Diabetic Mouse: From Mechanism to Treatment

A Dissertation submitted in partial satisfaction
of the requirements for the degree of

Doctor of Philosophy

in

Bioengineering

by

Sandeep Dhall

December 2014

Dissertation Committee:

Dr. Manuela Martins-Green, Chairperson
Dr. Victor G. J. Rodgers
Dr. Devin Binder

The Dissertation of Sandeep Dhall is approved:

Committee Chairperson

University of California, Riverside

Acknowledgments

I owe my profound sense of gratitude and sincerest appreciation to my advisor, Dr. Manuela Martins-Green. Dr. Martins-Greens' passionate advising and expectations throughout my time of doctoral studies is what has driven me to go beyond limits, critically analyze data and question every finding. Her emphasis of thinking at the bench while working is what has led to important findings. Dr. Martins-Greens' work ethics, professionalism and service to the institution and community has not allowed me to stay true to the science, but enabled me to work responsibly for the University while pursuing my doctoral studies. The patience and guidance from Dr. Martins-Green throughout my degree not only has left a sense of scientific sanctity but has also increased my confidence and faith to be able to unravel the pathway to a successful career.

I sincerely would like to thank my dissertation committee members, Dr. Victor G J Rodgers and Dr. Devin Binder for their insights into the project and pushing me to think beyond the conventional theories. I thank my research group for all their productive criticism and suggestions. I want to specially thank Dr. Allen Wang, Dr. Yan Liu and Dr. Joao Pedro, with whom I worked very closely and had a lot of scientific discussions. I thank all the undergraduate scholars that worked with me over the past few years (Monika Garcia, Raquelle Alamat, Jane Kim and Anthony Castro). It has been a pleasure mentoring you and I have developed a lot during the process. I would also like to thank our neighboring Dr. Frances Sladek's lab, for all the fun times, great food and scientific talk that I have had with every member of the lab.

I want to extend my gratitude to our collaborators Dr. Neal Schiller and Dr. Danh Do for all the microbiology expertise that was brought into this work, Dr. Shanaka Wijesinghe and Dr. Charles Chalfant for help with lipidomics, Dr. Fadi Khasawneh for support with platelet aggregation studies, Dr. Rakesh Patel for the nitric oxide metabolite estimations and Dr. Eugene Nothnagel for his knowledge on carbohydrates.

During my course of graduate studies I have received a lot of backing and encouragement from various people at the Department of Bioengineering. Dr. Victor G J Rodgers, who I look up to as my fatherly figure outside of my home country, has not only provided me with a lot of inspiration, but has also been present at every occasion providing confidence whenever I have faltered during the process. Also, Ms. Denise Sanders and Hong Xu were very supportive, caring and helpful during my stay at UCR.

During my stay at UCR, I also had the opportunity to work with the Graduate Student Association and hence the various University bodies that students are linked with. I would like to thank each and everybody for all their wonderful support and team effort provided while I worked as the President of the Association.

Dr. Yusuf Khan and Dr. Kaushik Nanda were my apartment mates for 4years of my graduate studies and I extend my sincerest of thank you for all the wonderful times we have spent together and being there for each other during the stressful times of doing PhD. Not only have you both left a lot of memories but I will treasure this friendship forever. I would also like to thank my friends and colleagues, Garima Goyal, Dr. Smruti Parichha, Dr. Dennis Jeffrey, Dr. Deepti Tanjore, Dr. Shruti Lal, Dr.Payal Biswas,

Dr. Shailender Singh, who have made this journey a memorable experience. You all have been my family away from home.

I thank my best friend, Dr. Ronald Gorham Jr., for sharing the ups and downs of graduate school with me and for being there whenever I have needed you. I will forever cherish the marathon training, outings, food and other adventurous hikes and events that we have done together. I also thank Dr. Prashanthi Vandrangi, who has been my friend and elder sister at UCR, who took care of me at the most demanding times, cooked food when I was stressed out and made sure that I ate properly, has altogether helped me a lot. I also thank you for sharing enthusiasm for my work and all the constructive suggestions.

I also thank two of my first undergraduates, Rico Santangelo and Ashish Sud, whom I taught and have become my friends forever.

My extended family in US- Buddhadev Samal, Suman Samal and Bibek Samal, who have helped me tremendously in not feeling home sick by sharing their love and warmth. I express gratitude to Sandy Gorham, my best friend's mom. Your prayers and blessings, along with all the cookies that I have got almost every month have helped me fulfill this path.

Last but not the least; I would like to thank my family for always showering me with all the love and blessings during each and every stride of graduate school. I know that the path to this moment wasn't easy or clear and would not have been successful without your support. I thank you all.

I dedicate this dissertation to my family -

to my parents (Dillip Kumar Dhall and Sucharita Dhall) for

being the reason for my existence and

all the love, support and independence that I have been bestowed upon with,

to my brother and sister (Sidhant and Shivangi)for all their affection,

to grandpa and grandma (Padmacharan Dhall and Nalini Dhall) and

to late grandpa and grandma (Padmacharan Mallick and Bilasini Mallick)

for their endless blessings.

ABSTRACT OF THE DISSERTATION

Strategies for Development of Chronic Wounds Using the LIGHT$^{-/-}$ Mouse and a Diabetic Mouse: From Mechanism to Treatment

by

Sandeep Dhall

Doctor of Philosophy, Graduate Program in Bioengineering
University of California, Riverside, December 2014
Dr. Manuela Martins-Green, Chairperson

Wound healing involves many cellular and molecular processes that are integrated in several sequential and overlapping phases, hemostasis, controlled oxidative stress, inflammation, granulation tissue formation, and remodeling. Impaired-healing and chronic wounds exhibit defective regulation of one or more of these processes that leads to conditions such as diabetic foot ulcers, and other similar chronic wounds that impact ~6.5M people and cost ~$25B/year in the US alone. Great efforts have been made to stimulate healing of these wounds, including the development of animal models mimicking chronic wounds in order to understand how they develop but success has been limited. Recently, we developed a mouse model of impaired healing that became chronic in presence of biofilm-forming bacteria. I took an integrated approach by using various cellular and molecular approaches to study the wound microenvironment. Using the LIGHT$^{-/-}$ model of impaired healing, I showed that the wounds in these mice, very early during the process of healing have elevated levels of reactive oxygen species (ROS) and reactive nitrogen species (RNS), increased lactate levels and reduced pH that could potentially damage the healing tissue. With the use of luminol I showed, for the very first

time, real time monitoring of increase in oxidative stress levels. In addition, I showed that the detrimental effects of increases in ROS and RNS significantly increased damage to DNA, lipid peroxidation and protein nitrosylation. Furthermore, using a lipidomics approach I showed an increase in inflammatory lipids and lipids involved in platelet function. The findings were confirmed by the increases in inflammation, platelet aggregation and reduced bleeding time post wounding. I then showed that by exacerbating the levels of ROS by inhibition major antioxidant enzymes, glutathione peroxidase and catalase, and introducing previously isolated biofilm forming bacteria on the wound bed, led to the development of chronic wounds. The wounds remained open and persistent inflammation was marked by the clear presence of neutrophils and macrophages in the wound tissue. The granulation tissue was poorly formed and there was loss of collagen bundles. Furthermore, I also showed that the bacteria were capable of forming biofilms and were resistant to antibiotics. These results confirmed that redox imbalance and presence of bacteria were crucial elements for chronic wound formation.

I then tested the possibility that exacerbated oxidative stress was critical for chronic wound development by performing similar experiment in a diabetic mouse model, the db/db. I showed that only one dose of inhibitors to the antioxidant enzymes at the time of wounding was sufficient to cause the wound to become chronic by 20 days and spontaneously harbor biofilm-forming bacteria. The chronic wounds in these mice did not heal for as long as 90 days. I also showed that the bacteria was resistant to antibiotics and that there were embedded in the extrapolysaccharide (EPS) matrix. To confirm the importance of redox stress, I reversed the stress levels by treating the wounds with

antioxidants, N-acetyl cysteine and α-tocopherol, and showed that the wounds healed with decreased levels of oxidative stress, reduction in biofilm forming bacteria, reduction in biofilm on the wound bed, better tissue structure with proper collagen bundles and proper differentiating epithelial cells.

The studies presented here provide an in vivo model of chronic wounds that captures many of the clinical aspects of human chronic wounds and that may provide insights into the mechanisms involved in chronic wound development, including the natural growth of biofilm *in situ*. These findings, taken together suggest the robustness of the LIGHT$^{-/-}$ and db/db models of impaired and chronic wounds respectively that warrants further research to capture the underlying mechanisms in the development of human chronic wounds and hence uncovering potential targets to treat such wounds.

TABLE OF CONTENTS

LIST OF FIGURES

INTRODUCTION

Wound healing, as a normal yet intricately woven biological process, is accomplished through four accurately and highly defined stages. Any deviations, caused by a myriad of factors, in any of the phases during the course of healing can derail the sequence of proper healing. A variety of factors, including age, increases in inflammation, redox imbalances, vascular complications and bacterial colonization have been proposed. Due to the steady increases in number of lifestyle related diseases, such as diabetes, obesity, and cardiovascular diseases, it is expected that the number of chronic wounds is set to increase worldwide. Two major categories have time and again been described to be consistently present in non-healing chronic wounds: oxidative stress and presence of biofilms.

In this document I first review the processes involved in normal wound healing and the recent animal models developed to mimic impaired wound healing (**Chapter 1**). I also discuss the animals models developed to mimic chronic wound in humans and the different approaches used to incorporate biofilm forming bacteria grown *in vitro* onto excisional and burn wounds. In these descriptions I describe the two mouse models of chronic wounds developed by us. By taking an integrative approach with various assays to study the redox environment during wound healing, affymetrix gene arrays to study gene expression, and flow experiments to study cell death, I investigate the cellular and molecular mechanisms of impaired wound healing. Furthermore, I manipulate the wound environment in the impaired model of wound healing to create chronic wounds (**Chapter 2**). Chapter 2 is a slight modification of the published paper: Dhall, S., Do, D., Garcia, M., Wijesinghe, D. S., Brandon, A., Kim, J., Sanchez, A., Lyubovitsky, J., Gallagher, S.,

Nothnagel, E. A., and Martins-Green, M. (2014). A novel model of chronic wounds: importance of redox imbalance and biofilm-forming bacteria for establishment of chronicity. *PLoS One* 9, e109848. I further studied the course of impaired healing by integrating lipidomics approaches and elucidating the state of inflammatory and platelet activating lipids. I also characterize the state of platelets and blood coagulation in the impaired LIGHT$^{-/-}$ mice model post wounding (**Chapter 3**). Because chronic wounds are primarily associated with diabetic patients, I describe, for the first time, the development of chronic wounds in a diabetic model of wound healing that mimic the parameters of a chronic wound in humans. I also identify the combination of antioxidants that we used to reverse chronicity and that led to improved tissue structure and caused the dismantling of the bacterial biofilm and made the biofilm forming bacteria susceptible to antibiotics (**Chapter 4**). Chapter 4 is slight modification from the published paper: Dhall, S., Do, D., Garcia, M., Kim, J., Mirebrahim, S., Lyubovitsky, J., Lonardi,S., Nothnagel, E. A., and Martins-Green, M. (2014). Generating and reversing chronic wounds in diabetic mice by manipulating wound redox parameters. *Journal of Diabetes Research*, e562625. Finally, I summarize the critical findings of the impaired and chronic wound models of healing and conclude by suggesting the importance of expanding our knowledge of underlying mechanisms by exploiting our novel model of chronic wound healing (**Chapter 5**).

CHAPTER 1

A BRIEF OVERVIEW OF NORMAL AND ABNORMAL HEALING

INTRODUCTION

Wound healing is a dynamic, interactive process involving soluble mediators, blood cells, extracellular matrix, and connective tissue cells. Overlapping in space and time, the phases are divided into four groups: homeostasis, inflammation, granulation tissue formation, and tissue remodeling (**Fig. 1.1**). Improper progression of these phases can lead to the derailment of the healing process resulting in impaired and/or chronic wounds (Lazarus et al., 1994). Chronic wounds impact approximately 6.5M people and cost approximately $25B/year in the US alone (Sen et al., 2009). Although large amounts of investment and research have gone into understanding the etiology of chronic wound development, success has been limited. This is primarily due to the multifactorial environment that leads to the stagnation of the healing process preventing it to progress to remodeling of the newly laid tissue. The consequences of chronic wounds are multiple often resulting in amputations severely decreasing quality of life and lifespan.

MAJOR PROCESSES INVOLVED IN NORMAL CUTANEOUS WOUND HEALING

Tissue injury causes the disruption of blood vessels and extravasation of blood constituents (**Fig. 1.1**). The blood clotting reestablishes hemostasis and provides a provisional extracellular matrix for cell migration. Numerous vasoactive mediators and chemotactic factors are generated by coagulation, activated-complement pathways and by injured or activated connective tissue cells. These molecules recruit inflammatory leukocytes to the site of injury initiating the inflammatory phase. Infiltrating neutrophils

clean the wound tissue of foreign particles and pathogens and are then extruded with the eschar or phagocytized by macrophages (Guo and Dipietro, 2010). In response to specific chemoattractants, such as fragments of extracellular-matrix proteins, transforming growth factor β (TGFβ), and monocyte chemoattractant protein 1 (MCP1), monocytes infiltrate the wound site, differentiate into macrophages that become activated and release growth factors to initiate the formation of the granulation tissue. One such factor is vascular endothelial growth factor (VEGF), which initiate the formation angiogenesis (Granata et al., 2010; Kiriakidis, 2002; Rodero and Khosrotehrani, 2010; Steed, 1997). Macrophages bind to specific proteins of the extracellular matrix by their integrin receptors, an action that stimulates phagocytosis of microorganisms and fragments of dead cells (Monick et al., 2002; Sorokin, 2010).

Re-epithelialization of wounds, another important part of the granulation tissue formation, begins within hours after injury. The hair follicle bulge contain stem cells that help repair the epidermis (Ito et al., 2005). In addition, the epidermal cells from the wound edge migrate over the wound tissue. Furthermore, dermal epidermal interactions are lost because of the disassembly of the hemidesmosomal junctions between the epidermis and the basement membrane, which allows the lateral movement of epidermal cells (Ozawa et al., 2010; Stadelmann et al., 1998). Once the wound is filled with new granulation tissue, angiogenesis ceases and many of the new blood vessels break down as a result of apoptosis during the remodeling phase of healing (Guo and Dipietro, 2010).

Collagen deposition, another very important aspect of granulation tissue development, occurs in a sequential manner, first collagen III followed by deposition of collagen I. The transition from collagen III to collagen I occurs in presence of controlled levels of metalloproteinases (MMPs) which are secreted by macrophages, epidermal cells, endothelial cells, as well as fibroblasts (Lobmann et al., 2002). Tissue inhibitors of metalloproteinases (TIMPs) are critical for the control of MMPs (Wynn and Ramalingam, 2012) and are required to act as checkpoints for proper collagen turnover and degradation. Perturbation or absence in TIMP activity compromises the quality of the healing process (Novo and Parola, 2008; Vaalamo et al., 1996). Furthermore, excessive deposition of matrix proteins, in particular collagen I, causes impairment of proper wound healing (Falanga, 2005). Other growth factors such as TGFβ, PDGF and FGF2, also play important roles in proper collagen deposition and extracellular matrix remodeling (Penn et al., 2012; Sun et al., 2014). The cross linking of collagen and organization of the fibers takes place in this final remodeling phase. Although the remodeling phase takes anywhere from 1 to 3 years, the restored tissue at the site of injury never returns to its original state.

IMPACT OF EXCESSIVE OXIDATIVE AND NITROSATIVE STRESS ON IMPAIRED WOUND HEALING

The direct involvement of reactive oxygen species (ROS) and reactive nitrogen species (RNS) in chronic wounds has been previously reported (Clark, 2008; Dhall et al., 2014b; Gordillo and Sen, 2003; Mudge et al., 2002; Novo and Parola, 2008; Sen and Roy, 2008). In chronic wounds, the detoxification process is hindered due to persistent and uncontrolled production of ROS and RNS during the inflammatory phase. Furthermore, the reduction in antioxidant activity and the inability to quench oxidants in chronic wounds, cause excessive damage (Dröge, 2002). Redox imbalance causes wound healing to be stagnant in the inflammatory phase without progression towards granulation tissue development and can lead to impaired and/or chronic wounds.

It has been previously shown that oxidative stress induces apoptosis in keratinocytes (Kanda and Watanabe, 2003; Ponugoti et al., 2013). This suggests that high oxidative stress in chronic wounds might play a major role in disrupting epidermis–connective tissue interaction and also causing senescence in wound fibroblasts (Werner et al., 2007). Senescent fibroblasts are unable to replicate but remain metabolically active with altered cell functions, are less motile, can accumulate in the tissue due to their resistance to apoptosis, and produce a different array of proteins, including elevated levels of MMPs and pro-inflammatory cytokines – all of which affect tissue integrity and normal healing (Campisi, 2013).

Reactive oxygen species (ROS)

Reactive oxygen species (ROS) have historically been viewed as toxic metabolic byproducts and causal agents in a myriad of human pathologies. ROS are produced by all cells during the course of normal metabolic processes, e.g. in the respiratory chain. Specifically, large amounts are produced in wounded and inflamed tissue by NADPH oxidase, an enzyme complex, that is expressed at particular high levels by inflammatory cells (Darr and Fridovich, 1994; Darvin et al., 2010). This phenomenon has been described as the "respiratory burst".

Upon activation of NADPH oxidase, cells produce the highly reactive superoxide anion radical. This anion is rapidly dismutated to hydrogen peroxide (H_2O_2) by superoxide dismutase (SOD). Although H_2O_2 is not a radical, it can cause severe cell damage due to the generation of hydroxyl radicals in the presence of iron or copper ions (Fenton reaction) (Clark, 2008). Hydroxyl radicals are highly aggressive, resulting in oxidation of cellular macromolecules. Therefore, H_2O_2 must be rapidly detoxified, and this can be achieved by catalase, various peroxidases and also by peroxiredoxins. The latter are also able to detoxify lipid peroxides. In addition to ROS-detoxifying enzymes, ROS defense is achieved by a variety of endogenous and exogenous low molecular weight antioxidants (Shukla et al., 2009).

During the inflammatory phase of wound-healing neutrophils and macrophages invade the wound. Neutrophils are the first inflammatory cells to arrive at the wound site; this occurs within 1–3 hours after wounding. Subsequently, monocytes also arrive to the

wound site and differentiate into macrophages (Dovi et al., 2004). Neutrophils and macrophages produce large amounts of superoxide radical anions. ROS is required for the defense against invading pathogens and at low levels are essential mediators of intracellular signaling (D'Autréaux and Toledano, 2007; Roy et al., 2006). However, excessive amounts of ROS are deleterious and cause oxidative stress due to their high reactivity, resulting in cell damage, premature aging or even neoplastic transformation (Bickers and Athar, 2006; Parihar et al., 2008; Wlaschek and Scharffetter-Kochanek, 2005).

Reactive nitrogen species (RNS)

Emerging evidence from both animal and human studies indicate that nitric oxide (NO) plays a key role in wound repair (Schaffer et al., 1996; Soneja et al., 2005). The beneficial effects of NO in wound repair may be attributed to its functional influences on angiogenesis, inflammation, cell proliferation, matrix deposition, and remodeling. NO is a highly diffusible intercellular signaling molecule implicated in a wide range of biological effects. The enzyme nitric oxide synthase (NOS) catalyzes the conversion of L-arginine to L-citrulline in the presence of oxygen and produces nitric oxide (Griffith and Stuehr, 1995). Three NOS isoforms have been characterized, each encoded by different chromosomes. Two enzyme isoforms are constitutively expressed (endothelial and neuronal NOS), whereas one isoform is an inducible enzyme (iNOS), initially found in macrophages. All three NOS isoforms exist in their active form as homodimers with molecular masses of approximately 135 kDa (eNOS), 150–160 kDa (nNOS), and 130

kDa (iNOS) (Campbell et al., 2013; Chen et al., 2008). eNOS can be detected in keratinocytes of the basal epidermal layer, dermal fibroblasts and endothelial capillaries, and iNOS can be induced in keratinocytes, fibroblasts, Langerhans, and endothelial cells. The expression and function of the iNOS is stimulated by a variety of cytokines, growth factors, and inflammatory stimuli leading to the release of high levels of NO and hence formation of RNS and a state of nitrosative stress (Qadoumi et al., 2002; Sirsjö et al., 1996).

Nitrosative stress has been shown to increase matrix degradation and apoptosis in ulcers. Also iNOS and arginase (used in catalysis of L-arginine) are increased in chronic venous and diabetic ulcers (Durante et al., 2007; Roy et al., 2009). Arginase is responsible for increased matrix deposition but due to high nitrosative stress and subsequent proteolytic activity, matrix deposition is defective in these ulcers. High levels of NO produced by iNOS interacts with oxygen free radicals from sources including neutrophils and macrophages to produce peroxynitrite. Peroxynitrite induces apoptosis/necrosis depending on its concentration in the ulcer site (Abd-El-Aleem et al., 2000). Taken together, lack of NO modulation can critically affect the inflammatory phase of wound healing and potentially lead to detrimental alterations to tissue remodeling.

ANIMAL MODELS OF IMPAIRED WOUNDS

The underlying mechanism of impaired wound healing has been a subject of extensive study by both clinicians and basic wound biologists. Impaired models of wound healing *in vivo* have been achieved via targeting specifically the immune response. Use of glucocorticoids, irradiation, inducing diabetes (induced either genetically or chemically), aging, causing obesity, immunosuppression, antibody depletion, and calorie restriction are some of the methods that have successfully been used in developing impaired models of wound healing (Barbul et al., 1989; Cromack et al., 1993; Gallucci et al., 2000; Guo and Dipietro, 2010; Leibovich and Ross, 1975; Tsuboi et al., 1992). A variety of genetically and/or chemically manipulated animal models have been developed to mimic impaired wound healing in humans. Studies involving murine models of wound healing have provided significant knowledge on the influx of different cells into the wound bed, their interactions, cytokine and chemokine release and signaling, extracellular matrix regeneration and other aspects of the wound microenvironment (Chen et al., 2013). Importantly, murine models of wound healing are economic, easy to sustain and provides the opportunity to investigate multiple wound healing parameters by targeted generation of genetically modified strains.

The first model to reproduce ischemic impaired wounds was developed by circumferential incision of all but caudal artery and three veins of rabbit ear. Similarly the authors interrupted the venous outflow completely but the caudal vein to make the congestion ulcer model (Ahn and Mustoe, 1990).

The first model of pressure wounds was developed in the greyhound dog. This model showed that pressure wounds with different severities can be developed by changing the level of limb padding. A casting material was used to pad the limb and/or then covering with stockinette material (Swaim et al., 1993). The authors took advantage of the angular conformation of the legs and thin skin of the dog to produce this model. Using this model, these investigators showed that the level of thromboxane B2 (TXB_2), a stable metabolite of TXA_2, was significantly increased in the wound bed and in the tissue immediately neighboring the site of injury. TXA_2 has been shown to cause tissue ischemia by inducing vasoconstriction and platelet aggregation, that has led to vascular thrombosis and constrained vascular flow to the site of ulcer tissue (Swaim, 1992). Another model of surface pressure ulcers was achieved using a computer-controlled pressure delivery system. Two cylindrical pressure columns were used to apply constant tissue interface pressure of 145mm Hg on the fuzzy strain of Sprague Dawley rats for 6 hours each day for 5 consecutive days. This resulted in the development of lesions associated with cutaneous ulceration (Richard et al., 1995). Another group of researchers developed a pig model of pressure wounds by using a load application system that could deliver sheer stress and normal stress (Goldstein and Sanders, 1998). The authors applied varying sheer stresses on the pig skin in 10 min intervals up to a total of 40 min to show that skin breakdown was dependent on the direction and magnitude of the stresses applied on the skin and that highest load resulted in the fastest tissue injury. The authors reported an increase in polymorphonuclear cells, edema and occasional extravasation of blood cells into the dermis of the site of stress. Furthermore, they reported that longer

periods (weeks) of repetitive stress would result in tissue adaptation to the stress applied and the injury would not occur (Goldstein and Sanders, 1998). The models described above incorporated the application of surface pressure for varied periods of time to form pressure wounds and study ischemic injury. A rat model of ischemia-reperfusion injury was later developed by performing periodic compression of skin. A steel sheet was implanted under the skin and periodic pressure of 50mm Hg was applied using a magnet. The authors showed that the tissue injury increased with increasing number of ischemic-repurfusion cycles, increase in duration, and frequency of the cycle. Furthermore, the authors showed that the site of injury had increased neutrophil infiltration, increased oxygen tension and problems in blood flow that led to tissue necrosis (Peirce et al., 2000). The ultimate goal of the pressure wound models described above and the systems established to develop these models was primarily to study variables such as pressure, blood flow, histopathology, and tissue environment.

With the advent of 21st century, a non-invasive technique was used to develop a mice model of ischemic reperfusion injury. The authors used magnetic plates to pinch the skin of mice for a period of 12hrs. The cycle was repeated 3 times to cause ischemia–reperfusion injury that led to lesions equivalent to stage III pressure ulcers. The authors also showed that the injury caused full thickness skin loss and necrosis of the subcutaneous tissue (Stadler et al., 2004). More recently, an invasive compression technique was used to create stage IV pressure ulcers. The authors used the BALB/c nude mice and implanted a steel disk under the great gluteus muscle. Upon full recovery of the incision where the steel disc was placed, pressure on the tissue was applied by using a

magnet to do 2hrs compression and 1hr recovery cycle for a total of 10 cycles. The authors showed the occurrence of necrosis in the fat and muscles layers was dependent on the number of ischemic-repurfusion cycles, however the infiltration of polymorphonuclear granulocyte was independent of the number of ischemic-repurfusion cycles (Wassermann et al., 2009). The notion behind the creation of the ischemic-repurfusion injury models of pressure wounds was to understand the pathological trigger for pressure ulcer development seen in humans. Investigators proposed the use of these models to discover therapeutic interventions for pressure wounds.

More recently, ischemic wounds were successfully created in a porcine model. Briefly, a bipedicle flap was created by electrocautery incision and was followed by placing sheeting material between the dermal flap and the underlying tissue. Upon suturing the flap, to hold the sheet it in place, full thickness excisional wounds were created on the bipedicle flap to result in ischemic wounds (Roy et al., 2009). Using this model, the authors performed a transcriptome analysis of the ischemic wounds over a period of time (Day 3, 7, 14, and 28) and showed elevated expression of arginase-1 and superoxide dismutase 2 (SOD2) during ischemia, similar to the elevated expression observed in human chronic wounds. Tissue oxidative stress is known to be induced by SOD2 creating H_2O_2, whereas arginase-1 is involved in increasing nitric oxide, involved in causing redox imbalance. This model was developed to elucidate the mechanism behind the development of ischemic cutaneous wounds. Nevertheless, all the studies and wound models described incorporated only the component of pressure and ischemia

without the inclusion of biofilm forming bacteria, clinically present in pressure ulcers (Dowd et al., 2008).

Tumor necrosis factor (TNF) is a member of a superfamily of ligands and receptors that are important in inflammation, proliferation and apoptosis (Aggarwal et al., 2012). During wound healing, TNF-α is released shortly after injury and it initiates the inflammatory phase by promoting neutrophil and macrophage recruitment into the wound tissues (Barrientos et al., 2008). **T**umor **N**ecrosis **F**actor **S**uper**F**amily 14 (TNFSF14), also known as **L**ymphotoxin-like **I**nducible protein that competes with **G**lycoprotein D for binding **H**erpesvirus entry mediator on **T** cells (LIGHT), is a ligand that binds to two known cellular receptors, lymphotoxin-β receptor (LTβR) and the herpesvirus entry mediator (HveA) and has been shown to stimulate the proliferation of T cells and trigger macrophage apoptosis (Petreaca et al., 2008; Rooney et al., 2000; Zhai et al., 1998). Recently, we have shown that a mouse model in which the LIGHT gene was deleted had impaired wound healing with characteristics of non-healing ulcers similar to those observed in humans (Petreaca et al., 2012). The wounds of $LIGHT^{-/-}$ phenotype had high levels of pro-inflammatory chemokines and cytokines and consequently prolonged inflammation. The wounds had defective basement membrane, impaired dermal/epidermal interactions, leaky blood vessels and complications in granulation tissue formation. More recently we showed that very early after wounding, the $LIGHT^{-/-}$ wounds display elevated levels of oxidative stress due to increases in ROS, and RNS, and reduced levels of antioxidant enzymes (Dhall et al., 2014; Chapter 2). The increase in stress led to lipid peroxidation, DNA damage and protein nitrosylation suggesting broad-

spectrum damage to the healing tissue. Using modern metabolomics approaches, we also performed lipidomics studies on LIGHT$^{-/-}$ wounds and found increases in pro-inflammatory lipids and those involved in vascular leakage and platelet aggregation (Chapter 3). Furthermore, we reported that exacerbation of redox stress in the wound microenvironment and the presence of previously isolated biofilm forming bacteria could lead to the development of chronic wounds (Dhall et al., 2014; Chapter 2). These studies suggest that increased redox stress shortly after injury when coupled with presence of biofilm-forming bacteria can lead to wound chronicity.

ANIMAL MODELS OF CHRONIC WOUNDS

Chronic wounds in a true clinical environment are defined as wounds which have failed to progress through a systematic and well-timed reparative process to produce anatomic and functional tissue integrity over a period of 3 months (Mustoe et al., 2006). In addition, previous reports using *in vivo* animals models have also defined chronic wounds as those that take more than 4 weeks to heal (Ganesh et al., 2014). The hallmark of chronic wounds is the presence of microbial biofilms. Biofilms are formed of multiple communities of microbial flora that in the wound microenvironment adhere to a substrate and secrete extracellular polymeric substances (EPS). In the case of bacterial biofilms, the EPS serves as a niche for the residing bacteria and also acts as a protective film for the bacterial colonies (Costerton et al., 1999). They are protected from antimicrobial agents, antibiotics inflammatory cells and the highly proteolytic environment. Importantly, some bacteria that make biofilms in the presence of a substrate might not behave similarly in a free flowing environment (James et al., 2007). Different types of bacterial population are present in different types of chronic wounds (Dowd et al., 2008; Flemming and Wingender, 2010; James et al., 2007). Recent findings have shown that certain strains of bacteria when grown individually ex vivo can form biofilm, but may behave differently in presence of other coexisting bacteria in the *in vivo* wound microenvironment (Dhall et al., 2014). Hence the longitudinal assessment of wound microbiota in a chronic wound setting is crucial for preserving the microbial environment and quorum sensing that exists between different species to help our understanding of biofilm dynamics.

Although *in vitro* biofilm models have been developed to study the interactions of multiple microbes, understanding host and microbial interactions in terms of immunity, control and tolerance of both commensal and pathogenic microorganisms needs to be addressed *in vivo* (Ganesh et al., 2014). *In vivo* models to study biofilms, with introduction of purified *in vitro* grown single species of bacteria have been developed in recent years (Gurjala et al., 2011). Recently, a study used multiple species of *in vitro* grown bacteria to inoculate mouse wounds. The authors showed the bacterial prevalence in the wound over time and concluded that only *Pseudomonas aeruginosa* dominated over the 12 day period of study (Dalton et al., 2011).

Burn models of chronic wounds

Recently, *in vivo* models of burn wounds in mice and pigs involving inoculation of single or multiples species of bacterial infections have been developed. In one case, inoculation of mixed species of bacteria (*Pseudomonas aeruginosa* and *Acinetobacter baumannii strain 19606*) on full-thickness burns using a porcine model was studied over a period of 56 days (Roy et al., 2014). Although the authors did not observe any significant difference in rate of wound closure, they reported high epidermal water loss at 30 days post infection, when the wound was considered to have achieved chronicity. This model of burn wounds with microbial infection showed that the mixed-biofilm adhered to the burn surface was persistent for a long period of time and presented resistance to anti-microbial treatment. Several other models of chronic wounds using burn as an injury

have been attempted but none have become truly chronic (Trøstrup et al., 2013; Turner et al., 2014).

Diabetic models of chronic wounds

People with type II diabetes account for one of the major patient population that acquires non-healing chronic wounds and results in more than 6.5 billion dollars spent every year in the US alone (Sen et al., 2009). Therefore, understanding how chronic wounds develop in diabetics can help generate targeted therapeutics. The db/db mouse model and the streptozotocin-induced diabetic mice and pigs have been used to study impaired wound healing (Greenhalgh et al., 1990; Velander et al., 2008). However, these models have not captured the presence of biofilm forming bacteria, commonly seen in human diabetic wounds preventing the wounds from healing. Similar studies were conducted on streptozotocin induced diabetic mice with full-thickness excisional wounds challenged with *Pseudomonas aeruginosa* that lasted 16 days post infection (Watters et al., 2013). This work determined the significance of biofilm forming bacteria in delaying wound healing compared with untreated controls. However, these *in vivo* models of biofilms in wounds encompassed the use of a purified single strain of bacteria that were cultured in vitro and were not a result of spontaneously acquired infections.

To capture the clinical characteristics of chronic wounds in human diabetic patients, we developed a diabetic model of chronic wounds that spontaneously acquired biofilms and can be used for the longitudinal assessment of wound and bacteria dynamics. We hypothesized that exacerbating oxidative stress at the time of wounding

would lead the impaired wounds to become chronic (**Fig. 1.2A,B**). These wounds became fully chronic in 20 days, did not heal for more than 90 days and consisted of complex microbiota similar to that seen in humans (Dhall et al., 2014a); Chapter 4).The capability of the bacteria to thrive in a hostile proteolytic and oxidative environment was largely due to the presence of biofilm. The mixed microbial population dynamics during chronicity progressed toward a monospecific infection dominated by biofilm-producing E. cloacae. Upon treatment of the wounds with antioxidants N-acetyl cysteine (NAC) and α-tocopherol (α-TOC), to reduce the oxidative stress, we show that the resistance of the biofilm forming bacteria to antibiotics was lost (Dhall et al., 2014). Furthermore, the redox imbalance that existed in the chronic wounds was partially corrected in the presence of antioxidant treatments. This recent model developed in our laboratory is the first to allow a longitudinal assessment of the spontaneously developed wound microbiome in its natural environment. Importantly, this model offers an opportunity to longitudinally understand the microbial dynamics in a competitive environment and also mechanistically decipher the host microbiome relationship in an effort to have a targeted approach to heal chronic wounds in humans.

FUTURE STUDIES

Whereas it is well established that understanding chronic wound development in humans is still in its infancy, there are currently a number of animal models that attempt to recapitulate the process. However, only our recently developed murine model approaches recapitulation of human diabetic chronic ulcers. With the development of this animal model of chronic wounds it is now possible to understand the underlying mechanism of wound chronicity at system's levels that integrates metabolomics, proteomics and genomics. Furthermore, future prospects include understanding the bacterial bioburden behavior in the wound microenvironment and its dynamic relationship with the host to gain mechanistic insights and develop therapeutics to treat problematic wounds.

REFERENCES

Abd-El-Aleem, S. a, Ferguson, M. W., Appleton, I., Kairsingh, S., Jude, E. B., Jones, K., McCollum, C. N. and Ireland, G. W. (2000). Expression of nitric oxide synthase isoforms and arginase in normal human skin and chronic venous leg ulcers. *J. Pathol.* **191**, 434–42.

Aggarwal, B. B., Gupta, S. C. and Kim, J. H. (2012). Historical perspectives on tumor necrosis factor and its superfamily: 25 years later, a golden journey. *Blood* **119**, 651–65.

Ahn, S. T. and Mustoe, T. A. (1990). Effects of ischemia on ulcer wound healing: A new model in the rabbit ear. *Ann. Plast. Surg.* **24**, 17–23.

Barbul, A., Shawe, T., Rotter, S. M., Efron, J. E., Wasserkrug, H. L. and Badawy, S. B. (1989). Wound healing in nude mice: a study on the regulatory role of lymphocytes in fibroplasia. *Surgery* **105**, 764–9.

Barrientos, S., Stojadinovic, O., Golinko, M. S., Brem, H. and Tomic-Canic, M. (2008). Growth factors and cytokines in wound healing. *Wound Repair Regen.* **16**, 585–601.

Bickers, D. R. and Athar, M. (2006). Oxidative stress in the pathogenesis of skin disease. *J. Invest. Dermatol.* **126**, 2565–75.

Campbell, L., Saville, C. R., Murray, P. J., Cruickshank, S. M. and Hardman, M. J. (2013). Local arginase 1 activity is required for cutaneous wound healing. *J. Invest. Dermatol.* **133**, 2461–70.

Campisi, J. (2013). Aging, cellular senescence, and cancer. *Annu. Rev. Physiol.* **75**, 685–705.

Chen, C.-A., Druhan, L. J., Varadharaj, S., Chen, Y.-R. and Zweier, J. L. (2008). Phosphorylation of endothelial nitric-oxide synthase regulates superoxide generation from the enzyme. *J. Biol. Chem.* **283**, 27038–47.

Chen, J. S., Longaker, M. T. and Gurtner, G. C. (2013). Murine models of human wound healing. *Methods Mol. Biol.* **1037**, 265–74.

Clark, R. A. F. (2008). Oxidative stress and "senescent" fibroblasts in non-healing wounds as potential therapeutic targets. *J. Invest. Dermatol.* **128**, 2361–4.

Costerton, J. W., Stewart, P. S. and Greenberg, E. P. (1999). Bacterial biofilms: a common cause of persistent infections. *Science* **284**, 1318–22.

Cromack, D. T., Porras-Reyes, B., Purdy, J. A., Pierce, G. F. and Mustoe, T. A. (1993). Acceleration of tissue repair by transforming growth factor beta 1: identification of in vivo mechanism of action with radiotherapy-induced specific healing deficits. *Surgery* **113**, 36–42.

D'Autréaux, B. and Toledano, M. B. (2007). ROS as signalling molecules: mechanisms that generate specificity in ROS homeostasis. *Nat. Rev. Mol. Cell Biol.* **8**, 813–24.

Dalton, T., Dowd, S. E., Wolcott, R. D., Sun, Y., Watters, C., Griswold, J. A. and Rumbaugh, K. P. (2011). An in vivo polymicrobial biofilm wound infection model to study interspecies interactions. *PLoS One* **6**, e27317.

Darr, D. and Fridovich, I. (1994). Free Radicals in Cutaneous Biology. *J. Invest. Dermatol.* **102**, 671–675.

Darvin, M. E., Haag, S. F., Lademann, J., Zastrow, L., Sterry, W. and Meinke, M. C. (2010). Formation of free radicals in human skin during irradiation with infrared light. *J. Invest. Dermatol.* **130**, 629–31.

Dhall, S., Do, D. C., Garcia, M., Kim, J., Mirebrahim, S., Lonardi, S., Nothnagel, E. A., Schiller, N. and Martins-Green, M. (2014a). Generating and Reversing Chronic Wounds in Diabetic Mice by Manipulating Wound Redox Parameters. *J. Diabetes Res.*

Dhall, S., Do, D., Garcia, M., Wijesinghe, D. S., Brandon, A., Kim, J., Sanchez, A., Lyubovitsky, J., Gallagher, S., Nothnagel, E. A., et al. (2014b). A novel model of chronic wounds: importance of redox imbalance and biofilm-forming bacteria for establishment of chronicity. *PLoS One* **9**, e109848.

Dovi, J. V., Szpaderska, A. M. and DiPietro, L. a. (2004). Neutrophil function in the healing wound: adding insult to injury? *Thromb. Haemost.* 275–280.

Dowd, S. E., Sun, Y., Secor, P. R., Rhoads, D. D., Wolcott, B. M., James, G. a and Wolcott, R. D. (2008). Survey of bacterial diversity in chronic wounds using pyrosequencing, DGGE, and full ribosome shotgun sequencing. *BMC Microbiol.* **8**, 43.

Dröge, W. (2002). Free radicals in the physiological control of cell function. *Physiol. Rev.* **82**, 47–95.

Durante, W., Johnson, F. K. and Johnson, R. a (2007). Arginase: a critical regulator of nitric oxide synthesis and vascular function. *Clin. Exp. Pharmacol. Physiol.* **34**, 906–11.

Falanga, V. (2005). Wound healing and its impairment in the diabetic foot. *Lancet* **366**, 1736–43.

Flemming, H.-C. and Wingender, J. (2010). The biofilm matrix. *Nat. Rev. Microbiol.* **8**, 623–33.

Gallucci, R. M., Simeonova, P. P., Matheson, J. M., Kommineni, C., Guriel, J. L., Sugawara, T. and Luster, M. I. (2000). Impaired cutaneous wound healing in interleukin-6-deficient and immunosuppressed mice. *FASEB J.* **14**, 2525–31.

Ganesh, K., Sinha, M., Mathew-Steiner, S. S., Das, A., Roy, S. and Sen, C. K. (2014). Chronic Wound Biofilm Model. *Adv. Wound Care* **00**, 141105140242008.

Goldstein, B. and Sanders, J. (1998). Skin Response to Repetitive Mechanical Stress: A New Experimental Model in Pig. *Arch Phys Med Rehabil* **79**, 265–272.

Gordillo, G. M. and Sen, C. K. (2003). Revisiting the essential role of oxygen in wound healing. *Am. J. Surg.* **186**, 259–263.

Granata, F., Frattini, A., Loffredo, S., Staiano, R. I., Petraroli, A., Ribatti, D., Oslund, R., Gelb, M. H., Lambeau, G., Marone, G., et al. (2010). Production of vascular endothelial growth factors from human lung macrophages induced by group IIA and group X secreted phospholipases A2. *J. Immunol.* **184**, 5232–41.

Greenhalgh, D. G., Sprugel, K. H., Murray, M. J. and Ross, R. (1990). PDGF and FGF stimulate wound healing in the genetically diabetic mouse. *Am. J. Pathol.* **136**, 1235–46.

Griffith, O. W. and Stuehr, D. J. (1995). Nitric oxide synthases: properties and catalytic mechanism. *Annu. Rev. Physiol.* **57**, 707–36.

Guo, S. and Dipietro, L. a (2010). Factors affecting wound healing. *J. Dent. Res.* **89**, 219–29.

Gurjala, A. N., Geringer, M. R., Seth, A. K., Hong, S. J., Smeltzer, M. S., Galiano, R. D., Leung, K. P. and Mustoe, T. A. (2011). Development of a novel, highly quantitative in vivo model for the study of biofilm-impaired cutaneous wound healing. *Wound Repair Regen.* **19**, 400–10.

Ito, M., Liu, Y., Yang, Z., Nguyen, J., Liang, F., Morris, R. J. and Cotsarelis, G. (2005). Stem cells in the hair follicle bulge contribute to wound repair but not to homeostasis of the epidermis. *Nat. Med.* **11**, 1351–4.

James, G. a, Swogger, E., Wolcott, R., Pulcini, E. deLancey, Secor, P., Sestrich, J., Costerton, J. W. and Stewart, P. S. (2007). Biofilms in chronic wounds. *Wound Repair Regen.* **16**, 37–44.

Kanda, N. and Watanabe, S. (2003). 17beta-estradiol inhibits oxidative stress-induced apoptosis in keratinocytes by promoting Bcl-2 expression. *J. Invest. Dermatol.* **121**, 1500–9.

Kiriakidis, S. (2002). VEGF expression in human macrophages is NF-kappaB-dependent: studies using adenoviruses expressing the endogenous NF-kappaB inhibitor IkappaBalpha and a kinase-defective form of the IkappaB kinase 2. *J. Cell Sci.* **116**, 665–674.

Lazarus, G. S., Cooper, D. M., Knighton, D. R., Margolis, D. J., Percoraro, R. E., Rodeheaver, G. and Robson, M. C. (1994). Definitions and guidelines for assessment of wounds and evaluation of healing. *Wound Repair Regen.* 165–170.

Leibovich, S. J. and Ross, R. (1975). The role of the macrophage in wound repair. A study with hydrocortisone and antimacrophage serum. *Am. J. Pathol.* **78**, 71–100.

Lobmann, R., Ambrosch, a, Schultz, G., Waldmann, K., Schiweck, S. and Lehnert, H. (2002). Expression of matrix-metalloproteinases and their inhibitors in the wounds of diabetic and non-diabetic patients. *Diabetologia* **45**, 1011–6.

Monick, M. M., Powers, L., Butler, N., Yarovinsky, T. and Hunninghake, G. W. (2002). Interaction of matrix with integrin receptors is required for optimal LPS-induced MAP kinase activation. *Am. J. Physiol. Lung Cell. Mol. Physiol.* **283**, L390–402.

Mudge, B. P., Harris, C., Gilmont, R. R., Adamson, B. S. and Rees, R. S. (2002). Role of glutathione redox dysfunction in diabetic wounds. *Wound Repair Regen.* **10**, 52–8.

Mustoe, T. a, O'Shaughnessy, K. and Kloeters, O. (2006). Chronic wound pathogenesis and current treatment strategies: a unifying hypothesis. *Plast. Reconstr. Surg.* **117**, 35S–41S.

Novo, E. and Parola, M. (2008). Redox mechanisms in hepatic chronic wound healing and fibrogenesis. *Fibrogenesis Tissue Repair* **1**, 5.

Ozawa, T., Tsuruta, D., Jones, J. C. R., Ishii, M., Ikeda, K., Harada, T., Aoyama, Y., Kawada, A. and Kobayashi, H. (2010). Dynamic relationship of focal contacts and hemidesmosome protein complexes in live cells. *J. Invest. Dermatol.* **130**, 1624–35.

Parihar, A., Parihar, M. S., Milner, S. and Bhat, S. (2008). Oxidative stress and anti-oxidative mobilization in burn injury. *Burns* **34**, 6–17.

Peirce, S. M., Skalak, T. C. and Rodeheaver, G. T. (2000). Ischemia-reperfusion injury in chronic pressure ulcer formation: a skin model in the rat. *Wound Repair Regen.* **8**, 68–76.

Penn, J. W., Grobbelaar, A. O. and Rolfe, K. J. (2012). The role of the TGF-β family in wound healing, burns and scarring: a review. *Int. J. Burns Trauma* **2**, 18–28.

Petreaca, M. L., Yao, M., Ware, C. and Martins-Green, M. M. (2008). Vascular endothelial growth factor promotes macrophage apoptosis through stimulation of tumor necrosis factor superfamily member 14 (TNFSF14/LIGHT). *Wound Repair Regen.* **16**, 602–14.

Petreaca, M. L., Do, D., Dhall, S., McLelland, D., Serafino, A., Lyubovitsky, J., Schiller, N. and Martins-Green, M. M. (2012). Deletion of a tumor necrosis superfamily gene in mice leads to impaired healing that mimics chronic wounds in humans. *Wound Repair Regen.* **20**, 353–66.

Ponugoti, B., Xu, F., Zhang, C., Tian, C., Pacios, S. and Graves, D. T. (2013). FOXO1 promotes wound healing through the up-regulation of TGF-β1 and prevention of oxidative stress. *J. Cell Biol.* **203**, 327–43.

Qadoumi, M., Becker, I., Donhauser, N., Röllinghoff, M. and Bogdan, C. (2002). Expression of inducible nitric oxide synthase in skin lesions of patients with american cutaneous leishmaniasis. *Infect. Immun.* **70**, 4638–42.

Richard, S., B.Steve, F., C.James, D., Mark, B., Charles, K., Rongzhao, L. and Legrand K.Edmund, C. M. J. (1995). An animal model and computer-controlled surface pressure delivery system for the production of pressure ulcers. *J. Rehabil. Res. Dev.* **32**, 149–161.

Rodero, M. P. and Khosrotehrani, K. (2010). Skin wound healing modulation by macrophages. *Int. J. Clin. Exp. Pathol.* **3**, 643–53.

Rooney, I. A., Butrovich, K. D., Glass, A. A., Borboroglu, S., Benedict, C. A., Whitbeck, J. C., Cohen, G. H., Eisenberg, R. J. and Ware, C. F. (2000). The Lymphotoxin-beta Receptor Is Necessary and Sufficient for LIGHT-mediated Apoptosis of Tumor Cells. *J. Biol. Chem.* **275**, 14307–14315.

Roy, S., Khanna, S., Nallu, K., Hunt, T. K. and Sen, C. K. (2006). Dermal wound healing is subject to redox control. *Mol. Ther.* **13**, 211–20.

Roy, S., Biswas, S., Khanna, S., Gordillo, G., Bergdall, V., Green, J., Marsh, C. B., Gould, L. J. and Sen, C. K. (2009). Characterization of a preclinical model of chronic ischemic wound. *Physiol. Genomics* **37**, 211–24.

Roy, S., Elgharably, H., Sinha, M., Ganesh, K., Chaney, S., Mann, E., Miller, C., Khanna, S., Bergdall, V. K., Powell, H. M., et al. (2014). Mixed-species biofilm compromises wound healing by disrupting epidermal barrier function. *J. Pathol.* **233**, 331–43.

Schaffer, M. R., Tantry, U., Gross, S. S., Wasserburg, H. L. and Barbul, a (1996). Nitric oxide regulates wound healing. *J. Surg. Res.* **63**, 237–40.

Sen, C. K. and Roy, S. (2008). Redox signals in wound healing. *Biochim. Biophys. Acta* **1780**, 1348–61.

Sen, C. K., Gordillo, G. M., Roy, S., Kirsner, R., Lambert, L., Hunt, T. K., Gottrup, F., Gurtner, G. C. and Longaker, M. T. (2009). Human skin wounds: a major and snowballing threat to public health and the economy. *Wound Repair Regen.* **17**, 763–71.

Shukla, A., Rasik, A. M. and Patnaik, G. K. (2009). Depletion of Reduced Glutathione, Ascorbic Acid, Vitamin E and Antioxidant Defence Enzymes in a Healing Cutaneous Wound.

Sirsjö, A., Karlsson, M., Gidlöf, A., Rollman, O. and Törmä, H. (1996). Increased expression of inducible nitric oxide synthase in psoriatic skin and cytokine-stimulated cultured keratinocytes. *Br. J. Dermatol.* **134**, 643–8.

Soneja, A., Drews, M. and Malinski, T. (2005). Role of nitric oxide, nitroxidative and oxidative stress in wound healing. *Pharmacol. Rep.* **57 Suppl**, 108–19.

Sorokin, L. (2010). The impact of the extracellular matrix on inflammation. *Nat. Rev. Immunol.* **10**, 712–23.

Stadelmann, W. K., Digenis, A. G. and Tobin, G. R. (1998). Physiology and Healing Dynamics of Chronic Cutaneous Wounds. *Am. J. Surg.* **176**, 26S–38S.

Stadler, I., Zhang, R.-Y., Oskoui, P., Whittaker, M. S. and Lanzafame, R. J. (2004). Development of a simple, noninvasive, clinically relevant model of pressure ulcers in the mouse. *J. Invest. Surg.* **17**, 221–7.

Steed, D. L. (1997). THE ROLE OF GROWTH FACTORS IN WOUND HEALING. *Surg. Clin. North Am.* **77**, 575–586.

Sun, B. K., Siprashvili, Z. and Khavari, P. A. (2014). Advances in skin grafting and treatment of cutaneous wounds. *Science (80-.).* **346**, 941–945.

Swaim, S. F. (1992). Use of a thromboxane synthetase inhibitor in the presence of dermal pressure. *Am. J. Hosp. Palliat. Med.* **9**, 21–23.

Swaim, F. S., Bradley, M. D., Vaughn, M. D., Powers, D. R. and Hoffman, E. C. (1993). The greyhound dog as a model for studying pressure ulcers. *Decubitus* **6**, 32–40.

Trøstrup, H., Thomsen, K., Christophersen, L. J., Hougen, H. P., Bjarnsholt, T., Jensen, P. Ø., Kirkby, N., Calum, H., Høiby, N. and Moser, C. (2013). Pseudomonas aeruginosa biofilm aggravates skin inflammatory response in BALB/c mice in a novel chronic wound model. *Wound Repair Regen.* **21**, 292–9.

Tsuboi, R., Shi, C. M., Rifkin, D. B. and Ogawa, H. (1992). A wound healing model using healing-impaired diabetic mice. *J. Dermatol.* **19**, 673–5.

Turner, K. H., Everett, J., Trivedi, U., Rumbaugh, K. P. and Whiteley, M. (2014). Requirements for Pseudomonas aeruginosa acute burn and chronic surgical wound infection. *PLoS Genet.* **10**, e1004518.

Vaalamo, M., Weckroth, M., Puolakkainen, P., Kere, J., Saarinen, P., Lauharanta, J. and Saarialho-Kere, U. K. (1996). Patterns of matrix metalloproteinase and TIMP-1 expression in chronic and normally healing human cutaneous wounds. *Br. J. Dermatol.* **135**, 52–9.

Velander, P., Theopold, C., Hirsch, T., Bleiziffer, O., Zuhaili, B., Fossum, M., Hoeller, D., Gheerardyn, R., Chen, M., Visovatti, S., et al. (2008). Impaired wound healing in an acute diabetic pig model and the effects of local hyperglycemia. *Wound Repair Regen.* **16**, 288–93.

Wassermann, E., van Griensven, M., Gstaltner, K., Oehlinger, W., Schrei, K. and Redl, H. (2009). A chronic pressure ulcer model in the nude mouse. *Wound Repair Regen.* **17**, 480–4.

Watters, C., DeLeon, K., Trivedi, U., Griswold, J. a, Lyte, M., Hampel, K. J., Wargo, M. J. and Rumbaugh, K. P. (2013). Pseudomonas aeruginosa biofilms perturb wound resolution and antibiotic tolerance in diabetic mice. *Med. Microbiol. Immunol.* **202**, 131–41.

Werner, S., Krieg, T. and Smola, H. (2007). Keratinocyte-fibroblast interactions in wound healing. *J. Invest. Dermatol.* **127**, 998–1008.

Wlaschek, M. and Scharffetter-Kochanek, K. (2005). Oxidative stress in chronic venous leg ulcers. *Wound Repair Regen.* **13**, 452–61.

Wynn, T. A. and Ramalingam, T. R. (2012). Mechanisms of fibrosis: therapeutic translation for fibrotic disease. *Nat. Med.* **18**, 1028–40.

Zhai, Y., Guo, R., Hsu, T. L., Yu, G. L., Ni, J., Kwon, B. S., Jiang, G. W., Lu, J., Tan, J., Ugustus, M., et al. (1998). LIGHT, a novel ligand for lymphotoxin beta receptor and TR2/HVEM induces apoptosis and suppresses in vivo tumor formation via gene transfer. *J. Clin. Invest.* **102**, 1142–51.

FIGURE CAPTIONS

Figure 1.1. Schematic illustration of the sequence of events during normal/acute wound healing. At the site of injury, there occurs a phase of hemostasis, followed by the inflammatory phase where chemotaxis of inflammatory cells (neutrophils, macrophages and lymphocytes) and release of growth factors and cytokines occurs. Granulation tissue formation overlaps the inflammatory phase. Collagen III production and deposition, keratinocyte migration and fibroblast proliferation and migration, angiogenesis, and extracellular matrix (ECM) deposition, takes place in this phase. The final phase is the tissue remodeling phase which ensues crosslinking of collagen fibers, changes in ECM deposition, and collagen III replaced by collagen I

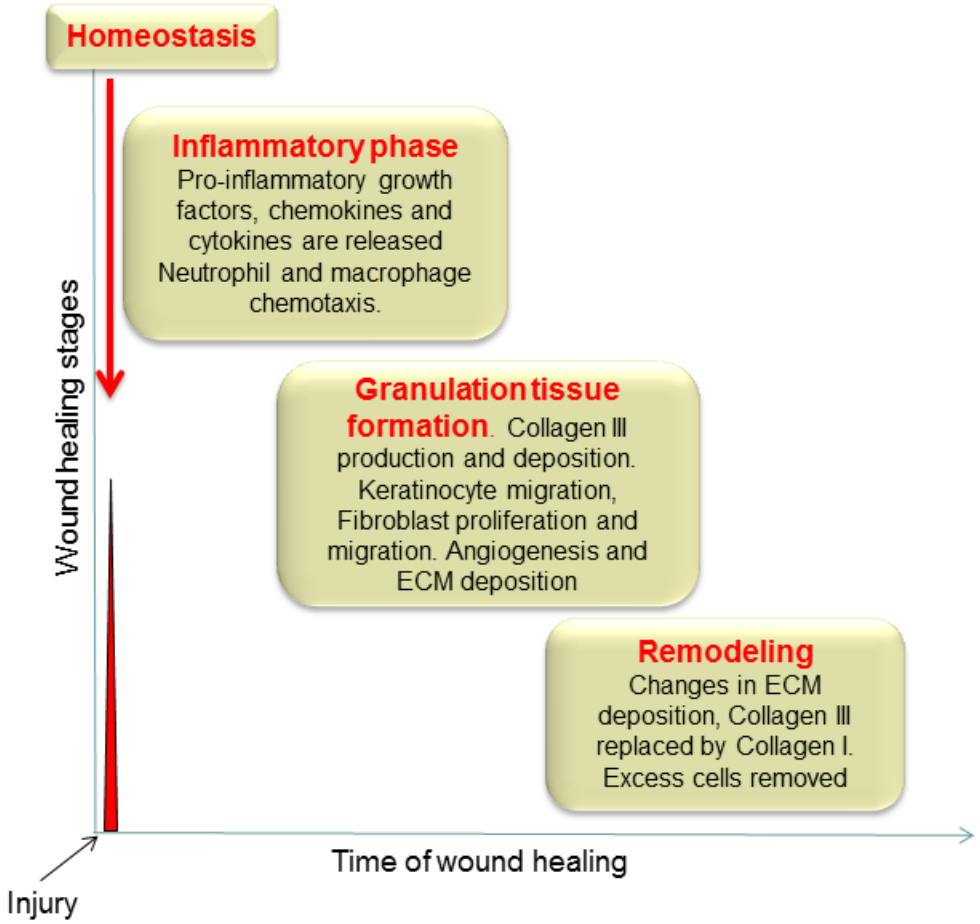
Homeostasis
Inflammatory phase
Pro-inflammatory growth factors, chemokines and cytokines are released Neutrophil and macrophage chemotaxis.
Granulation tissue formation. Collagen III production and deposition. Keratinocyte migration, Fibroblast proliferation and migration. Angiogenesis and ECM deposition
Remodeling
Changes in ECM deposition, Collagen III replaced by Collagen I. Excess cells removed
Wound healing stages
Time of wound healing
Injury

Figure 1.1

Figure 1.2. Schematic representation of schedule of inflammation during acute and chronic healing. (A) Upon injury in an environment of normal healing, there is an exponential rise in inflammation seen as with the onset of neutrophil recruitment, followed by the progression phase while there is the presence of macrophages and incoming T-lymphocytes. The phase is followed by the resolution phase where inflammation ceases and the tissue returns to hemostasis. (**B**) In case of a chronic wound, upon injury, there is an exponential rise in inflammatory cells along with exacerbated levels of reactive oxygen species. The wound progresses on a path of continuous inflammation and stress, damaging the tissue in repair and surrounding tissue and harbors biofilm forming bacteria. Such an environment does not enter the phase of resolution and hemostasis. This leads to the formation of chronic wounds.

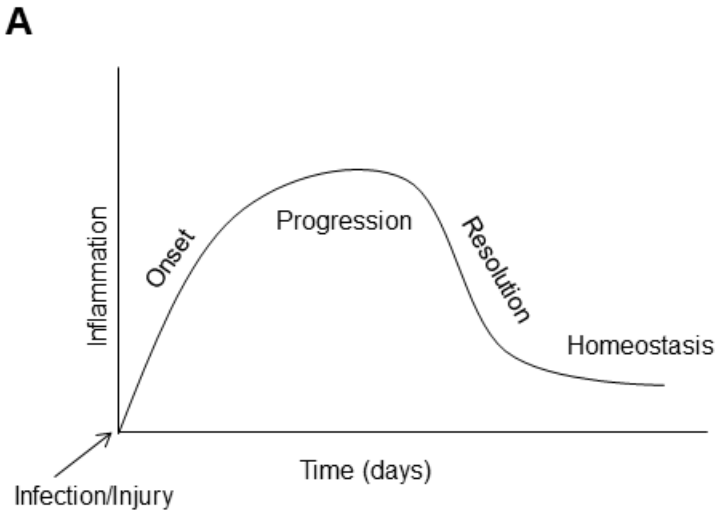
A
Inflammation
Onset
Progression
Resolution
Homeostasis
Time (days)
Infection/Injury

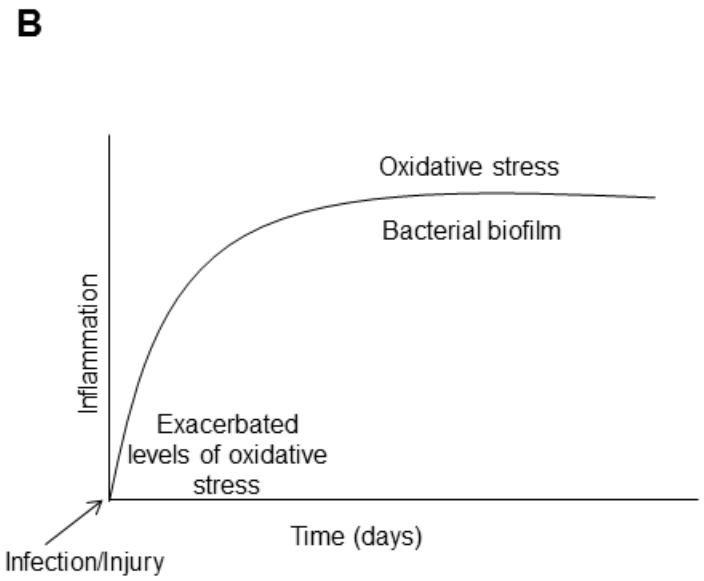
B
Oxidative stress
Bacterial biofilm
Inflammation
Exacerbated
levels of oxidative
stress
Time (days)
Infection/Injury

Figure 1.2

SECTION 1

IMPAIRED WOUNDS

CHAPTER 2

IMPORTANCE OF REDOX IMBALANCE AND BIOFILM-FORMING BACTERIA FOR ESTABLISHMENT OF CHRONICITY

ABSTRACT

Chronic wounds have a large impact on health, affecting ~6.5M people and costing ~$25B/year in the US alone (Sen et al., 2009). We previously discovered that a genetically modified mouse model displays impaired healing similar to problematic wounds in humans and that sometimes the wounds become chronic. Here we show how and why these impaired wounds become chronic, describe a way whereby we can drive impaired wounds to chronicity at will and propose that the same processes are involved in chronic wound development in humans. We hypothesize that exacerbated levels of oxidative stress are critical for initiation of chronicity. We show that, very early after injury, wounds with impaired healing contain elevated levels of reactive oxygen and nitrogen species and, much like in humans, these levels increase with age. Moreover, the activity of anti-oxidant enzymes is not elevated, leading to buildup of oxidative stress in the wound environment. To induce chronicity, we exacerbated the redox imbalance by further inhibiting the antioxidant enzymes and by infecting the wounds with biofilm-forming bacteria isolated from the chronic wounds that developed naturally in these mice. These wounds do not re-epithelialize, the granulation tissue lacks vascularization and interstitial collagen fibers, they contain an antibiotic-resistant mixed bioflora with biofilm-forming capacity, and they stay open for several weeks. These findings are highly significant because they show for the first time that *chronic wounds* can be generated in an animal model effectively and consistently. The availability of such a model will significantly propel the field forward because it can be used to develop strategies to

regain redox balance that may result in inhibition of biofilm formation and result in restoration of healthy wound tissue. Furthermore, the model can lead to the understanding of other fundamental mechanisms of chronic wound development that can potentially lead to novel therapies.

INTRODUCTION

Failure of acute wounds to proceed through the normal regulated repair process results in wounds that have impaired healing and/or become chronic (Lazarus et al., 1994; Wong and Gurtner, 2012). Diabetic foot ulcers, venous ulcers, and other similar chronic wounds have a large impact on health, currently affecting ~6.5M patients and costing ~$25B/year in the US alone (Sen et al., 2009). Although great efforts have been made to switch the course of repair from non-healing wounds to healing wounds, success has been limited. This is primarily due to the pathophysiological complexity of changing an acute wound into a chronic wound and the lack of good animal models.

Injury causes the early generation of reactive oxygen species (ROS) in the presence of vascular membrane-bound nicotinamide-adenine-dinucleotide (NADH)-dependent oxidases (NOXs) that are produced by resident endothelial cells and fibroblasts (Roy et al., 2006). ROS are required for defense against invading pathogens and low levels of ROS act as essential mediators of intracellular signaling that leads to proper healing (D'Autréaux and Toledano, 2007; Sen and Roy, 2008). However, uncontrolled production of ROS early after injury leads to an altered detoxification process caused by reduction in antioxidant production and activity (Dröge, 2002). Studies have provided evidence that non-healing ulcers in humans have high oxidative and nitrosative stress (Wlaschek and Scharffetter-Kochanek, 2005; Yang et al., 2013; Yeoh-Ellerton and Stacey, 2003). Furthermore, tissue hypoxia as well as anaerobic glycolysis, contribute to the production of lactate and its accumulation under inflammatory

conditions (Britland et al., 2012; Hopf and Rollins, 2007). Even in well-oxygenated wounds (Hopf and Rollins, 2007), when the number of neutrophils is high (Fazli et al., 2011), lactate and ROS become significantly elevated as a result of aerobic glycolysis -- the so-called "Warburg effect" (Warburg, 1956). This environment leads to a stagnant inflammatory phase. If the inflammatory cells are not removed from the wound tissue, they can promote further tissue damage through excessive production of inflammatory cytokines, proteases, and reactive oxygen intermediates, and increased cell death that, together, result in abnormal granulation tissue development and lead to wounds with impaired healing (Dovi et al., 2004; Hunt et al., 2000; McCarty et al., 2012).

Nitric oxide (NO) also plays a key role in wound repair (Luo and Chen, 2005; Schäfer and Werner, 2008). The beneficial effects of NO in wound repair relate to its functions in angiogenesis, inflammation, cell proliferation, matrix deposition, and remodeling. However, high levels of NO produced by inducible nitric oxide synthase (iNOS) produce peroxynitrite ($ONOO^-$), a reactive nitrogen species (RNS). $ONOO^-$ causes damage to DNA, lipids and proteins which invariably leads to cell apoptosis and/or necrosis depending on its concentration at the injury site (Abd-El-Aleem et al., 2000).

It is virtually impossible to study the development of chronic wounds in humans. By the time these wounds appear in the clinic, the initial stage of development is well passed. Therefore, animal models to conduct studies on the genesis of non-healing chronic wounds are needed. We recently showed that a mouse in which the Tumor

Necrosis Factor Superfamily Member 14 (TNFSF14/LIGHT) gene has been knocked out (LIGHT$^{-/-}$ mice) has impaired healing and that the wounds heal poorly and show many of the characteristics of impaired wounds in humans (Petreaca et al., 2012). When compared to control, the wounds of LIGHT$^{-/-}$ mice show defects in epithelial-dermal interactions, high degree of inflammation, damaged microvessels with virtually no basement membrane or periendothelial cells, the collagen in the granulation tissue is mostly degraded, matrix metalloproteinases (MMPs) are elevated and tissue inhibitors of metalloproteinase (TIMPs) are down-regulated. In addition, we also found that sometimes the LIGHT$^{-/-}$ wounds become chronic, and when they do, these defects are highly accentuated. In addition, the wounds become heavily infected with *Staphylococcus epidermidis* (Petreaca et al., 2012), a gram-positive bacterium frequently found in human chronic wounds (Howell-Jones et al., 2005). All of these characteristics are very similar to those found in chronic wounds in humans (Guo and Dipietro, 2010; James et al., 2007; Martin et al., 2010). Mechanistically, we have shown that LIGHT mediates macrophage cell death induced by vascular endothelial growth factor (VEGF) and that this occurs in a LTβ receptor-dependent manner (Petreaca et al., 2008), indicating that LIGHT is involved in the resolution of macrophage-induced inflammation**.** In addition, LIGHT$^{-/-}$ mice also show increased levels of Forkhead box protein A1 (FOXA1), Cytochrome P450 2E1 (CYP2E1), and Toll-like receptor 6 (TLR6) which are genes involved in oxidative stress (Gonzalez, 2005; Kuhlicke et al., 2007; Kundu et al., 2012; Song et al., 2009)**.** Furthermore, Aldehyde oxidase 4 (AOX4) is also elevated in these knockout mice. This enzyme leads to the generation of $O_2^{\cdot -}$ that then aids in release of iron from

ferritin (Shaw and Jayatilleke, 1992). Here we show that by manipulating the microenvironment at wounding we can cause the impaired wounds to become chronic 100% of the time and propose that the same processes are involved in chronic wound development in humans. This model provides an opportunity to understand fundamental mechanisms involved in chronic wound development that can potentially lead to identifying diagnostic molecules and to the discovery of novel treatments.

MATERIALS AND METHODS

Dermal excisional wound model: Animals were housed at the University of California, Riverside (UCR) vivarium. All experimental protocols were approved by the UCR Institutional Animal Care and Use Committee (IACUC). Experiments were performed using 12–16 week old mice categorized as adult mice and 85–92 week old mice as old mice. The procedure used was performed as previously described (Petreaca et al., 2012).

Superoxide dismutase activity assay: Total tissue superoxide dismutase (SOD) activity was measured by using a commercially available kit (Cayman Chemical, Catalog# 706002, Ann Arbor, USA) that measures all three types of SOD (Cu/Zn-, Mn-, and EC-SOD). One unit of SOD is defined as the amount of enzyme needed to cause 50% dismutation of the superoxide radical**.** Extracts obtained from tissues collected at 4hr, 12hr, 24hr and 48hr post-wounding were processed for total SOD activity according to the protocol provided by the assay kit manufacturer. The SOD activities of the samples were calculated from the linear regression of a standard curve that was determined using the SOD activity of bovine erythrocytes at various concentrations run under the same conditions. The SOD activity was expressed as U/ml of tissue extract.

Hydrogen peroxide activity assay: Tissue hydrogen peroxide (H_2O_2) levels were measured by using a commercially available kit (Cell Technology Inc., Catalog# FLOH 100-3, Mountain View, USA) that utilizes a non-fluorescent detection reagent. The assay is based on the peroxidase-catalyzed oxidation by H_2O_2 of the nonfluorescent substrate 10-acetyl-3,7-dihydroxyphenoxazine to a fluorescent resorufin. Fluorescent intensities

were measured at 530 nm (excitation)/590 nm (emission) using a Victor 2 microplate reader. The amounts of H_2O_2 in the supernatants were derived from a seven-point standard curve generated with known concentrations of H_2O_2**.**

Catalase activity assay: Tissue catalase activity was measured by using a commercially available kit (Cayman Chemical, Catalog# 707002, Ann Arbor, USA). The enzyme assay for catalase is based on the peroxidatic function of catalase with methanol to produce formaldehyde in the presence of an optimal concentration of H_2O_2. The formaldehyde produced was measured spectrophotometrically, with 4-amino-3-hydrazino-5-mercapto-1,2,4-triazole (purpald) as the chromogen, at 540 nm in a 96-well place. The catalase activity was expressed as nmol/min/ml of tissue extract.

Glutathione peroxidase activity assay: Tissue glutathione peroxidase (GPx) activity was measured using a commercially available kit (Cayman Chemical, Catalog# 703102, Ann Arbor, USA). The activity was measured indirectly by a coupled reaction with glutathione reductase (GR). GPx reduces H_2O_2 to H_2O and in the process oxidized glutathione (GSSG) is produced that in turn is recycled to its reduced state by GR and NADPH. Furthermore, oxidation of NADPH to $NADP^+$ is accompanied by a decrease in absorbance at 340nm. Under conditions in which GPx activity is rate limiting, the rate of decrease in the absorbance measured at 340nm, in a 96-well plate at 1-min interval for a total of 5min using a Victor 2 microplate reader, is directly proportional to the GPx activity of the sample. GPx activity was expressed as nmol/min/ml of tissue extract.

Lactate measurement assay: Tissue lactate levels were measured using a commercially available kit (Biovision Inc, Catalog# K638-100, Milipitas, USA). Tissue lactate extracts were specifically oxidized to form an intermediate that reacts with a colorless probe to generate fluorescence that was measured at 530nm (excitation)/590nm (emission) using Victor 2 microplate reader. The intensity was directly proportional to the amount of lactate measured in nmol/ml.

pH measurements: Wound pH levels were measured using a Beetrode micro pH electrode with a 100 µm tip diameter, 2 mm receptacle (World Precision Instruments, Catalog# NMPH5,Sarasota, USA). A separate reference electrode of 450µm diameter tip was used (World Precision Instruments, Catalog# DRIREF-450, Sarasota, USA) along with a small, battery-operated compensator (World Precision Instruments, Catalog# SYS-Beecal, Sarasota, USA) to generate mV readings in the range of the standard pH meter used (Beckman Coulter, Catalog# A58754, Brea, USA). The compensator helped adjust the electrode-offset potential. Calibration of the electrodes was done at 37^0C (temperature of the mouse body) in pH buffers 4, 7 and 10. A linear Nernstian plot was obtained and was used to convert the mV readings that were obtained from the mouse wound. Measurements on every mouse wound were done at five different locations, four of which were at the periphery of the wound at 90^o angle and one in the center.

Nitrate nitrite analysis: Tissues collected were weighed and introduced into eppendorf tubes with equal weights of zirconium oxide beads. Nitrite free methanol at 2 ml/g tissue was added to the tubes. Tissues were homogenized for 10mins in a bullet blender at 4^OC.

The extracts were then centrifuged at 10000rpm for 10 mins at 4^{O}C. The methanolic supernatant was collected and analysis was performed as previously described (Stapley et al., 2012).

Lipid peroxide assay using thiobarbituric acid reactive substances: Tissue thiobarbituric acid reactive substances (TBARS) were measured by using a commercially available kit (Cell Biolabs Inc., Catalog# STA-300, San Diego, USA). Lipid peroxidation forms unstable lipid peroxides that further decompose into natural byproducts such as malondialdehyde (MDA) and 4-hydroxynonenal (4-HNE). MDA forms adducts with TBARS in a 1:2 proportion. These aducts were measured fluorometrically at an excitation of 540 nm and emission at 590 nm. TBARS levels were then calculated in µM by comparison with a predetermined MDA standard curve.

Isolation of DNA and 8-hydroxy-2-deoxy Guanosine (8-OH-dG) analysis: Tissue DNA was extracted by using a commercially available kit (Qiagen, Catalog# 69504, Valencia, USA). Eluted DNA was digested using nuclease P1 and the pH adjusted to 7.5-8.5 using 1M Tris. The DNA was incubated for 30min at 37^{o}C with 1U of alkaline phosphatase per 100µg of DNA and then boiled for 10min. The 8-OH-dG DNA damage assay was performed by using a commercially available kit (Cayman Chemical, Catalog# 589320, Ann Arbor, USA). The measurements are based on a competitive enzyme immunoassay between 8-OH-dG and an 8-OH-dG-acetylcholinesterase (AChE) conjugate (8-OH-dG tracer) with a limited amount of 8-OH-dG monoclonal antibody. After conjugation, Ellman's reagent (used to quantify the number or concentration of thiol groups) was used

as a developing agent and read spectrophotometrically at 412nm. The intensity measured was proportional to the amount of 8-OH-dG that was expressed in pg/ml.

Nitrotyrosine ELISA: Tissue nitrotyrosine levels were measured by using a commercially available kit (Cell Biolabs Inc., Catalog# STA-305 San Diego, USA). The measurements are based on a competitive enzyme immunoassay. The tissue sample or nitrated BSA were bound to an anti-nitrotyrosine antibody, followed by an HRP conjugated secondary antibody and enzyme substrate. The absorbance was measured spectrophotometrically at 412nm and the nitrotyrosine content in the unknown sample was then determined by comparing with a standard curve that was prepared from predetermined nitrated BSA standards.

Cell death: Tissue cell death level was measured by using Annexin V apoptosis kits (Southern Biotech, Catalog# 10010-09, Birmingham, USA) according to the manufacturer's instructions and our previously published methodology (Petreaca et al., 2008). Percoll gradients were used to collect the wound cells from the homogenized wound tissue, and the cell stained with the kit reagents. Cells that lose membrane integrity allow propidium iodide to enter and bind to DNA, a phenomenon seen in case of cell death due to necrosis, whereas apoptotic cells only stain for Annexin V. The cells were then separated by FACS analysis to separate the populations staining with propidium iodide from those staining with Annexin V.

Scanning Electron Microscopy: Tissues collected were fixed in 4% paraformaldehyde for 4hrs at room temperature. Samples were then dehydrated in 25%, 50%, 75%, 95%

and 100% ethanol for 20min each at room temperature. Critical point drying of the tissues was performed using Critical-point-dryer Balzers CPD0202 followed by Au/Pd sputtering for 1min in the Sputter coater Cressington 108 auto. The coated samples were attached to carbon taped aluminum stubs and were imaged using an XL30 FEG scanning electron microscope.

In Vivo Imaging: Live animal images were captured using the iBox Scientia Small Animal Imaging System (UVP, LLC. Upland, CA, an Analytik Jena Company). Mice were anesthetized and placed on the imaging stage maintained at 37^{o}C for the duration of each imaging experiment. For each time point, age-matched C57BL/6 and LIGHT$^{-/-}$ mice was imaged using the ImageEM 1K EM-CCD (Hamamatsu, Japan), cooled to -55°C, and an optical system consisting of a 50mm f/1.2 lens. Images were captured separately for each time point without an emission filter and at 1x1 binning. Bright field images using a white light channel were captured first at an exposure time of 150 milliseconds followed by a luminescent channel at an exposure time at 10-20min.

***Preparation of tissue extracts*:** The tissues collected were prepared as previously described (Petreaca et al., 2012).

Immunoblotting: Wound tissue extracts were probed for iNOS and phospho eNOS as previously described (Petreaca et al., 2012).

Lipidomics: 1ml of LCMS grade ethanol containing 0.05% BHT and 10ng of each internal standard was added to frozen wound tissues. Internal standards used were, (d_4) 8-iso $PGF_{2\alpha,}$ (d_{11}) 5-iso $PGF_{2\alpha}$-VI, (d_4) 6k $PGF_{1\alpha}$, (d_4) $PGF_{2\alpha}$, (d_4) PGE_2, (d_4) PGD_2, (d_4)

LTB_4, (d4) TXB_2, (d_4) LTC_4, (d_5) LTD_4, (d_5) LTE_4, (d_8) 5-hydroxyeicosatetranoic acid (5HETE), (d_8) 15-hydroxyeicosatetranoic acid (15HETE), (d_8) 14,15 epoxyeicosatrienoic acid, (d_8) arachidonic Acid, and (*d5*) eicosapentaenoic acid. Samples were mixed using a bath sonicator incubated overnight at -20^{0}C for lipid extraction. The insoluble fraction was precipitated by centrifuging at 12,000xg for 20min and the supernatant was transferred into a new glass tube. Lipid extracts were then dried under vacuum and reconstituted in of LCMS grade 50:50 EtOH:dH_2O (100 µl) for eicosanoid quantitation via UPLC ESI-MS/MS analysis. A 14min reversed-phase LC method utilizing a Kinetex C18 column (100 x 2.1mm, 1.7µm) and a Shimadzu UPLC was used to separate the eicosanoids at a flow rate of 500µl/min at 50°C. The column was first equilibrated with 100% Solvent A [acetonitrile:water:formic acid (20:80:0.02, v/v/v)] for two minutes and then 10µl of sample was injected. 100% Solvent A was used for the first two minutes of elution. Solvent B [acetonitrile:isopropanol (20:80, v/v)] was increased in a linear gradient to 25% Solvent B to 3min, to 30% by 6 minutes, to 55% by 6.1min, to 70% by 10min, and to 100% by 10.1min. 100% Solvent B was held until 13min, then decreased to 0% by 13.1min and held at 0% until 14min. The eluting eicosanoids were analyzed using a hybrid triple quadrapole linear ion trap mass analyzer (ABSciex 6500 QTRAP®,) via multiple-reaction monitoring in negative-ion mode. Eicosanoids were monitored using species specific precursor → product MRM pairs. The mass spectrometer parameters were: curtain gas: 30; CAD: High; ion spray voltage: -3500V; temperature: 300°C; Gas 1: 40; Gas 2: 60; declustering potential, collision energy, and cell exit potential were optimized per transition.

Antioxidant inhibition and biofilm formation model: Catalase activity was inhibited by intraperitonial injection of 3-Amino-1,2,4-triazole (ATZ) at a concentration of 1g/kg body weight 20min prior to creating the excisional wound. GPx activity inhibition was performed by topical application of mercaptosuccinic acid at concentration of 150mg/kg body weight immediately after wounding and the wound was covered with sterile tegaderm. 24hrs post-wounding, 20µl *Staphylococcus epidermidis C2* suspension at a concentration of $1x10^8$ CFU/mL was added onto the wound and this covered with sterile tegaderm. The wounds were kept moist at all times and tegaderm was replaced as soon as the sealant of the tegaderm was seen to be compromised to avoid wound contamination. All procedures were carried out in a sterile environment. The inhibitor injection protocol and application of the bacteria were repeated every week.

Bacteria isolation and characterization: Wound exudates from $LIGHT^{-/-}$ mice were collected using sterile cotton swabs and stored at -80^oC in 1.0% w/v proteose peptone and 20.0% v/v glycerol solution until analyzed. Samples were thawed on ice, vortexed and cultured for 16-24 hrs at 37^oC on tryptic soy agar plates containing 5.0% v/v defibrinated sheep blood and 0.08% w/v Congo red dye. Viable colonies were counted and then differentiated based on size, hemolytic patterns, and Congo red uptake. The cultures were examined for Grams stain reactivity and visualized using a compound light microscope. Grams negative rods were characterized using the API 20E identification kit (Biomerieux, Durham USA), grown on *Pseudomonas* Isolation Agar, oxidase activity, growth at 42^oC in LB, and motility. Grams positive cocci differentiated based on catalase activity, coagulase activity, growth in 6.5% w/v NaCl tolerance test, and hemolytic

activity. Biofilm production was quantified using adherence and staining of extracellular polysaccharide (slime), produced by bacteria, using Congo red staining to deduce whether or not the bacteria was a biofilm former using previously published procedures and criteria (Christensen et al., 1985; Cui et al., 2013).

Community Minimal antibiotic inhibitory concentration assay: Community minimal inhibitory concentration (CMIC) assay was carried out with amoxicillin as described by DeLoney and Schiller (DeLoney and Schiller, 1999) with the following modification. Wound exudates (containing the bacteria) were challenged with antibiotic for 12hr with concentrations ranges from 100 to 0.78µg/mL in tryptic soy broth after being seeded at 37oC in a humidified incubator for 4hr prior to the assay. The CMIC is defined as the lowest antibiotic concentration that resulted in a ≤50% increase in the optical density measured at 595nm compared to the optical density reading prior to the introduction of antibiotic.

Tissue preparation for histology: Tissues collected were prepared as previously described (Petreaca et al., 2012).

Statistical analysis: For the statistical analysis of experiments, we used Graphpad Instat Software (Graphpad, La Jolla, CA, USA) and Sigmaplot Software (SigmaPlot, San Jose, USA). Analysis of variance (ANOVA) was used to test the significance of group differences between two or more groups. In experiments with only two groups, statistical analysis was conducted using a Student's t-test.

RESULTS

In order to identify parameters in the wounds with impaired healing that, when changed, may lead these wounds to become chronic, we first characterized the state of ROS/RNS in the early stages of impaired healing by examining a variety of components of the oxidative and nitrosative stress cycle as represented schematically in **Figure 1** Superoxide dismutase (SOD) dismutates superoxide anions ($O_2^{\cdot -}$) to generate H_2O_2, which can then be detoxified by catalase to H_2O+O_2 and by glutathione peroxidase (GPx) to H_2O. ROS can also enter the Fenton reaction in the presence of ferrous ions to give rise to $^{\cdot}OH+OH^-$. $O_2^{\cdot -}$ can also interact with nitric oxide (NO) produced by nitric oxide synthase (NOS) to give rise to peroxinitrite anion ($ONOO^-$). The effects of oxidative and nitrosative stress are shown in terms of lipid peroxidation, DNA damage, protein modification and cell death. Secondly, we will present the data on the manipulation of the redox balance that leads to development of chronic wounds including the characterization of the polymicrobial environment that favors growth of biofilm-forming aerobic and anaerobic bacteria. For all figures (**Figures 2.2-2.5**) except (**Figure 2.3C**), time t=0 represents unwounded skin.

Characterization of the redox environment in wounds with impaired healing

ROS

Oxidative stress: To determine whether the wounds with impaired healing have increased oxidative stress, we measured the levels of SOD. SOD activity, measuring Cu/Zn-, Mn-, and EC-SOD, was already significantly elevated by 4hrs post-wounding in the LIGHT$^{-/-}$ wounds compared to the C57BL/6 wounds and remains high through 48hrs (**Figure 2.2A**). H_2O_2 levels also were significantly elevated as early at 4hrs post-wounding in the LIGHT$^{-/-}$ wounds, decreasing to control levels by 48hrs (**Figure 2.2B**). Furthermore, we observed that in LIGHT$^{-/-}$ mice, both catalase and GPx activities were similar to control mice, suggesting that accumulation of H_2O_2 was primarily caused by the inability of the antioxidant system to keep up with the oxidative stress (**Figure 2.2C,D**).

It is well known that, in human wounds, oxidative stress increases with age. We determined that oxidative stress in wounds of old LIGHT$^{-/-}$ mice also increased with age; higher levels of SOD activity were seen in wounds of old LIGHT$^{-/-}$ mice than in their adult counterparts (**Figure 2.2E**). H_2O_2 levels in the wounds of old LIGHT$^{-/-}$ mice were at least 10 times higher than those in the adult mice (compare **Figure 2.1F** with **Figure 2.2B**). In contrast, the level of catalase activity was significantly lower in wounds of old LIGHT$^{-/-}$ mouse than in wounds of old C57BL/6 mice (**Figure 2.2G**) but was comparable to the wounds of adult LIGHT$^{-/-}$ mice (compare **Figure 2.2G** with **Figure 2.2C**). Similarly, GPx activity was significantly lower in the wounds of old LIGHT$^{-/-}$ mice than in old C57BL/6 mice (**Figure 2.2H**) and was much lower than in either type of adult

mice (compare **Figure 2.2H** with **Figure 2.2D**). Taken together, these results suggest that adult LIGHT$^{-/-}$ wounds have high levels of oxidative stress and that, much like in humans, these levels are exacerbated with age (Guo and Dipietro, 2010; Moor et al., 2014).

To further confirm the elevated presence of ROS we performed real time *in vivo* imaging of excision wounds at various time points after wounding. Imaging was initiated immediately after IP injection of luminol that emits light in the presence of an oxidizing agent such as H_2O_2. We detected a signal on the edges of the wound in the LIGHT$^{-/-}$ mouse as early as 4hrs after wounding. The level of intensity was increased significantly in LIGHT$^{-/-}$ mice compared to C57BL/6 throughout the early hours post-wounding (**Figure 2.3A)**. Similar results were obtained when imaging old LIGHT$^{-/-}$ and C57BL/6 mice (data not shown). These real-time images show for the first time that, *in vivo,* ROS can be detected *in situ* as early as 4hrs after wounding.

The presence of oxidative stress leads to increase in enzymatic activity of lactate dehydrogenase (LDH), which results in lactate generation. Because ROS-generated oxidative stress is elevated in the LIGHT$^{-/-}$ wounds, we investigated production of lactate in the wound microenvironment (Hunt et al., 2000; Schneider et al., 2007). Higher levels of lactate production were seen at 12hrs post-wounding in the control mice whereas LIGHT$^{-/-}$ mice showed a delayed, but significant, accumulation during days 1 and 2 post-wounding (**Figure 2.3B**). The levels of lactate accumulation in wounds of old LIGHT$^{-/-}$

mice were similar to the wounds of adult LIGHT$^{-/-}$ mice and also were significantly higher than wounds in old C57BL/6 mice (**Figure 2.4A**).

The pH in a wound milieu is a dynamic factor that can change rapidly and affect healing. Studies have shown that the presence of acidic pH correlates with compromised, chronic, and infected wounds (Schreml et al., 2010). pH measurements of the wound bed were collected immediately, within 3 minutes after wounding and then at the indicated hrs. Relative to the control, the pH obtained from LIGHT$^{-/-}$ wounds was more acidic by 4hrs post-wounding and remained so through at least 48hrs (**Figure 2.3C**). Similar results were obtained with old LIGHT-/- mice (**Figure 2.4B**). Unwounded skin surface pH was not measured because the glass microelectrodes we used require moisture and the skin is dry. Humidifying the skin with water will alter the pH because of the presence of free fatty acids on the skin that releases H+ ions into the water applied and can give measurements that are not accurate (Stefaniak et al., 2013). Correlations between lactate and pH (proton transport) have previously been shown to increase in parallel to each other (Gethin, 2007; Lotito et al., 1989). The same occurs in these wounds.

Nitrosative stress, protein modification, and damage of lipids and DNA: To determine whether wounds of LIGHT$^{-/-}$ mice have high nitrosative stress, we examined the metabolites of NO, nitrite (NO_2^-) and nitrate (NO_3^-) and found that shortly after wounding the levels of nitrite in the adult LIGHT$^{-/-}$ mice wounds were very much higher than those in the control at 4 and 12hrs but declined to normal by day 1 (**Figure 2.3D**). Nitrate

levels showed the same pattern of elevation as nitrite (**Figure 2.3E**). Old mice showed a similar pattern of elevation but the levels were even higher than in adult LIGHT$^{-/-}$ wounds between 4-12hrs post-wounding (**Figure 2.4C,D**). To determine whether the elevated levels of NO_2^- and NO_3^- early post-wounding were due to changes in nitric oxide synthase (NOS), both endothelial NOS (eNOS) and inducible NOS (iNOS) were examined for phosphorylation/activation of eNOS and elevated expression of iNOS in LIGHT$^{-/-}$ mouse wounds. We found that the levels were significantly elevated but that elevation did not occur until 12hrs and 24hrs post-wounding, respectively (**Figure 2.3F,G**), suggesting that the increase in NO production must be due to activation of other systems/factors occurring very early after wounding.

Modification of tyrosine residues to 3-nitrotyrosine in proteins by $ONOO^-$ or other potential nitrating agents occurs when tissues are subject to nitrosative stress. Because we show the presence of nitrosative stress, we examined the levels of 3-nitrotyrosine (3-NT) to assess the effects of this stress on protein modification during healing of the LIGHT$^{-/-}$ mice. We found that the levels of 3-NT were significantly elevated in LIGHT$^{-/-}$ mouse wounds 1 day post-wounding and, except for day 5, remained significantly elevated throughout the course of healing (**Figure 2.5A**), confirming the deleterious effects of the presence of nitrosative stress. These effects were almost doubled in the old LIGHT$^{-/-}$ mice (**Figure 2.6A**).

It is known that increase in ROS/RNS can cause lipid peroxidation. Lipid peroxides are unstable markers of oxidative stress that decompose to form

malondialdehyde (MDA) and 4-hydroxynonenal (4-HNE). We found a significant increase in MDA levels 48hrs after wounding that remained significantly elevated throughout healing (**Figure 2.5B**). We also found that the levels of lipid peroxidation were exacerbated in wounds of old LIGHT$^{-/-}$ mice after 48hr post-wounding (**Figure 2.6B**). Furthermore, we used mass spectroscopy to examine whether ROS-induced non-enzymatic peroxidation products of arachidonic acid, such as isoprostanes, were present in the wounds. We found that 8-isoprostane (8-epi-$PGF_{2\alpha}$) and 5-isoprostane were significantly elevated in the LIGHT$^{-/-}$ mouse wounds, suggesting the breakdown of arachidonic acid in the presence of ROS (**Figure 2.5C,D**). These results confirm that there is lipid damage in the LIGHT$^{-/-}$ wounds.

Another detrimental effect caused by excessive oxidative stress and nitrosative stress is 8-hydroxylation of the DNA guanine base (8OHdG) that results in DNA damage. The overall levels of this stress marker were increased in wounds of adult LIGHT$^{-/-}$ mice (**Figure 3E**), with significant increase at days 3 and 9 post-wounding. We also found that the levels of 8-OHdG in the old LIGHT$^{-/-}$ mouse wounds were significantly more elevated throughout the course of healing (**Figure 2.6C**).

Levels of cell death by both apoptosis and necrosis: Given that excessive redox stress results in damage of DNA, proteins, and lipids that are critical for cell survival and function, we examined cell death both by apoptosis and necrosis (**Figure 2.5F**). Apoptosis was significantly increased 12hrs post-wounding and increased even more by

48hrs post-wounding. Cell death by necrosis was predominantly found at 24hrs and 48hrs. Particularly striking is the difference in cell death by necrosis between control and LIGHT$^{-/-}$ mice. This elevated cell death is potentially due to the higher levels of oxidative stress and can lead to chronic inflammation, impaired healing and delayed wound closure.

Manipulation of redox balance and the presence of biofilm-forming bacteria lead to development of chronic wounds

Our previous results (Petreaca et al., 2012) and the results presented above strongly suggest that the LIGHT$^{-/-}$ impaired healing is caused by redox imbalance established shortly after injury, resulting in excessive cell death which then creates an environment that increases inflammation and is propitious for the growth of biofilm-forming bacteria, thereby setting the wound on a course that leads to development of chronic ulcers. To test this possibility we significantly increased the oxidative stress in the wound by further inhibiting the antioxidant enzymatic activity and applying the biofilm-forming bacteria, S. *epidermidis* C2, that we isolated from the spontaneously-developed chronic wounds of the LIGHT$^{-/-}$ mice (Petreaca et al., 2012). Inhibition of catalase by 3-Amino-1,2,4-triazole (ATZ) and GPx by mercaptosuccinic acid (MSA) immediately post-wounding and application of S. *epidermidis* C2 24hrs later was sufficient to turn the wounds with impaired healing into chronic wounds 100% of the time (**Figure 2.7A**). Chronic wounds were successfully created in 30 animals used in 10 different experiments. Wounds of C57BL/6 mice treated under the same conditions

closed in 15-19 days whereas the LIGHT$^{-/-}$ wounds remained open for > 4 weeks (**Figure 2.7B**). The wounds were kept covered at all times using sterile tegaderm and changed upon compromised sealant of the bandage.

Following the application of inhibitors post-wounding, and bacteria 24 hours later, we evaluated the levels of ROS to determine whether the levels of oxidative stress increased. With antioxidant inhibitor treatment, SOD (**Figure 2.7C**) and H_2O_2 levels (**Figure 2.7D**) were significantly elevated by 12hours post-wounding. Corresponding to the increase in ROS, antioxidant enzymes catalase and GPx, that were inhibited by ATZ and MSA respectively, were decreased significantly (**Figure 2.7E,F**). These experiments were conducted simultaneously, under identical conditions.

Histological examination of chronic LIGHT$^{-/-}$ wounds showed that the migrating tongue of the epidermis was blunted and tortuous **(Figure 2.8A,B)** rather than thin and linear as in the control (**Figure 2.9A**). Also, the granulation tissue was poorly developed (**Figure 2.8A**) when compared to normal granulation tissue (**Figure 2.9B,C**). Collagen IV, a component of the basal lamina, was well-formed behind the migrating tongue but was absent under the tortuous migrating edge (**Figure 2.8C-E**). We also found that these wounds contain macrophages, indicating that inflammation has not been resolved (**Figure 2.8F,H**; inserts show higher magnification of one macrophage). Furthermore, the interstitial collagen deposition and organization were abnormal in the LIGHT$^{-/-}$ chronic wounds as revealed by Masson trichrome staining (**Figure 2.8I**) and by second harmonic generation imaging microscopy (SHIM) (**Figure 2.8J,K**). Although interstitial collagen

was present, the collagen fibers were not clearly visible and did not form proper bundles (**Figure 2.8J**). This is similar to the finding we published on the impaired wounds of LIGHT-/- wounds (Petreaca et al., 2012) but much more exaggerated.

To determine whether the application of the bacteria alone or in the presence of a single inhibitor could induce chronicity in the LIGHT$^{-/-}$ wounds, we introduced S. *epidermidis* C2 24hrs post-wounding without any inhibitor treatment (**Figure 2.10A**) or with just ATZ treatment (**Figure 2.10B**) or with just MSA treatment (**Figure 2.10C**). In all three cases, both in the C57BL/6 and LIGHT$^{-/-}$ mice, the wounds healed by day 15-19, suggesting that development of chronic wounds requires all three of these elements: inhibition of both catalase and GPx to greatly decrease the antioxidant enzymes in the wound, plus addition of biofilm-forming bacteria.

It has been established that the bioflora that colonize chronic wounds in humans is commonly polymicrobial (Bowler, 2002; Dowd et al., 2008). Therefore, we determined whether the LIGHT$^{-/-}$ chronic wounds also exhibited this polymicrobial phenotype. Wound exudates from both adult and old LIGHT$^{-/-}$ mice were collected and the bacteria genus/species determined as described in Materials and Methods. In addition, staining of adherent cells with Hucker crystal violet, which has been widely used as readout for biofilm-production (Christensen et al., 1985; Kolodkin-Gal et al., 2012; O'Toole and Kolter, 1998; Stepanovic et al., 2000), was used as a qualitative measure for biofilm formation in our bacteria isolates. As expected, we found that biofilm-forming (OD570nm $\geq$ 0.125) coagulase-negative *Staphylococcus epidermidis* was present in the

wounds throughout healing, given that we infected the wounds with *S. epidermidis* C2. However, co-colonizing bacteria were also isolated. These co-colonizers were identified as non-biofilm forming hemolytic *Streptococcus sp.*, biofilm-producing oxidase-positive aerobic Gram-negative rods (presumptively *Pseudomonas*), and *Enterobacter cloacae* (dotted line in **Figure 2.11A** defines the minimum optical density for biofilm formation).

Quantification of the relative bacterial prevalence showed that the dynamics of the colonizing bioflora in adult LIGHT$^{-/-}$ mouse wounds changes over time (**Figure 2.11B**). These changes are marked by the decreased concentration of *S. epidermidis* populations coupled with the appearance of the oxidase positive Gram-negative rods followed by *E. cloacae.* As the wound progresses to a non-healing/chronic stage at ~20 days post-wounding, the *E. cloacae* population dominates the wound with traces of *S. epidermidis* (**Figure 2.11B**). Irrespective of the shift in bacterial population of the wounds, the overall degree in biofilm production by these polymicrobial communities (dotted line in **Figure 2.11C**) did not change significantly over time at least until 22 days. However, the individual contribution to biofilm production varies and is dependent on the time of isolation and is species specific (**Figure 2.11C**). Eight days post-wounding, biofilm-producing *Staphylococcus epidermidis* (C2) is significantly different from the non-biofilm-producing negative control, *Staphylococcus hominis* (SP2, ATCC 35982). SP2 does not adhere to polystyrene plates, does not produce extracellular polysaccharide and is a commensal bacterium found on human skin (Kloos and Schleifer, 1975). Because of these characteristics, this strain has been widely used as a negative control for

biofilm production (Christensen et al., 1985; Cui et al., 2013; Qu et al., 2010). Similar observations were made in the old LIGHT$^{-/-}$ mice (**Figure 2.12A-C**).

It has been well established that biofilm-associated wound infections are extremely resistant to antimicrobial therapy (Parsek and Singh, 2003; Percival et al., 2010). The community minimal inhibitory concentration (CMIC) of amoxicillin required to inhibit the growth of biofilm-producing microbial flora from LIGHT$^{-/-}$ adult chronic wounds was determined to be 50μg/mL (day 22/24) compared to the 0.4-0.8μg/mL required for non-biofilm producing colonizers (day 5) (**Figure 2.11D**). This suggests that biofilm-producing microbial flora isolated from LIGHT$^{-/-}$ chronic wounds are ~50X more resistant to killing by amoxicillin compared to their non-biofilm producing counterparts.

It has been reported that the majority of chronic wounds in humans have bacterial contamination and high levels of bacterial burden will likely result in impaired healing (Siddiqui and Bernstein, 2010). At 5 and 8 days post-wounding, colony-forming unit counts (CFU/mL of exudate) from adult and old LIGHT$^{-/-}$ mouse exudates show low levels of bacterial burden ($1.6x10^3$ CFU/mL and $2.0x10^3$ CFU/mL respectively). However, these levels reach $4.0x10^7$ CFU/mL and $7.4x10^7$ CFU/mL by 22-24 days of healing (**Figure 2.11E and Figure 2.12D).**

In order to determine whether the skin of mice contain the bacteria that eventually make biofilm in the chronic wounds, we took skin swabs from unwounded C57 and LIGHT$^{-/-}$ mice and cultured them *in vitro* (**Figure 2.11F**). The majority of the cultured bacteria belong to the Firmicutes phylum, specifically *Staphylococcus spp. and*

Streptococcus spp. We also documented the presence of bacteria that belong to the Proteobacteria phylum (e.g. various Gram-negative rods and *Enterobacter*). These bacteria are all known to be associated with the human skin microbiota (Cho and Blaser, 2012).

To further confirm the presence of biofilm-forming bacteria in these wounds we performed scanning electron microscopy on LIGHT$^{-/-}$ chronic wounds. An abundance of bacteria was observed in the wound and some of those bacteria were embedded in a biofilm-like matrix (**Figure 2.13A)**, with some of them appearing to reside in a defined niche surrounded by matrix (**Figure 2.13B**). Beneath the biofilm we observed the presence of numerous inflammatory cells adherent to extracellular matrix (**Figure 2.13C**). Furthermore, analysis of the glycosyl composition of the exudate collected from the chronic wounds showed high levels of N-acetylglucosaminyl (GlcNAc), galacturonosyl (GalU), mannosyl, galactosyl and glucosyl residues (data not shown**)**. This glycosyl composition is consistent with the presence of extracellular polysaccharide material, and possibly N-glycoproteins, in the chronic wound. These carbohydrates have also been shown to be present in human chronic wounds during *P. aeruginosa* infections (Stevens et al., 1984) and more recently exopolysaccharides with glycosyl compositions including these residues have been characterized in other species such as *Staphylcococcus* and *Enterobacter* which are pathogens commonly found in humans (Bales et al., 2013).

DISCUSSION

We have shown that we can *create chronic wounds* by manipulation of the impaired wounds of LIGHT$^{-/-}$ mice using antioxidant enzyme inhibitors to further increase ROS/RNS and by adding biofilm-forming bacteria previously isolated from the naturally occurring chronic wounds of these transgenic mice. This approach leads to the generation of chronic wounds 100% of the time. These wounds: (1) Contain high levels of reactive oxygen and nitrogen species and, much like in humans, these levels increase with age; (2) have decreased levels of anti-oxidant enzymes indicating the buildup of oxidative stress in the wound environment; (3) contain increased peroxynitrite and lipid peroxidation-derived products, increased 3-nitrotyrosine levels, increased DNA damage and high levels of cell death, contributing to redox imbalance in the wound microenvironment; (4) do not heal for weeks.

Our data show that SOD enzymatic activity is highly elevated in the first 48hrs post-wounding which likely is the cause for continued increase of H_2O_2 at the wound site. This is particularly important because the activities of the antioxidant enzymes, catalase and GPx, are not elevated to compensate for the extra H_2O_2 produced. In old animals, catalase and GPx activity is even lower than in the control, exacerbating the levels of H_2O_2. Furthermore, not only can H_2O_2 cause damage directly, it can also enter the Fenton reaction in the presence of divalent iron ions to produce hydroxyl radicals ($^{\cdot}OH$) that lead to additional tissue damage (Bryan et al., 2012; Sindrilaru et al., 2011; Yeoh-Ellerton and Stacey, 2003).

The LIGHT$^{-/-}$ wounds also have high levels of inflammatory cells early after wounding that persist for a long time (Petreaca et al., 2012). Increase in inflammation in a hypoxic wound tends to drive lactate accumulation that, in turn, leads to an unchecked proton gradient. As a consequence, lactate plays an important role in maintaining the fine acid-base milieu (Britland et al., 2012; Fazli et al., 2011; Hopf and Rollins, 2007). LIGHT$^{-/-}$ wounds showed increases in lactate levels both in adult and old mice, suggesting a pH imbalance. Recent findings on successful acceptance of skin grafts on chronic wounds was higher at elevated pH (alkaline) than at lower (acidic) pH (Lotito et al., 1989; Messonnier et al., 2007; Shorrock et al., 2000). In the control wounds, the pH shifted to alkaline at 4hrs whereas in the LIGHT$^{-/-}$ wounds it shifted to more acidic and the levels remained acidic throughout at least the first 2 days in both adult and old LIGHT$^{-/-}$ mice, potentially contributing to the impaired healing in the wounds of these mice. Although we do not know whether increases in anaerobic metabolism are due to the down regulation of oxidative phosphorylation in an effort to alleviate oxidative stress, we are currently studying the gene expression profiles of the LIGHT$^{-/-}$ wound very early post wounding to obtain in-depth insight into the genes/proteins responsible for such processes.

The levels of nitrite and nitrate, end products of NO metabolism, were significantly elevated very early post-wounding in the adult and old LIGHT$^{-/-}$ mice. This suggests excessive levels of NO production at the wound site that in the presence of $O_2^{\cdot -}$ can generate $ONOO^-$. It has been reported that phosphorylation of eNOS modulates both the production of NO and $O_2^{\cdot -}$ (Chen et al., 2008) and also that increase in H_2O_2 may

exert effects on endothelial cell dysfunction and uncoupling of NOS. Our data show that there is increased phosphorylation/activation of eNOS and increased iNOS levels. However, the elevated levels of phospho-eNOS and of iNOS appear after the increase in nitrite and nitrate levels in LIGHT$^{-/-}$ wounds, hence these enzymes cannot be the reason for the increases in nitrite and nitrate. It is possible that elevation of NO could be the result of either dephosphorylation of Thr495 on eNOS (Sullivan and Pollock, 2006) or increases in L-arginine (Erez et al., 2011) and decrease in endogenous NOS inhibitors (Miyazaki et al., 1999). Furthermore, the elevation in eNOS and iNOS at later times after wounding suggests an increase in NO that can combine with $O_2^{\cdot -}$ to give rise to $ONOO^-$, a highly damaging ion species.

Clinical studies on chronic wounds in humans have shown free-radical-induced damage of proteins, lipids and DNA (Abd-El-Aleem et al., 2000; Goel et al., 2012; Moseley et al., 2004; Schäfer and Werner, 2008). We found that the levels of malondialdehyde (MDA), a byproduct of lipid peroxidation, were significantly elevated throughout the course of healing in LIGHT$^{-/-}$ mice, indicating lipid damage. We also show the presence of F_2 isoprostanes that are considered to be the gold standard of oxidative stress and lipid peroxidation. Levels of 8- and 5-isoprostanes detected in LIGHT$^{-/-}$ mice were significantly elevated when compared to the control mice.

DNA damage induced by ROS and RNS can cause modifications that impair DNA repair (Freeman et al., 2009). Levels of excretion of the free, water soluble, 8-OHdG are reduced, resulting in failing exonuclease activity; this is especially seen with

aging, leading to cell damage (Fraga et al., 1990; Kikuchi et al., 2012). Our results show two waves of DNA damage in LIGHT$^{-/-}$ mouse wounds. The first wave suggests that the initial accumulation of 8-OHdG in these wounds is potentially controlled by existing exonuclease activity. However, once this activity is exhausted, the cells are no longer able to handle DNA damage. Increased levels of DNA damage in old mice are seen early and remain elevated, underscoring the continuous increase in oxidative and nitrosative stress with aging of this mouse model much as is seen in humans.

NO is a dynamic molecule that reacts with $O_2^{\cdot -}$ at a rate constant three times higher than the rate constant reaction of $O_2^{\cdot -}$ with SOD, giving rise to $ONOO^-$ production (Beckman and Koppenol, 1996) that causes nitration of tyrosine residues which damages proteins. Previous studies have shown that changes on tyrosine residues in proteins is an irreversible process that, in turn, severely impairs the regulatory components that undergo phosphorylation or adenylation in signal transduction events (Berlett et al., 1996). The increased levels of nitrotyrosine in adult and exacerbation in old LIGHT$^{-/-}$ mice suggest an increase in tissue damage.

NO plays a crucial role in bacterial biofilm dispersion (Barraud et al., 2006). Recent studies have shown that the use of low doses of NO in conjunction with antibiotics can lead to bacterial biofilm dispersion and induce these biofilm-forming bacteria to behave in a planktonic manner, hence reducing biofilm formation (Cathie et al., 2014; Kaplan, 2010; Schreiber et al., 2011). Although NO also has been widely considered an important immune cell regulator and a chemoattractant that plays a vital

role in signaling events in wound healing (Rizk et al., 2004), the chemistry of excessive NO changes in the presence of oxygen. These two molecules readily react with each other, giving rise to RNS that cause damage in the wound tissue (Bedard and Krause, 2007; Wink et al., 2011). Formation of $ONOO^-$, triggered by combination of NO and $O_2^{\cdot -}$, has been known to cause nitrosative damage. We show that there are elevated levels of nitrosative damage in $LIGHT^{-/-}$ wounds after we increase the oxidative stress in the wounds. Therefore, we speculate that the complexity of the microbiota and varying levels of NO, due to the presence of ROS, can lead to restricted levels of biofilm dispersion.

Occurrence of oxidative stress and maintenance of redox balance following stress is an essential component for proper wound healing. Stress is triggered by increases in ROS produced by (i) inflammatory cells (termed as oxidative burst), (ii) a family of NADPH oxidase (NOX), consisting of NOX1-5, and DUOX1&2, (Bedard and Krause, 2007)and (iii) wound fibroblasts when stimulated by pro-inflammatory cytokines (Clark, 2008). Although moderate increases in ROS regulate various signaling processes and act against invading bacteria, prolonged and excessive presence of ROS and inflammation can lead to hypoxia and tissue damage caused primarily by lipid peroxidation, DNA damage, protein nitrosylation, and cell death. Furthermore, excessive levels of ROS due to tissue damage create an environment that can serve as an inviting substrate for bacteria to thrive upon. The relationship between exacerbated levels of ROS and bacteria has been reported previously (Boles and Singh, 2008; Liu et al., 2013). Studies have suggested that DNA double-stranded breaks in bacteria caused by oxidative stress lead to mutagenic repair via DNA repair protein RecA, rendering the variants with increased antibiotic

resistance and adaptability to the surrounding microenvironment (Boles and Singh, 2008). Furthermore, during excessive oxidative stress, these bacteria upregulate genes that increase their virulence (Liu et al., 2013). In an effort to obtain excessive and persistent levels of oxidative stress, we manipulated the early wound microenvironment by inhibiting catalase (Heck et al., 2010) and GPx activities (Chaudiere et al., 1984) and introduced our previously isolated S. epidermidis bacterial strain. The intensified levels in redox stress and the presence of biofilm-forming bacteria led to reproducible generation of chronic wounds.

Chronic wounds, and difficult-to-heal wounds are postulated to have an underlying biofilm-associated microbial contribution that is complex and dynamic (Costerton et al., 1999; James et al., 2007; Siddiqui and Bernstein, 2010; Zhao et al., 2012). We show that chronicity in LIGHT$^{-/-}$ wounds is accompanied by a persistent bacterial infection that is polymicrobial and contains biofilm-producing bacteria. The colonizing bacterial species associated and/or responsible for the formation of chronic wounds in the LIGHT$^{-/-}$ mice, are biofilm-producing and the capacity of these organisms to produce biofilms varies depending on the time of isolation. Furthermore, we showed that the source of infection arises from the LIGHT$^{-/-}$ mouse skin microbiota. Similar observations have been documented for human chronic wounds (Scales and Huffnagle, 2013; Youmans et al., 1980).

The presence of biofilm-producing *S. epidermidis* in human chronic wounds (James et al., 2007) and the contribution of *E. cloacae* in nosocomial infections are well

known (Dalben et al., 2008). However, much less is known about *E. cloacae* infection in chronic wounds, although its presence is often reported (Madsen et al., 1996) in diabetic foot infection (Gerding, 1995; Sapico et al.), diabetic gangrene (Sharp et al.), and chronic venous leg ulcers (Gjødsbøl et al., 2006; Hansson et al., 1995). Perhaps the lack of consideration of *E. cloacae* contribution to the development of chronic wounds may be in part due to their relatively lower initial abundance compared to the more commonly isolated bacteria *Staphylococcus spp.*, *Enterococcus spp.*, and *Pseudomonas aeruginosa* (Brook and Frazier, 1998; Gjødsbøl et al., 2006; Siddiqui and Bernstein, 2010).

CONCLUSIONS

The chronic wound model we present in this publication is the first to effectively mimic chronic wounds in humans. The model wounds stay open for weeks and capture many of the characteristics of human chronic wounds. LIGHT$^{-/-}$ mice have elevated levels of genes involved in oxidative and nitrosative stress that lead to imbalanced redox levels in the wound tissue that are exacerbated with age. As a consequence, redox burden causes deleterious effects in the wound tissue that lead to impaired healing. Manipulation of the wound microenvironment to increase oxidative stress in the presence of biofilm-forming bacteria leads inevitably to development of chronic wounds, identifying high levels of oxidative stress in the wound tissue as a critical factor for chronic wound development. Furthermore, because of the nature and complexity of the mixed wound microbiota, the model presented here can provide insight into the biology of bacterial dynamics and host interaction and the factors that promote biofilm production. This model system, in which a genetic alteration leads to an imbalance in redox levels in wound tissue, has the potential to lead to the understanding of other fundamental cell and molecular mechanisms of chronic wound development and, by implication, to the development of new therapies. Having established a system where 100% of wounds are chronic, we are currently working on reversing chronicity in LIGHT$^{-/-}$ and other genetically-modified mice.

REFERENCES

Abd-El-Aleem, S. a, Ferguson, M. W., Appleton, I., Kairsingh, S., Jude, E. B., Jones, K., McCollum, C. N. and Ireland, G. W. (2000). Expression of nitric oxide synthase isoforms and arginase in normal human skin and chronic venous leg ulcers. *J. Pathol.* **191**, 434–42.

Bales, P. M., Renke, E. M., May, S. L., Shen, Y. and Nelson, D. C. (2013). Purification and Characterization of Biofilm-Associated EPS Exopolysaccharides from ESKAPE Organisms and Other Pathogens. *PLoS One* **8**, e67950.

Barraud, N., Hassett, D. J., Hwang, S.-H., Rice, S. a, Kjelleberg, S. and Webb, J. S. (2006). Involvement of nitric oxide in biofilm dispersal of Pseudomonas aeruginosa. *J. Bacteriol.* **188**, 7344–53.

Beckman, J. S. and Koppenol, W. H. (1996). Nitric oxide , superoxide , and peroxynitrite : the good , the bad , and the ugly. *AJP Cell Physiol.* **271**, 1424–1437.

Bedard, K. and Krause, K. (2007). The NOX Family of ROS-Generating NADPH Oxidases : Physiology and Pathophysiology. *Physiol. Rev.* **87**, 245–313.

Berlett, B. S., Friguet, B., Yim, M. B., Chock, P. B. and Stadtman, E. R. (1996). Peroxynitrite-mediated nitration of tyrosine residues in Escherichia coli glutamine synthetase mimics adenylylation: relevance to signal transduction. *Proc. Natl. Acad. Sci. U. S. A.* **93**, 1776–80.

Boles, B. R. and Singh, P. K. (2008). Endogenous oxidative stress produces diversity and adaptability in biofilm communities. *Proc. Natl. Acad. Sci. U. S. A.* **105**, 12503–8.

Bowler, P. G. (2002). Wound pathophysiology, infection and therapeutic options. *Ann. Med.* **34**, 419–27.

Britland, S., Ross-Smith, O., Jamil, H., Smith, A. G., Vowden, K. and Vowden, P. (2012). The lactate conundrum in wound healing: clinical and experimental findings indicate the requirement for a rapid point-of-care diagnostic. *Biotechnol. Prog.* **28**, 917–24.

Brook, I. and Frazier, E. H. (1998). Aerobic and anaerobic microbiology of chronic venous ulcers. *Int. J. Dermatol.* **37**, 426–8.

Bryan, N., Ahswin, H., Smart, N., Bayon, Y., Wohlert, S. and Hunt, J. a (2012). Reactive oxygen species (ROS)--a family of fate deciding molecules pivotal in constructive inflammation and wound healing. *Eur. Cell. Mater.* **24**, 249–65.

Cathie, K., Howlin, R., Carroll, M., Clarke, S., Connett, G., Cornelius, V., Daniels, T., Duignan, C., Hall-Stoodley, L., Jefferies, J., et al. (2014). Reducing Antibiotic Tolerance using Nitric Oxide in Cystic Fibrosis : report of a proof of concept clinical trial. *Arch. Dis. Child.* **99**, A159–A159.

Chaudiere, J., Wilhelmsen, E. C. and Tappel, a L. (1984). Mechanism of selenium-glutathione peroxidase and its inhibition by mercaptocarboxylic acids and other mercaptans. *J. Biol. Chem.* **259**, 1043–50.

Chen, C.-A., Druhan, L. J., Varadharaj, S., Chen, Y.-R. and Zweier, J. L. (2008). Phosphorylation of endothelial nitric-oxide synthase regulates superoxide generation from the enzyme. *J. Biol. Chem.* **283**, 27038–47.

Cho, I. and Blaser, M. J. (2012). The human microbiome: at the interface of health and disease. *Nat. Rev. Genet.* **13**, 260–70.

Christensen, G. D., Simpson, W. a, Younger, J. J., Baddour, L. M., Barrett, F. F., Melton, D. M. and Beachey, E. H. (1985). Adherence of coagulase-negative staphylococci to plastic tissue culture plates: a quantitative model for the adherence of staphylococci to medical devices. *J. Clin. Microbiol.* **22**, 996–1006.

Clark, R. A. F. (2008). Oxidative stress and "senescent" fibroblasts in non-healing wounds as potential therapeutic targets. *J. Invest. Dermatol.* **128**, 2361–4.

Costerton, J. W., Stewart, P. S. and Greenberg, E. P. (1999). Bacterial biofilms: a common cause of persistent infections. *Science* **284**, 1318–22.

Cui, B., Smooker, P. M., Rouch, D. a, Daley, A. J. and Deighton, M. a (2013). Differences between two clinical Staphylococcus capitis subspecies as revealed by biofilm, antibiotic resistance, and pulsed-field gel electrophoresis profiling. *J. Clin. Microbiol.* **51**, 9–14.

D'Autréaux, B. and Toledano, M. B. (2007). ROS as signalling molecules: mechanisms that generate specificity in ROS homeostasis. *Nat. Rev. Mol. Cell Biol.* **8**, 813–24.

Dalben, M., Varkulja, G., Basso, M., Krebs, V. L. J., Gibelli, M. a, van der Heijden, I., Rossi, F., Duboc, G., Levin, a S. and Costa, S. F. (2008). Investigation of an outbreak of Enterobacter cloacae in a neonatal unit and review of the literature. *J. Hosp. Infect.* **70**, 7–14.

DeLoney, C. R. and Schiller, N. L. (1999). Competition of Various beta -Lactam Antibiotics for the Major Penicillin-Binding Proteins of Helicobacter pylori: Antibacterial Activity and Effects on Bacterial Morphology. *Antimicrob. Agents Chemother.* **43**, 2702–2709.

Dovi, J. V., Szpaderska, A. M. and DiPietro, L. a. (2004). Neutrophil function in the healing wound: adding insult to injury? *Thromb. Haemost.* 275–280.

Dowd, S. E., Sun, Y., Secor, P. R., Rhoads, D. D., Wolcott, B. M., James, G. a and Wolcott, R. D. (2008). Survey of bacterial diversity in chronic wounds using pyrosequencing, DGGE, and full ribosome shotgun sequencing. *BMC Microbiol.* **8**, 43.

Dröge, W. (2002). Free radicals in the physiological control of cell function. *Physiol. Rev.* **82**, 47–95.

Erez, A., Nagamani, S. C. S., Shchelochkov, O. a, Premkumar, M. H., Campeau, P. M., Chen, Y., Garg, H. K., Li, L., Mian, A., Bertin, T. K., et al. (2011). Requirement of argininosuccinate lyase for systemic nitric oxide production. *Nat. Med.* **17**, 1619–26.

Fazli, M., Bjarnsholt, T., Kirketerp-Møller, K., Jørgensen, A., Andersen, C. B., Givskov, M. and Tolker-Nielsen, T. (2011). Quantitative analysis of the cellular inflammatory response against biofilm bacteria in chronic wounds. *Wound Repair Regen.* **19**, 387–91.

Fraga, C. G., Shigenaga, M. K., Park, J. W., Degan, P. and Ames, B. N. (1990). Oxidative damage to DNA during aging: 8-hydroxy-2'-deoxyguanosine in rat organ DNA and urine. *Proc. Natl. Acad. Sci. U. S. A.* **87**, 4533–7.

Freeman, T. a, Parvizi, J., Della Valle, C. J. and Steinbeck, M. J. (2009). Reactive oxygen and nitrogen species induce protein and DNA modifications driving arthrofibrosis following total knee arthroplasty. *Fibrogenesis Tissue Repair* **2**, 5.

Gerding, D. N. (1995). Foot infections in diabetic patients: the role of anaerobes. *Clin. Infect. Dis.* **20 Suppl 2**, S283–8.

Gethin, G. (2007). The significance of surface pH in chronic wounds. *Wounds* **3**, 52–56.

Gjødsbøl, K., Christensen, J. J., Karlsmark, T., Jørgensen, B., Klein, B. M. and Krogfelt, K. A. (2006). Multiple bacterial species reside in chronic wounds: a longitudinal study. *Int. Wound J.* **3**, 225–31.

Goel, A., Spitz, D. R. and Weiner, G. J. (2012). Manipulation of cellular redox parameters for improving therapeutic responses in B-cell lymphoma and multiple myeloma. *J. Cell. Biochem.* **113**, 419–25.

Gonzalez, F. J. (2005). Role of cytochromes P450 in chemical toxicity and oxidative stress: studies with CYP2E1. *Mutat. Res.* **569**, 101–10.

Guo, S. and Dipietro, L. a (2010). Factors affecting wound healing. *J. Dent. Res.* **89**, 219–29.

Hansson, C., Hoborn, J., Möller, A. and Swanbeck, G. (1995). The microbial flora in venous leg ulcers without clinical signs of infection. Repeated culture using a validated standardised microbiological technique. *Acta Derm. Venereol.* **75**, 24–30.

Heck, D. E., Shakarjian, M., Kim, H. D., Laskin, J. D. and Vetrano, A. M. (2010). Mechanisms of oxidant generation by catalase. *Ann. N. Y. Acad. Sci.* **1203**, 120–5.

Hopf, H. W. and Rollins, M. D. (2007). Wounds: an overview of the role of oxygen. *Antioxid. Redox Signal.* **9**, 1183–92.

Howell-Jones, R. S., Wilson, M. J., Hill, K. E., Howard, a J., Price, P. E. and Thomas, D. W. (2005). A review of the microbiology, antibiotic usage and resistance in chronic skin wounds. *J. Antimicrob. Chemother.* **55**, 143–9.

Hunt, T. K., Hopf, H. and Hussain, Z. (2000). Physiology of wound healing. *Adv. Skin Wound Care* **13**, 6–11.

James, G. a, Swogger, E., Wolcott, R., Pulcini, E. deLancey, Secor, P., Sestrich, J., Costerton, J. W. and Stewart, P. S. (2007). Biofilms in chronic wounds. *Wound Repair Regen.* **16**, 37–44.

Kaplan, J. B. (2010). Biofilm dispersal: mechanisms, clinical implications, and potential therapeutic uses. *J. Dent. Res.* **89**, 205–18.

Kikuchi, S., Kobune, M., Iyama, S., Sato, T., Murase, K., Kawano, Y., Takada, K., Ono, K., Kaneko, Y., Miyanishi, K., et al. (2012). Improvement of iron-mediated oxidative DNA damage in patients with transfusion-dependent myelodysplastic syndrome by treatment with deferasirox. *Free Radic. Biol. Med.* **53**, 643–8.

Kloos, W. and Schleifer, K. (1975). Isolation and Characterization of Staphylococci from Human Skin. *Int. J. Syst. Bacteriol.* **25**, 62–79.

Kolodkin-Gal, I., Cao, S., Chai, L., Böttcher, T., Kolter, R., Clardy, J. and Losick, R. (2012). A self-produced trigger for biofilm disassembly that targets exopolysaccharide. *Cell* **149**, 684–92.

Kuhlicke, J., Frick, J. S., Morote-Garcia, J. C., Rosenberger, P. and Eltzschig, H. K. (2007). Hypoxia inducible factor (HIF)-1 coordinates induction of Toll-like receptors TLR2 and TLR6 during hypoxia. *PLoS One* **2**, e1364.

Kundu, T. K., Velayutham, M. and Zweier, J. L. (2012). Aldehyde Oxidase Functions as a Superoxide Generating NADH Oxidase: An Important Redox Regulated Pathway of Cellular Oxygen. *Biochemistry* **51**, 2930–2939.

Lazarus, G. S., Cooper, D. M., Knighton, D. R., Margolis, D. J., Percoraro, R. E., Rodeheaver, G. and Robson, M. C. (1994). Definitions and guidelines for assessment of wounds and evaluation of healing. *Wound Repair Regen.* 165–170.

Liu, X., Sun, X., Wu, Y., Xie, C., Zhang, W., Wang, D., Chen, X., Qu, D., Gan, J., Chen, H., et al. (2013). Oxidation-sensing regulator AbfR regulates oxidative stress responses, bacterial aggregation, and biofilm formation in Staphylococcus epidermidis. *J. Biol. Chem.* **288**, 3739–52.

Lotito, S., Blonder, P., Francois, A. I. and Rdmy, C. (1989). Correlation between intracellular pH and lactate levels in the rat brain during potassium cyanide induced metabolism blockade : a combined 31p-1H in vivo nuclear magnetic spectroscopy study. **97**, 91–96.

Luo, J. and Chen, A. F. (2005). Nitric oxide: a newly discovered function on wound healing. *Acta Pharmacol. Sin.* **26**, 259–64.

Madsen, S. M., Westh, H., Danielsen, L. and Rosdahl, V. T. (1996). Bacterial colonization and healing of venous leg ulcers. *APMIS* **104**, 895–9.

Martin, J. M., Zenilman, J. M. and Lazarus, G. S. (2010). Molecular microbiology: new dimensions for cutaneous biology and wound healing. *J. Invest. Dermatol.* **130**, 38–48.

McCarty, S. M., Cochrane, C. a, Clegg, P. D. and Percival, S. L. (2012). The role of endogenous and exogenous enzymes in chronic wounds: a focus on the implications of aberrant levels of both host and bacterial proteases in wound healing. *Wound Repair Regen.* **20**, 125–36.

Messonnier, L., Kristensen, M., Juel, C. and Denis, C. (2007). Importance of pH regulation and lactate/H+ transport capacity for work production during supramaximal exercise in humans. *J. Appl. Physiol.* **102**, 1936–44.

Miyazaki, H., Matsuoka, H., Cooke, J. P., Usui, M., Ueda, S., Okuda, S. and Imaizumi, T. (1999). Endogenous Nitric Oxide Synthase Inhibitor : A Novel Marker of Atherosclerosis. *Circulation* **99**, 1141–1146.

Moor, A. N., Tummel, E., Prather, J. L., Jung, M., Lopez, J. J., Connors, S. and Gould, L. J. (2014). Consequences of age on ischemic wound healing in rats: altered antioxidant activity and delayed wound closure. *Age (Dordr).* **36**, 733–48.

Moseley, R., Hilton, J. R., Waddington, R. J. and Harding, K. G. (2004). Original Research Articles – Basic Science Comparison of oxidative stress biomarker profiles between acute and chronic wound environments. *Wound Repair Regen.* **12**, 419–429.

O'Toole, G. a and Kolter, R. (1998). Initiation of biofilm formation in Pseudomonas fluorescens WCS365 proceeds via multiple, convergent signalling pathways: a genetic analysis. *Mol. Microbiol.* **28**, 449–61.

Parsek, M. R. and Singh, P. K. (2003). Bacterial biofilms: an emerging link to disease pathogenesis. *Annu. Rev. Microbiol.* **57**, 677–701.

Percival, S. L., Hill, K. E., Malic, S., Thomas, D. W. and Williams, D. W. (2010). Antimicrobial tolerance and the significance of persister cells in recalcitrant chronic wound biofilms. *Wound Repair Regen.* **19**, 1–9.

Petreaca, M. L., Yao, M., Ware, C. and Martins-Green, M. M. (2008). Vascular endothelial growth factor promotes macrophage apoptosis through stimulation of tumor necrosis factor superfamily member 14 (TNFSF14/LIGHT). *Wound Repair Regen.* **16**, 602–14.

Petreaca, M. L., Do, D., Dhall, S., McLelland, D., Serafino, A., Lyubovitsky, J., Schiller, N. and Martins-Green, M. M. (2012). Deletion of a tumor necrosis superfamily gene in mice leads to impaired healing that mimics chronic wounds in humans. *Wound Repair Regen.* **20**, 353–66.

Qu, Y., Daley, A. J., Istivan, T. S., Garland, S. M. and Deighton, M. a (2010). Antibiotic susceptibility of coagulase-negative staphylococci isolated from very low birth weight babies: comprehensive comparisons of bacteria at different stages of biofilm formation. *Ann. Clin. Microbiol. Antimicrob.* **9**, 16.

Rizk, M., Witte, M. B. and Barbul, A. (2004). Nitric oxide and wound healing. *World J. Surg.* **28**, 301–6.

Roy, S., Khanna, S., Nallu, K., Hunt, T. K. and Sen, C. K. (2006). Dermal wound healing is subject to redox control. *Mol. Ther.* **13**, 211–20.

Sapico, F. L., Witte, J. L., Canawati, H. N., Montgomerie, J. Z. and Bessman, A. N. The infected foot of the diabetic patient: quantitative microbiology and analysis of clinical features. *Rev. Infect. Dis.* **6 Suppl 1**, S171–6.

Scales, B. S. and Huffnagle, G. B. (2013). The microbiome in wound repair and tissue fibrosis. *J. Pathol.* **229**, 323–31.

Schäfer, M. and Werner, S. (2008). Oxidative stress in normal and impaired wound repair. *Pharmacol. Res.* **58**, 165–71.

Schneider, L. A., Korber, A., Grabbe, S. and Dissemond, J. (2007). Influence of pH on wound-healing: a new perspective for wound-therapy? *Arch. Dermatol. Res.* **298**, 413–20.

Schreiber, F., Beutler, M., Enning, D., Lamprecht-Grandio, M., Zafra, O., González-Pastor, J. E. and de Beer, D. (2011). The role of nitric-oxide-synthase-derived nitric oxide in multicellular traits of Bacillus subtilis 3610: biofilm formation, swarming, and dispersal. *BMC Microbiol.* **11**, 111.

Schreml, S., Szeimies, R. M., Prantl, L., Karrer, S., Landthaler, M. and Babilas, P. (2010). Oxygen in acute and chronic wound healing. *Br. J. Dermatol.* **163**, 257–68.

Sen, C. K. and Roy, S. (2008). Redox signals in wound healing. *Biochim. Biophys. Acta* **1780**, 1348–61.

Sen, C. K., Gordillo, G. M., Roy, S., Kirsner, R., Lambert, L., Hunt, T. K., Gottrup, F., Gurtner, G. C. and Longaker, M. T. (2009). Human skin wounds: a major and snowballing threat to public health and the economy. *Wound Repair Regen.* **17**, 763–71.

Sharp, C. S., Bessman, A. N., Wagner, F. W. and Garland, D. Microbiology of deep tissue in diabetic gangrene. *Diabetes Care* **1**, 289–92.

Shaw, S. and Jayatilleke, E. (1992). The Role of Cellular Oxidases and Catalytic iron in the pathogenesis of Ethanol-Induced Liver Injury. *Life Sci.* **50**, 2045–2052.

Shorrock, S. M., Kun, S., Peura, R. A. and Dum, R. M. (2000). Determination of a Relationship between Bacteria Levels and Tissue pH in Wounds : Animal Studies. *IEEE* 117–118.

Siddiqui, A. R. and Bernstein, J. M. (2010). Chronic wound infection: facts and controversies. *Clin. Dermatol.* **28**, 519–26.

Sindrilaru, A., Peters, T., Wieschalka, S., Baican, C., Baican, A., Peter, H., Hainzl, A., Schatz, S., Qi, Y., Schlecht, A., et al. (2011). An unrestrained proinflammatory M1 macrophage population induced by iron impairs wound healing in humans and mice. **121**, 985–997.

Song, L., Wei, X., Zhang, B., Luo, X., Liu, J., Feng, Y. and Xiao, X. (2009). Role of Foxa1 in regulation of bcl2 expression during oxidative-stress-induced apoptosis in A549 type II pneumocytes. *Cell Stress Chaperones* **14**, 417–25.

Stapley, R., Owusu, B. Y., Brandon, A., Cusick, M., Rodriguez, C., Marques, M. B., Kerby, J. D., Barnum, S. R., Weinberg, J. A., Lancaster, J. R., et al. (2012). Erythrocyte storage increases rates of NO and nitrite scavenging: implications for transfusion-related toxicity. *Biochem. J.* **446**, 499–508.

Stefaniak, A. B., Plessis, J. Du, John, S. M., Eloff, F., Agner, T., Chou, T.-C., Nixon, R., Steiner, M. F. C., Kudla, I. and Linn Holness, D. (2013). International guidelines for the in vivo assessment of skin properties in non-clinical settings: part 1. pH. *Skin Res. Technol.* **19**, 59–68.

Stepanovic, S., Vukovic, D., Dakic, I., Savic, B. and Svabic-Vlahovic, M. (2000). A modified microtiter-plate test for quantification of staphylococcal biofilm formation. *J. Microbiol. Methods* **40**, 175–9.

Stevens, D., Lieberman, M., McNitt, T. and Price, J. (1984). Demonstration of uronic acid capsular material in the cerebrospinal fluid of a patient with meningitis caused by mucoid Pseudomonas aeruginosa. *J. Clin. Microbiol.* **19**, 942–943.

Sullivan, J. C. and Pollock, J. S. (2006). Coupled and uncoupled NOS: separate but equal? Uncoupled NOS in endothelial cells is a critical pathway for intracellular signaling. *Circ. Res.* **98**, 717–9.

Warburg, O. (1956). On the Origin of Cancer Cells. *Science (80-.).* **123**, 309–314.

Wink, D. a, Hines, H. B., Cheng, R. Y. S., Switzer, C. H., Flores-Santana, W., Vitek, M. P., Ridnour, L. a and Colton, C. a (2011). Nitric oxide and redox mechanisms in the immune response. *J. Leukoc. Biol.* **89**, 873–91.

Wlaschek, M. and Scharffetter-Kochanek, K. (2005). Oxidative stress in chronic venous leg ulcers. *Wound Repair Regen.* **13**, 452–61.

Wong, V. W. and Gurtner, G. C. (2012). Tissue engineering for the management of chronic wounds: current concepts and future perspectives. *Exp. Dermatol.* **21**, 729–34.

Yang, Q., Phillips, P. L., Sampson, E. M., Progulske-Fox, A., Jin, S., Antonelli, P. and Schultz, G. S. (2013). Development of a novel ex vivo porcine skin explant model for the assessment of mature bacterial biofilms. *Wound Repair Regen.* **21**, 704–14.

Yeoh-Ellerton, S. and Stacey, M. C. (2003). Iron and 8-isoprostane levels in acute and chronic wounds. *J. Invest. Dermatol.* **121**, 918–25.

Youmans, G. P., Paterson, P. Y. and Sommers, H. M. (1980). The Biologic and clinical basis of infectious diseases. *J. Am. Med. Assoc.* **244**, 849.

Zhao, G., Usui, M. L., Underwood, R. A., Singh, P. K., James, G. A., Stewart, P. S., Fleckman, P. and Olerud, J. E. (2012). Time course study of delayed wound healing in a biofilm-challenged diabetic mouse model. *Wound Repair Regen.* **20**, 342–52.

FIGURE CAPTIONS

Figure 2.1. Schematic illustration of oxidative and nitrosative stress cycle. Superoxide dismutase (SOD) dismutates superoxide anions ($O_2^{\cdot -}$) to generate H_2O_2. The latter can be detoxified by catalase to H_2O+O_2 and by glutathione peroxidase (GPx) to H_2O. H_2O_2 can also enter the Fenton reaction in the presence of ferrous ions to give rise to $^{\cdot}OH+OH-$. We also depict the $O_2^{\cdot -}$ interaction with nitric oxide (NO) produced by nitric oxide synthetase (NOS) to give rise to peroxinitrite anion ($ONOO^-$). The arrows directed towards Fig.2.1 depict the parameters involved in oxidative stress. The arrows toward Figs. 2.2 and 2.3 include the parameters of nitrosative stress and the detrimental effects of reactive species respectively (supplementary references 1,2).

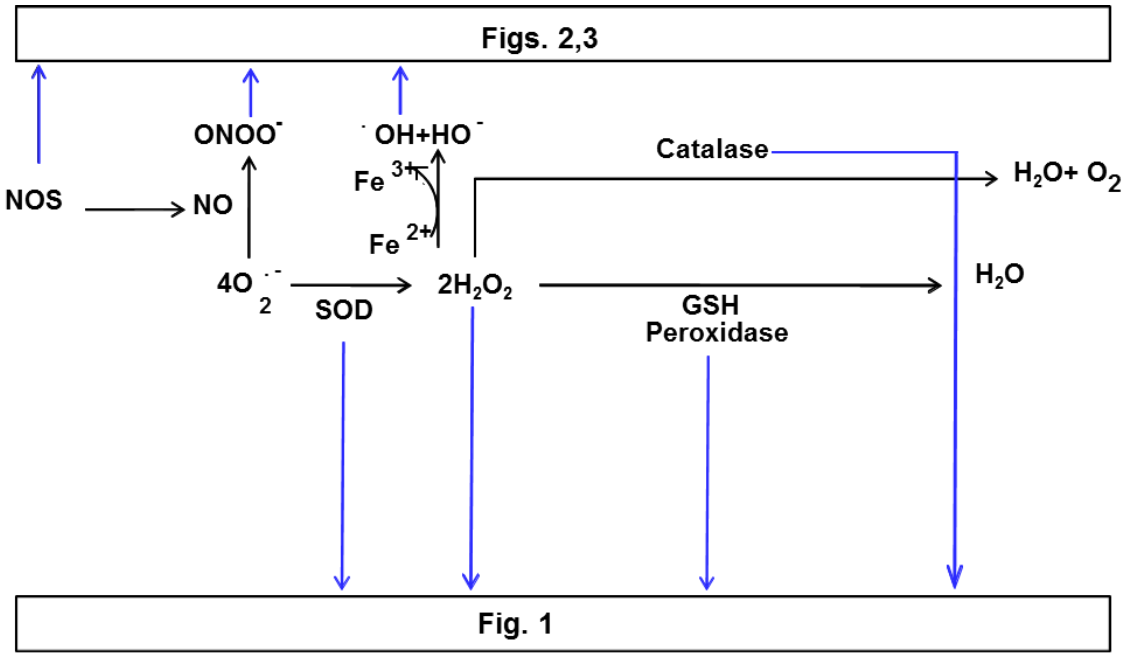
Figs. 2,3
ONOO-
·OH+HO-
Catalase
NOS
NO
Fe 3+
H2O+ O2
Fe 2+
4O ·- 2
SOD
2H2O2
H2O
GSH
Peroxidase
Fig. 1

Figure 2.1

Figure 2.2. Oxidative stress is elevated in LIGHT$^{-/-}$ wounds. (A) SOD activity was measured using a tetrazolium salt that converts into a formazan dye detectable at 450nm. SOD activity remains significantly elevated in LIGHT$^{-/-}$ mice in the first 48hrs post-wounding. *n=6.* **(B)** Resofurin formation, detected at 590nm, was used to determine H_2O_2 levels. Significant increases in H_2O_2 very shortly post-wounding were seen. *n=8.* **(C)** Enzymatic reaction of catalase and methanol in the presence of H_2O_2 gives rise to formaldehyde, spectrophotometrically detected with purpald chromogen, at 540nm. Catalase activity in adult LIGHT$^{-/-}$ and control wounds was similar. *n=6.* **(D)** GPx detoxifying activity was measured indirectly at 340nm by a coupled reaction with glutathione reductase where GPx activity was rate-limiting. The level of GPx activity in the adult LIGHT$^{-/-}$ wounds was essentially identical to that of the controls. *n= 6.* **(E-H)** The findings in old LIGHT$^{-/-}$ mice were exacerbated in all four parameters when compared to adult LIGHT$^{-/-}$ mice. *n=6. Time zero represents unwounded skin. All data are Mean ± SD. *p<0.05,**p<0.01,***p<0.001.*

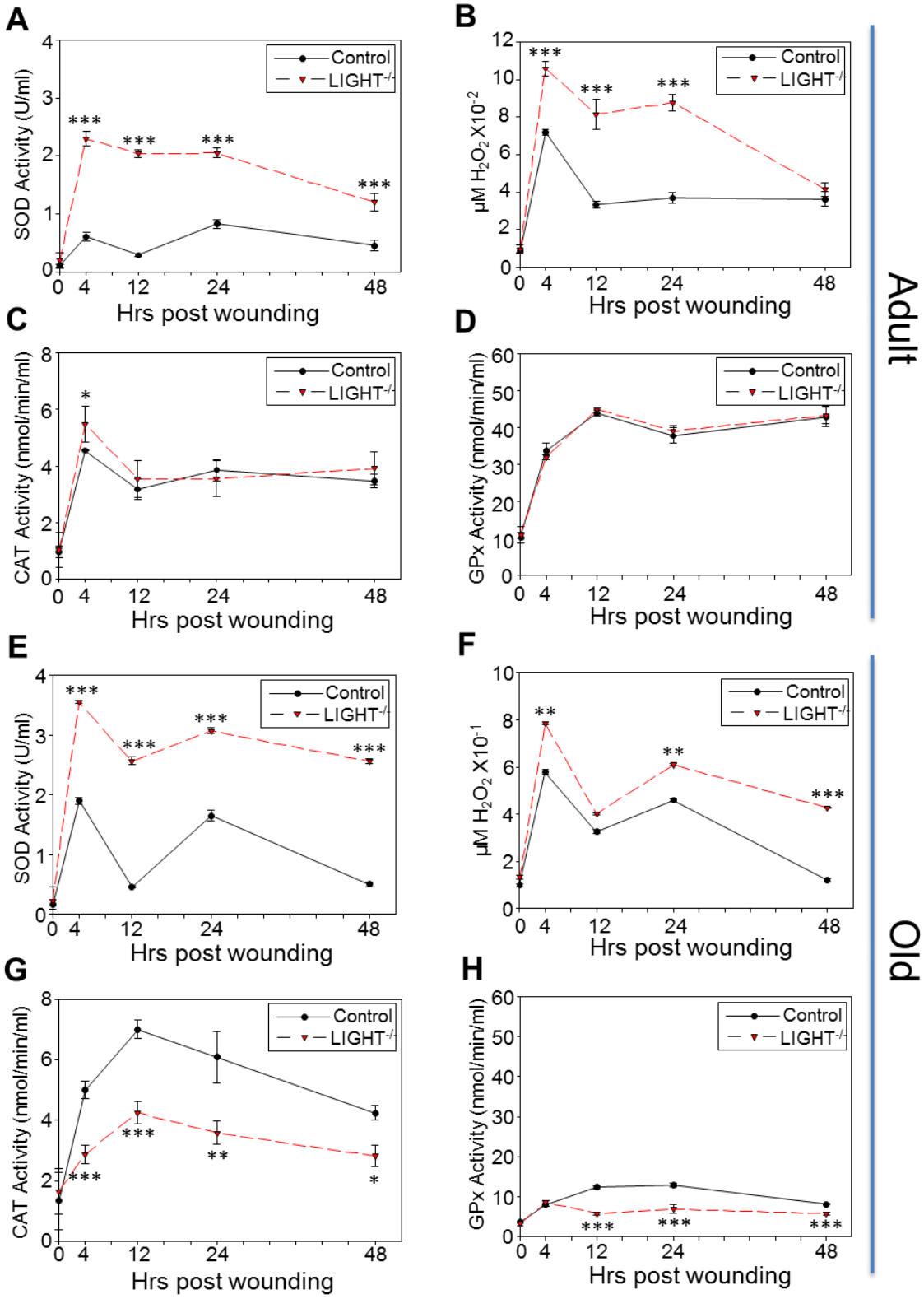
A
SOD Activity (U/ml)
Control
LIGHT-/-
Hrs post wounding
B
µM H2O2 X10-2
C
CAT Activity (nmol/min/ml)
D
GPx Activity (nmol/min/ml)
E
F
µM H2O2 X10-1
G
H
Adult
Old

Figure 2.2

Figure 2.3. Microscopic, biochemical and chemical markers show imbalanced redox in LIGHT$^{-/-}$ mice. **(A)** *In vivo* imaging of ROS was carried out using the ImageEM 1K EM-CCD camera with an optical system consisting of a 50mm f/1.2 lens. Signals were obtained around the periphery of the wound as early as 4hrs post-wounding in the LIGHT$^{-/-}$ mice and significantly higher signals captured in LIGHT$^{-/-}$ mice peaked at 24hrs post-wounding. **(B)** Lactate measurements: An oxidized intermediate was formed when extracted lactate reacted with a probe to give fluorescence detectable at 605nm. There was significant increase in levels of lactate accumulation in LIGHT$^{-/-}$ mice at 24-48hrs post wounding. *n=6.* **(C)** pH levels were measured using a beetrode microelectrode and micro-reference electrode. The LIGHT$^{-/-}$ wounds were systematically more acidic than controls. *n=25.* **(D,E)** Methanolic-extracted nitrite (**D**) and nitrate **(E)** were analyzed. Both were greatly increased in LIGHT$^{-/-}$ mice during early response to wounding. *n= 8.* **(F-G)** Phospho-eNOS levels and iNOS expression in LIGHT$^{-/-}$ wounds were examined by western blotting (representative experiment shown). Analysis by densitometry (normalized to C57BL/6 mouse wound). *Time zero represents unwounded skin except in Figure 2.2C. All data are Mean ± SD. *p<0.05,**p<0.01,***p<0.001.*

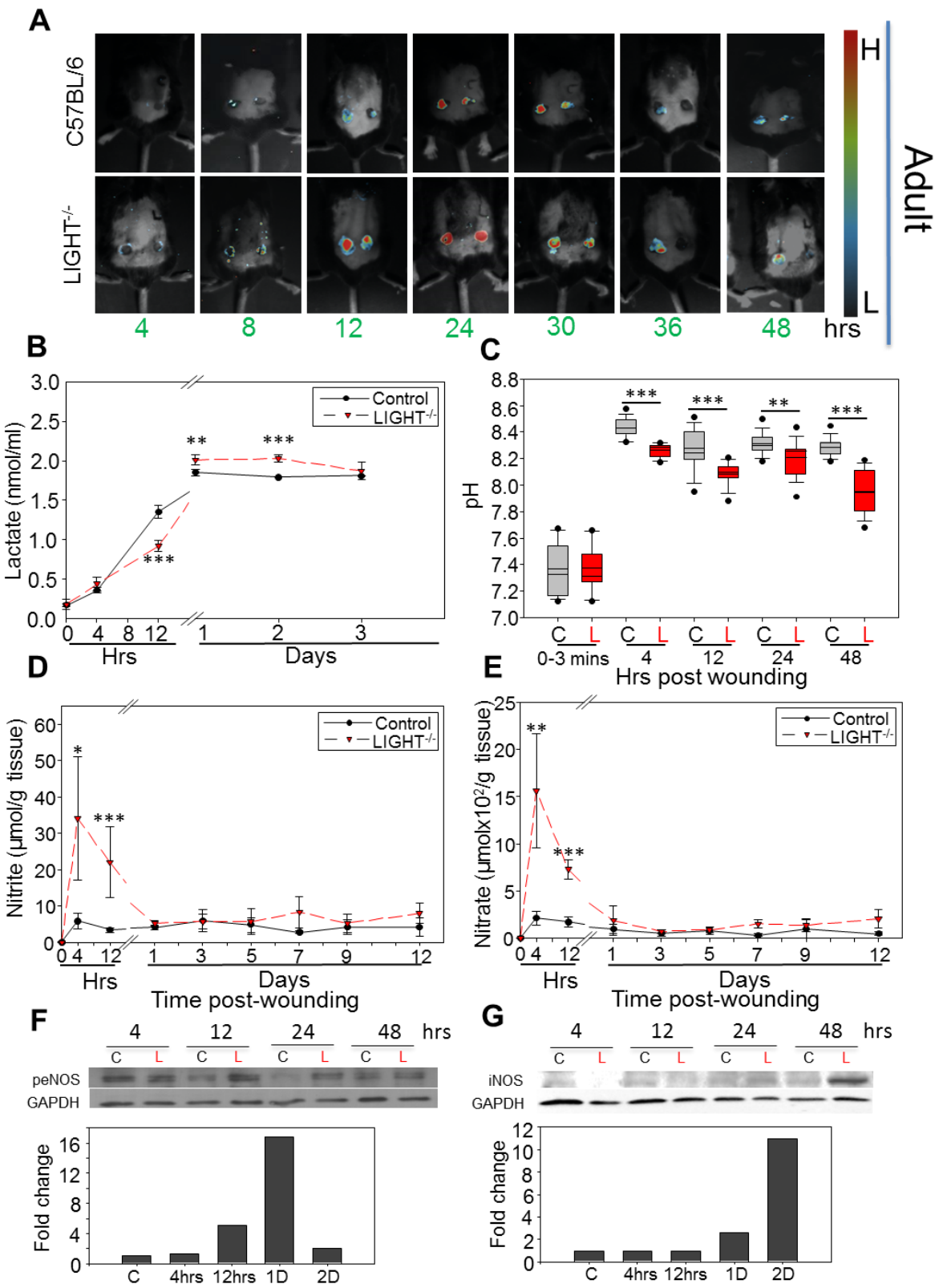
A
C57BL/6
LIGHT-/-
H
L
Adult
4
8
12
24
30
36
48
hrs
B
Lactate (nmol/ml)
Control
LIGHT-/-
Hrs
Days
C
pH
0-3 mins
Hrs post wounding
D
Nitrite (µmol/g tissue)
Time post-wounding
E
Nitrate (µmolx10²/g tissue)
F
peNOS
GAPDH
Fold change
C
4hrs
12hrs
1D
2D
G
iNOS
GAPDH

Figure 2.2

Figure 2.4. Lactate levels, pH, and nitrosative stress are exacerbated in old LIGHT$^{-/-}$ mice. (A) Lactate levels were measured in old LIGHT$^{-/-}$ mice during the first 48hrs of healing. Extraction of lactate was done using lactate buffer provided by the manufacturer. Oxidized intermediates reacted with a probe to give fluorescence detectable at an emission of 605nm. Data are mean ± SD, *n= 6*. (**B**) pH levels were measured using a microelectrode. A micro reference electrode was used at the same time as the pH electrode made contact with the wound tissue. Data are mean ± SD, *n= 25.* **(C,D)** Nitrite and nitrate levels were measured in old LIGHT$^{-/-}$ mice throughout the course of healing. Nitrite free methanol was used for extraction. Data shown here are representative of several independent experiments. Data are mean ± SD, *n= 8. * p <0.05, ** p <0.01, *** p<0.001*.

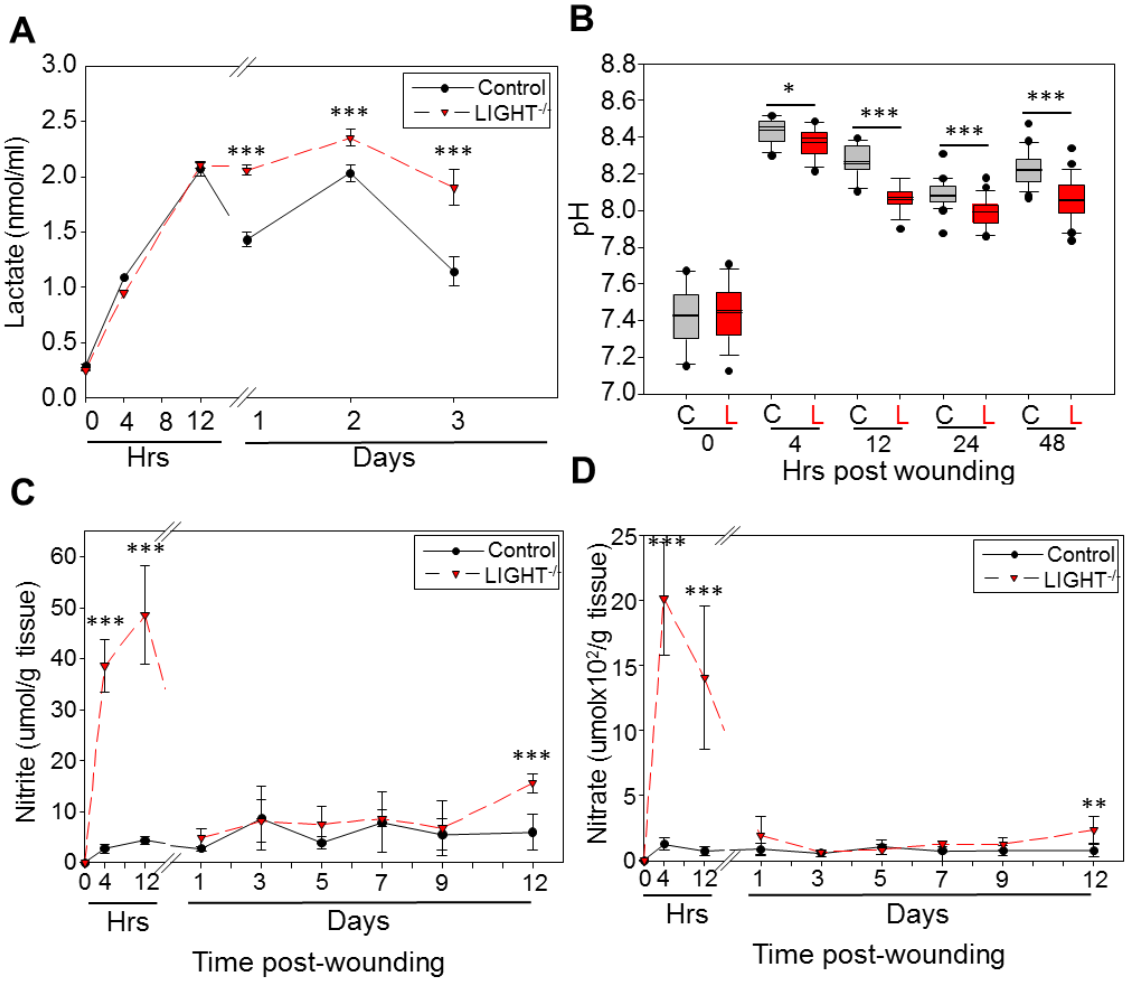
A
Lactate (nmol/ml)
Control
LIGHT-/-
***
Hrs
Days
B
pH
*
C L
0
4
12
24
48
Hrs post wounding
C
Nitrite (umol/g tissue)
Time post-wounding
D
Nitrate (umolx10²/g tissue)
**

Figure 2.4

Figure 2.5. Early oxidative and nitrosative stress in LIGHT$^{-/-}$ wounds have damaging effects on proteins, lipids and DNA and increased cell death. (A) Protein modification measurements were based on a competitive enzyme immunoassay; nitrotyrosine levels in the LIGHT$^{-/-}$ mice were significantly different from control throughout healing. **(B)** Lipid peroxidation levels were measured fluorometrically at an Ex/Em of 540nm/590 nm using thiobarbituric acid reactive substances (TBARS); the MDA levels were significantly elevated throughout the course of wound healing in LIGHT$^{-/-}$ mice. *n= 6.* **(C, D)** F_2 isoprostanes, were measured using the approach described in the M&M section; levels of 8- and 5-isoprostanes detected in LIGHT$^{-/-}$ mice were much higher than those in the control mice at early times. This correlates with the MDA levels that are the stable byproducts of lipid peroxidation. *n= 5.* **(E)** Levels of 8-OH-dG, were based on a competitive enzyme immunoassay; the samples were read spectrophotometrically at 412nm using Ellman's reagent. 8-OH-dG levels were found to be significantly elevated during the course of healing in LIGHT$^{-/-}$ mice. *n=4.* **(F)** Cell death by apoptosis and necrosis was determined by staining with Annexin V-FITC and propidium iodide, respectively, followed by FACS analysis. Cell death was increased significantly in the LIGHT$^{-/-}$ mice. The greatest difference occurred with necrosis, which showed to be much higher in LIGHT$^{-/-}$ mice. *Time zero represents unwounded skin. All data are Mean ± SD. *p<0.05,**p<0.01,***p<0.001.*

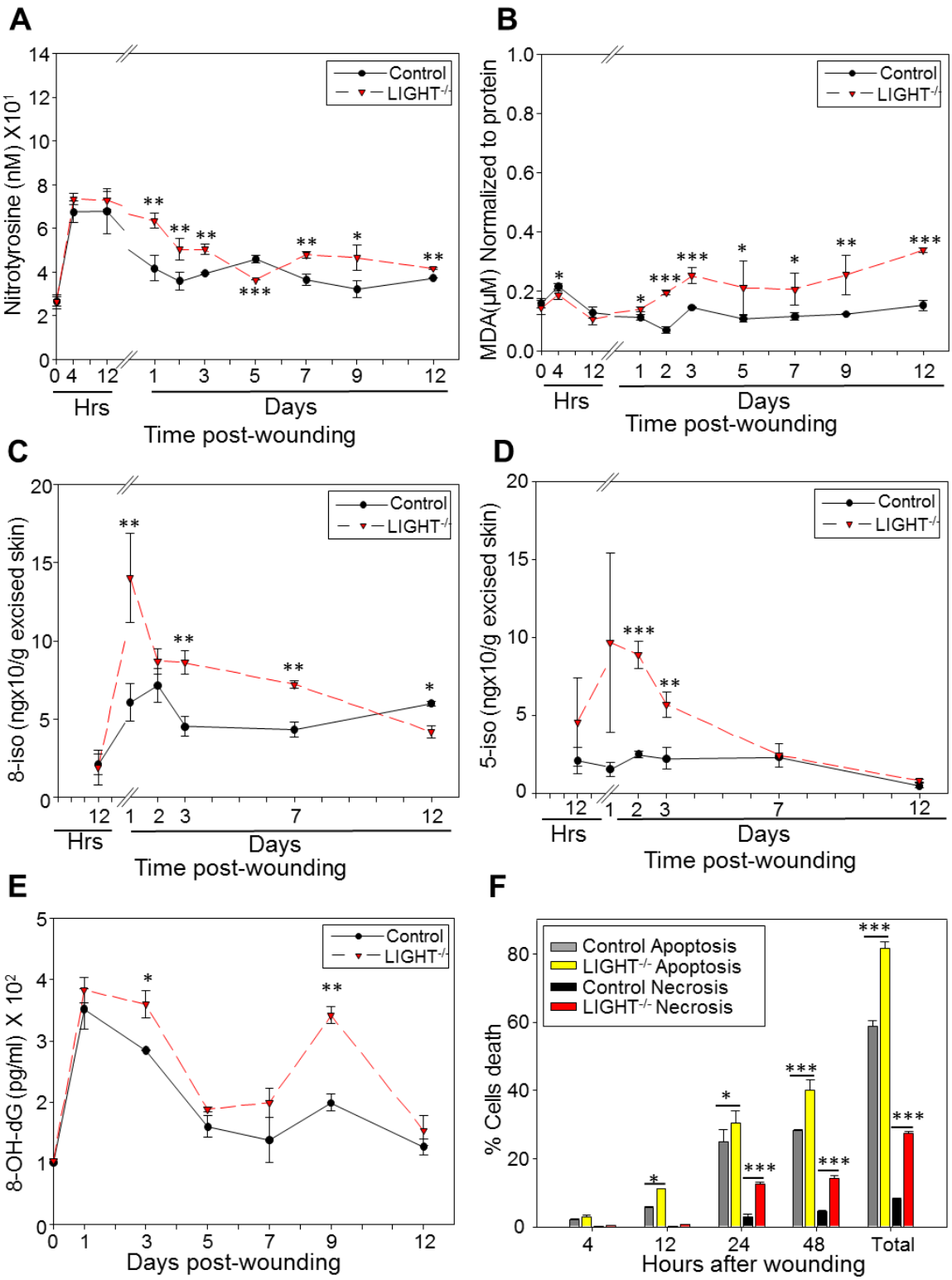
A
Nitrotyrosine (nM) X10¹
Control
LIGHT-/-
Hrs
Days
Time post-wounding
B
MDA(μM) Normalized to protein
Control
LIGHT-/-
Hrs
Days
Time post-wounding
C
8-iso (ngx10/g excised skin)
Control
LIGHT-/-
Hrs
Days
Time post-wounding
D
5-iso (ngx10/g excised skin)
Control
LIGHT-/-
Hrs
Days
Time post-wounding
E
8-OH-dG (pg/ml) X 10²
Control
LIGHT-/-
Days post-wounding
F
% Cells death
Control Apoptosis
LIGHT-/- Apoptosis
Control Necrosis
LIGHT-/- Necrosis
4
12
24
48
Total
Hours after wounding

Figure 2.5

Figure 2.6. Detrimental effects of exacerbated stress on protein modification, lipid peroxidation, and DNA damage in old mice. (A) Nitrotyrosine levels were measured in old LIGHT-/- mice and in age matched controls using an anti-nitrotyrosine antibody and an HRP conjugated secondary antibody. Data are mean ± SD, *n=6*. **(B)** Lipid peroxidation levels were measured using thiobarbituric acid reactive substances (TBARS). The absorbance was measured spectrophotometrically at 412nm. Data are mean ± SD. *n= 6* **(C)** DNA damage was measured at various time points post-wounding by determining the levels of 8-OH-dG. Isolated DNA from the wound tissue was digested to release 8-OH-dG and measurements were based on competitive enzyme immunoassay between 8-OH-dG and an 8-OH-dG-acetylcholinesterase conjugate with a limited amount of 8-OH-dG monoclonal antibody. Data are mean ±SD. *n=4.* *p<0.05,**p<0.01,***p<0.001.

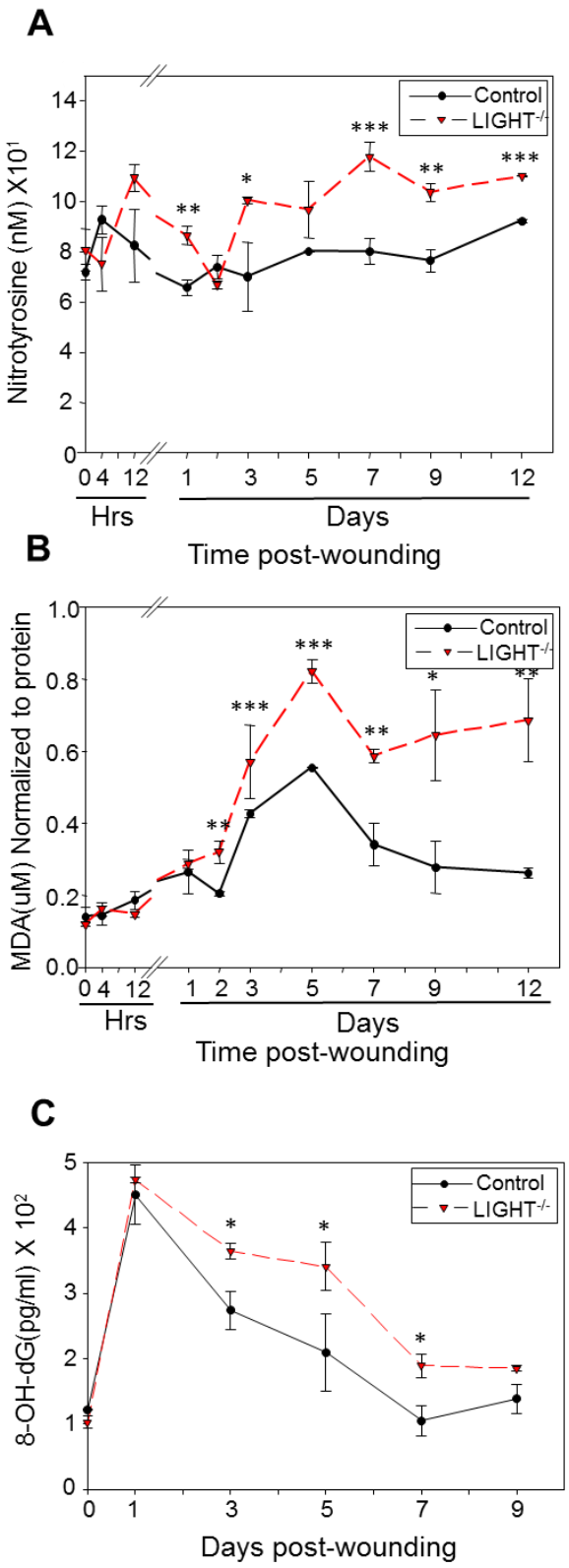
A
Nitrotyrosine (nM) X10¹
Control
LIGHT-/-
0 4 12 1 3 5 7 9 12
Hrs
Days
Time post-wounding
B
MDA(uM) Normalized to protein
Control
LIGHT-/-
0 4 12 1 2 3 5 7 9 12
Hrs
Days
Time post-wounding
C
8-OH-dG(pg/ml) X 10²
Control
LIGHT-/-
0 1 3 5 7 9
Days post-wounding

Figure 2.6

Figure 2.7. Manipulating redox parameters leads to development of chronic wounds. (A) C57BL/6 and LIGHT$^{-/-}$ mice were wounded and immediately treated with inhibitors for GPx and catalase followed by the application of biofilm-forming bacteria 24hrs later. The wounds were covered with sterile tegaderm to maintain a moist wound environment and prevent external infection. The LIGHT$^{-/-}$ wounds became chronic and remained open for more than 30 days. *n=30*. **(B)** Wound areas were traced using ImageJ and % open wound area was calculated. The LIGHT$^{-/-}$ wounds remained open for significantly longer time than the C57BL/6 wounds with similar treatment. *n=8.* **(C-F)** SOD activity (C); H_2O_2 levels (D); Catalase activity (E); and GPx Activity (F) were measured as described in Fig. 2.1. All were greatly different from controls. For all tests *n=6* at minimum. *Time zero in C-F represents unwounded skin. All data are Mean ± SD. *p<0.05,**p<0.01,***p<0.001.*

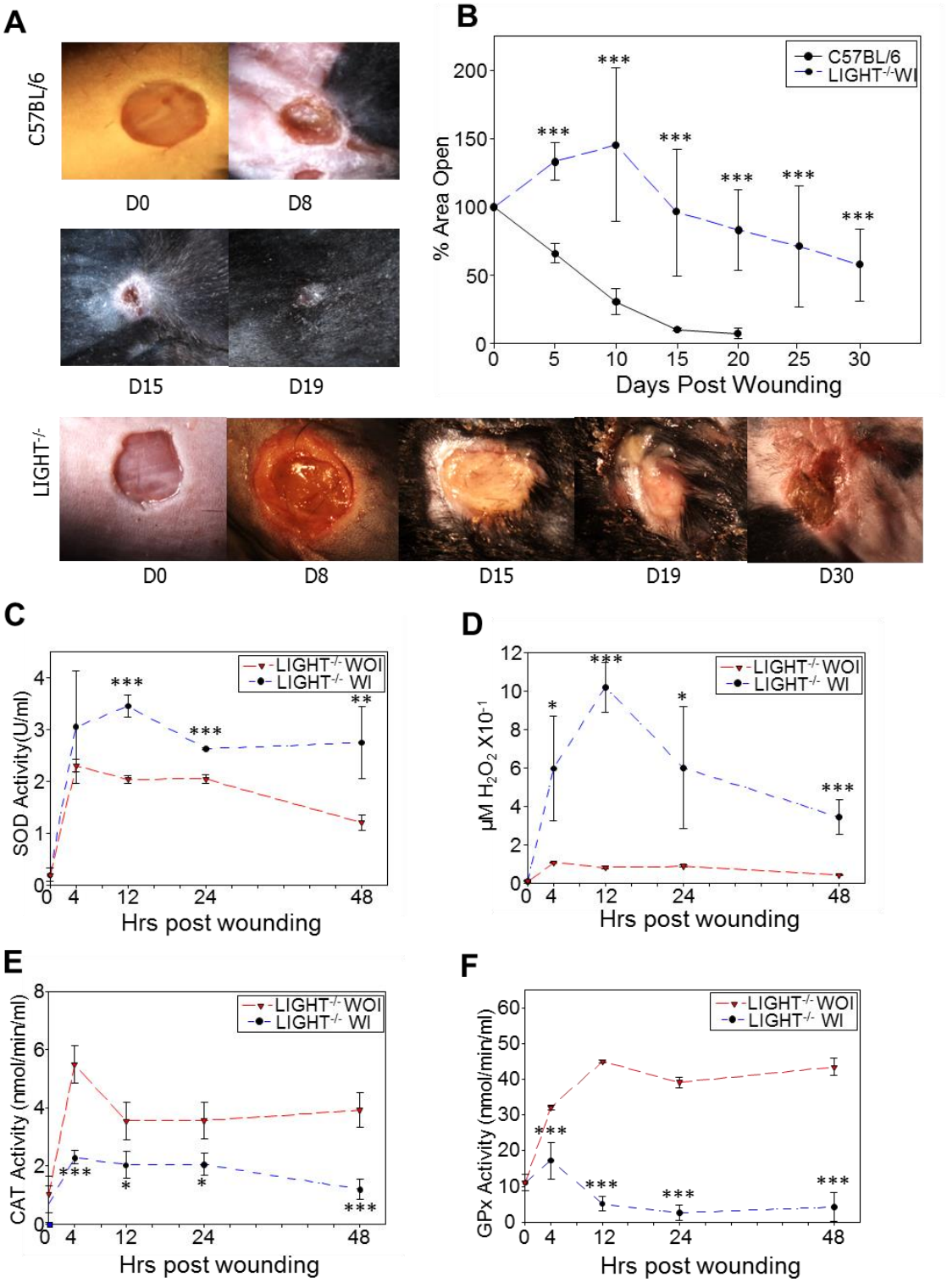
A
C57BL/6
D0
D8
D15
D19
LIGHT-/-
D0
D8
D15
D19
D30
B
C57BL/6
LIGHT-/-WI
% Area Open
Days Post Wounding
C
LIGHT-/- WOI
LIGHT-/- WI
SOD Activity(U/ml)
Hrs post wounding
D
LIGHT-/- WOI
LIGHT-/- WI
µM H2O2 X10-1
Hrs post wounding
E
LIGHT-/- WOI
LIGHT-/- WI
CAT Activity (nmol/min/ml)
Hrs post wounding
F
LIGHT-/- WOI
LIGHT-/- WI
GPx Activity (nmol/min/ml)
Hrs post wounding

Figure 2.7

Figure 2.8. Histological evaluation of chronic wounds. (**A**) Representative picture of H&E-stained sections of a LIGHT$^{-/-}$ chronic wounds from an animal treated with catalase and GPx inhibitors and the application of bacteria. The epithelium does not cover the wound tissue and the granulation tissue is poorly formed. Scale bar 500μm. **(B)** Higher magnification of the boxed area in (A). Epithelial tongue is outlined with a dotted line (**compare with Fig 2.S4A**). Scale bar 100μm. **(C)** Immunolabeling for Collagen IV delineates the presence of basement membrane; dotted line marks where basement membrane is missing in the migrating tongue. **(D)** propidium iodide staining identifies cell nuclei. **(E)** Merger of (C) & (D). **(F)** Immunolabeling for F4/80, a marker for macrophages, to illustrate the presence of inflammation; **(G)** propidium iodide staining identifies cell nuclei. **(H)** Merger of (F) & (G). Inserts are high magnifications of a single macrophage. **(I)** Representative Masson-trichrome (blue color) stained section illustrating loss of collagen bundles; scale bar 100μm. **(J,K)** SHIM analysis of a similar section (J) confirms results in (I) and, for comparison, collagen in the granulation tissue of a normal wound similarly analyzed by SHIM (K) showing filamentous collagen (red arrow); scale bar 10μm.

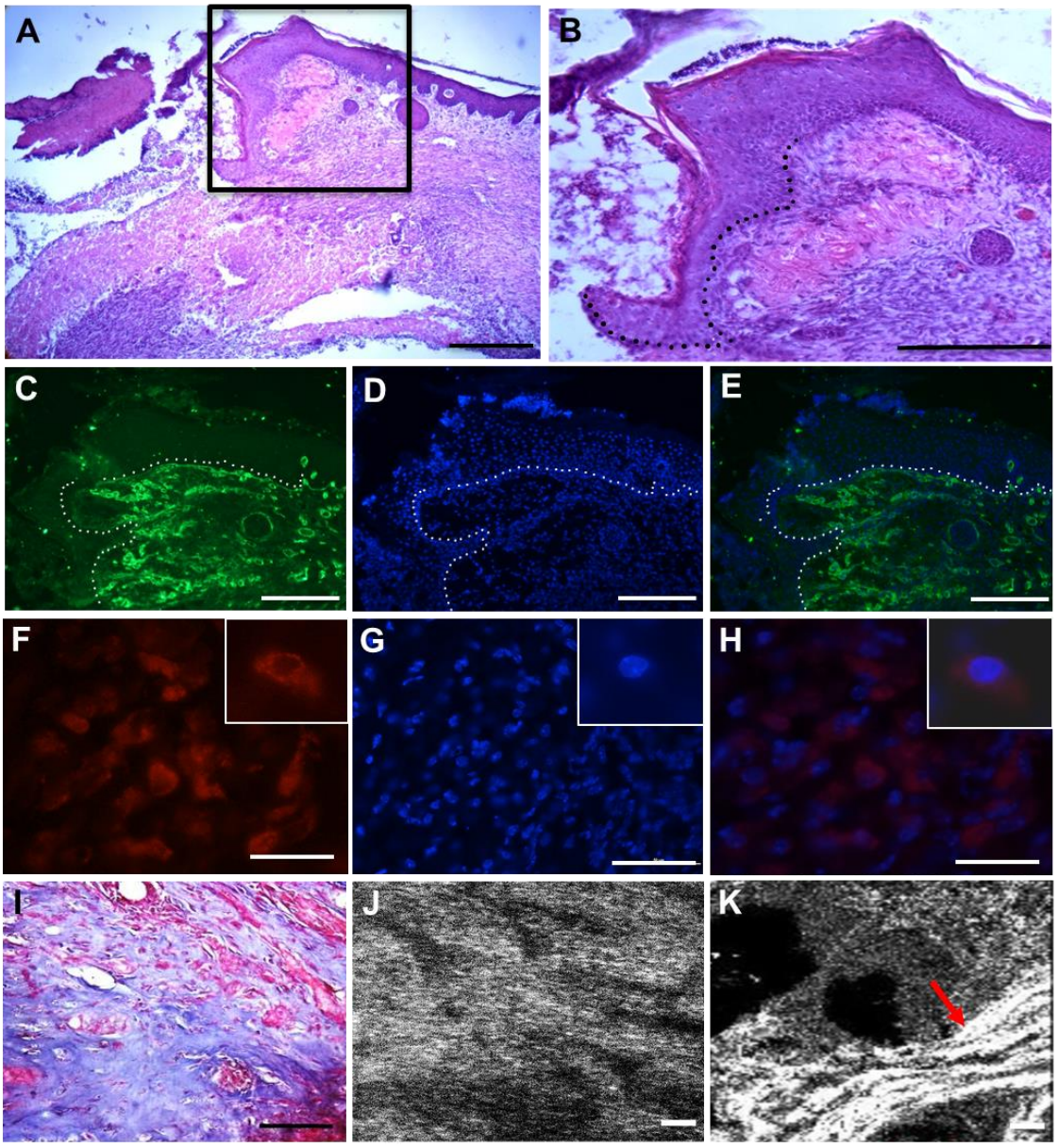

Figure 2.8

Figure 2.9. Histology of normal wound healing. (A) Migration tongue (delineated by dots) during normal wound healing. The epidermal cells form a well-defined straight migrating tongue that eventually meets the counterpart on the other side to close the wound. **(B)** Normal granulation tissue and epidermis after closure of the wound during normal healing. **(C)** Enlargement of the area depicted in the rectangle in B to show that the epidermis is well-adherent to the granulation tissue and the latter is well developed. Scale bars 50μm for (A) and (C) and 500μm for (B). Image in (A) modified from Fig. 1C of Liu et al., *BMC Cell Biology* 2009, **10**:1-15.

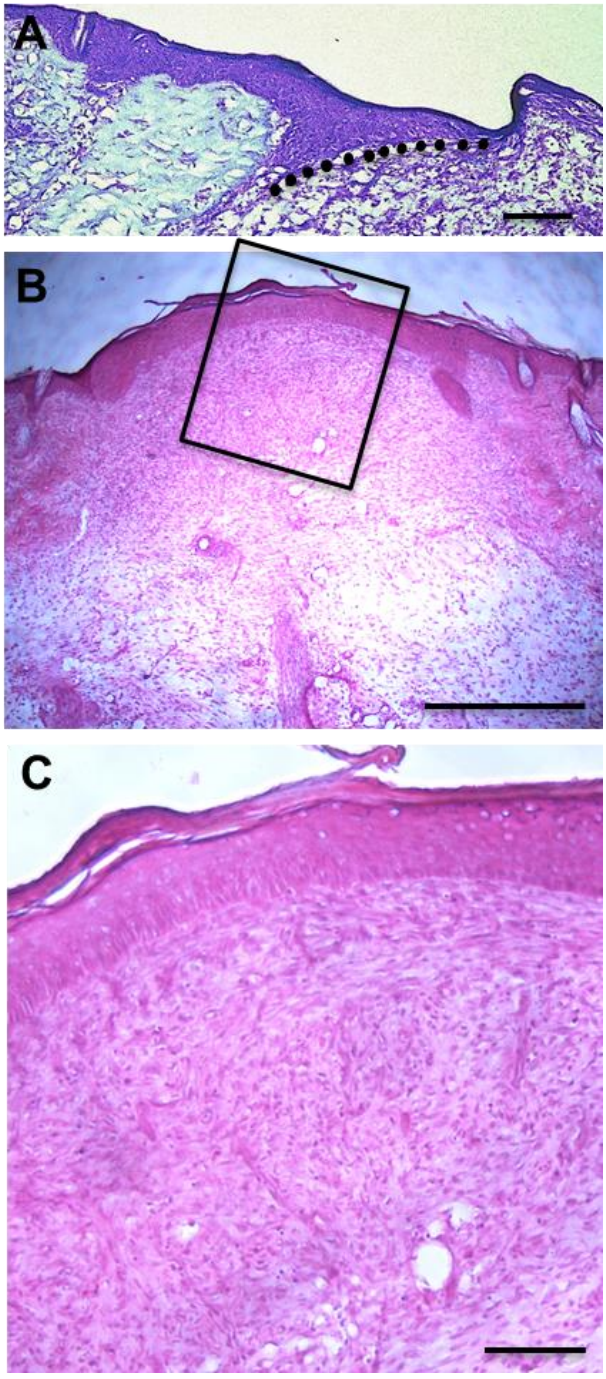

Figure 2.9

Figure 2.10. Manipulation of LIGHT$^{-/-}$ wounds with bacteria or individual antioxidant inhibitors does not lead to chronic wound development. (A) C57BL/6 and LIGHT$^{-/-}$ mice were topically treated with S. *epidermidis* C2 . Data are mean ± SD, *n= 4*. **(B)** C57BL/6 and LIGHT$^{-/-}$ mice were injected with 3-Amino-1,2,4-triazole (catalase inhibitor), 20 min prior to wounding and topical application of S. *epidermidis* C2 was done 1 day post wounding. Data are mean ± SD, *n= 4*. **(C)** C57BL/6 and LIGHT$^{-/-}$ mice were topically treated with mercaptosuccinic acid (GPx inhibitor) and topical application of S. *epidermidis* C2 was done 1 day post wounding. Data are mean ± SD, *n= 4*. * $p<0.05$,** $p<0.01$,***$p<0.001$.

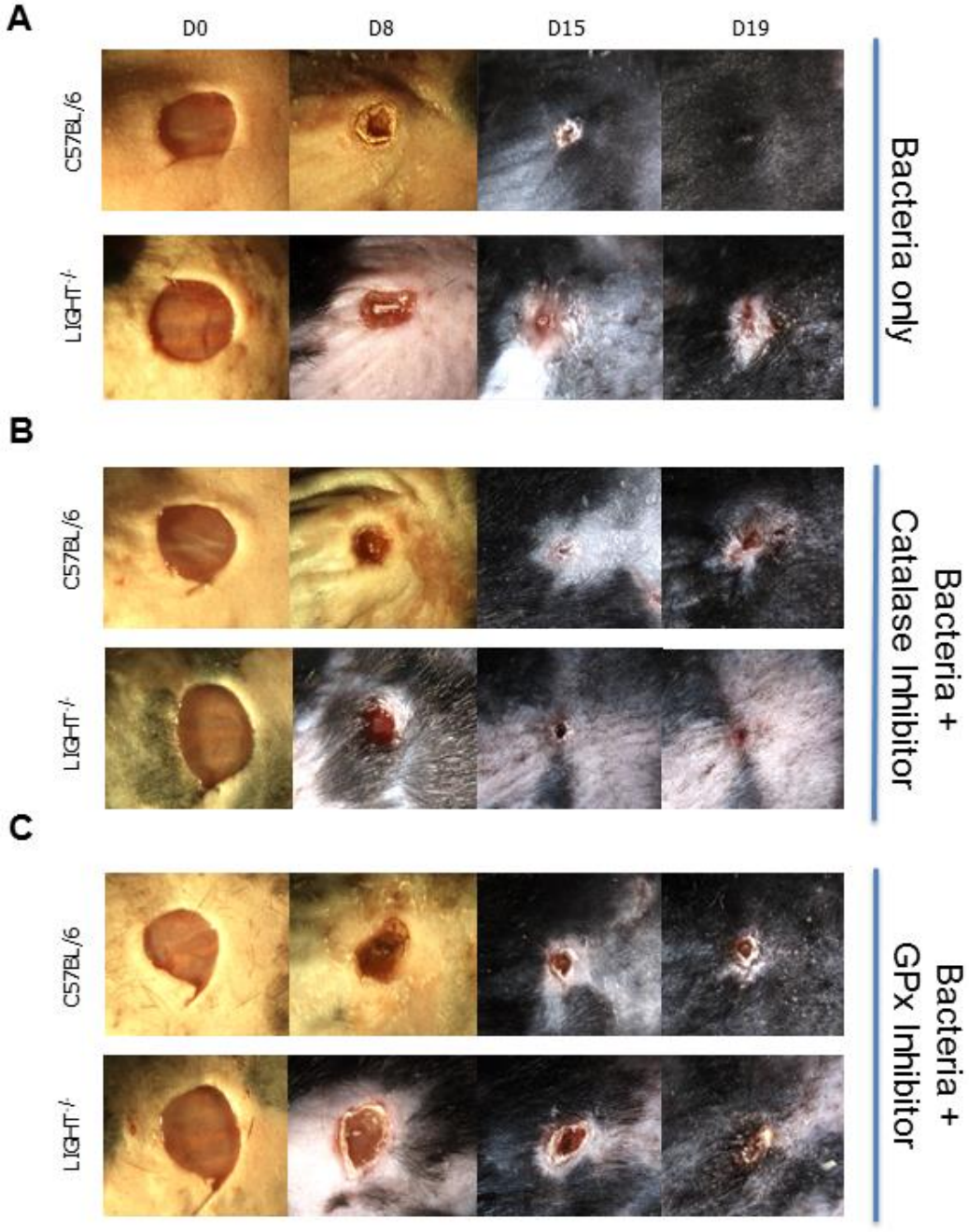
A
D0
D8
D15
D19
C57BL/6
LIGHT-/-
Bacteria only
B
C57BL/6
LIGHT-/-
Bacteria +
Catalase Inhibitor
C
C57BL/6
LIGHT-/-
Bacteria +
GPx Inhibitor

Figure 2.10

Figure 2.11. Identification and characterization of the microflora that colonizes the LIGHT$^{-/-}$ chronic wounds. (A) Biofilm production was quantified by measuring the optical densities of stained bacterial films adherent to plastic tissue culture plates. Biofilm forming capacity of *S. epidermidis* was seen throughout the time course of chronic wounds. *n= 7*. **(B)** Bacterial identification was carried out by growing bacteria on tryptic soy agar. Gram-negative rods were characterized using the API®20E identification kit. *n= 7*. **(C)** Biofilm quantification of exudate obtained from wounds was performed at OD570nm. The dynamics of the polymicrobial community in the wounds does not seem to affect the overall degree of biofilm production during the later stages of healing. Controls used were biofilm-negative (OD570nm < 0.125) *S. hominis* SP2 and biofilm-positive *S. epidermidis* C2. *n= 8*. **(D)** Antibiotic challenge on wound exudates collected from LIGHT$^{-/-}$ mice was done using Amoxicillin. The CMIC of amoxicillin on the bacteria found in the chronic LIGHT$^{-/-}$ wound exudate at day 22/24 was 50μg/ml, much higher than exudate collected at day 5 when biofilm is not yet abundant. **(E)** Bacterial burden was evaluated by colony forming unit counts. The CFU/mL was relatively low during the early phases of healing and was highest during the impaired and chronic stages of healing. *n= 7*. **(F)** Normal skin swabs were collected from LIGHT and C57BL/6 mice to evaluate resident organisms. The microbiota of the skin was similar in both C57BL/6 and LIGHT$^{-/-}$ mice.

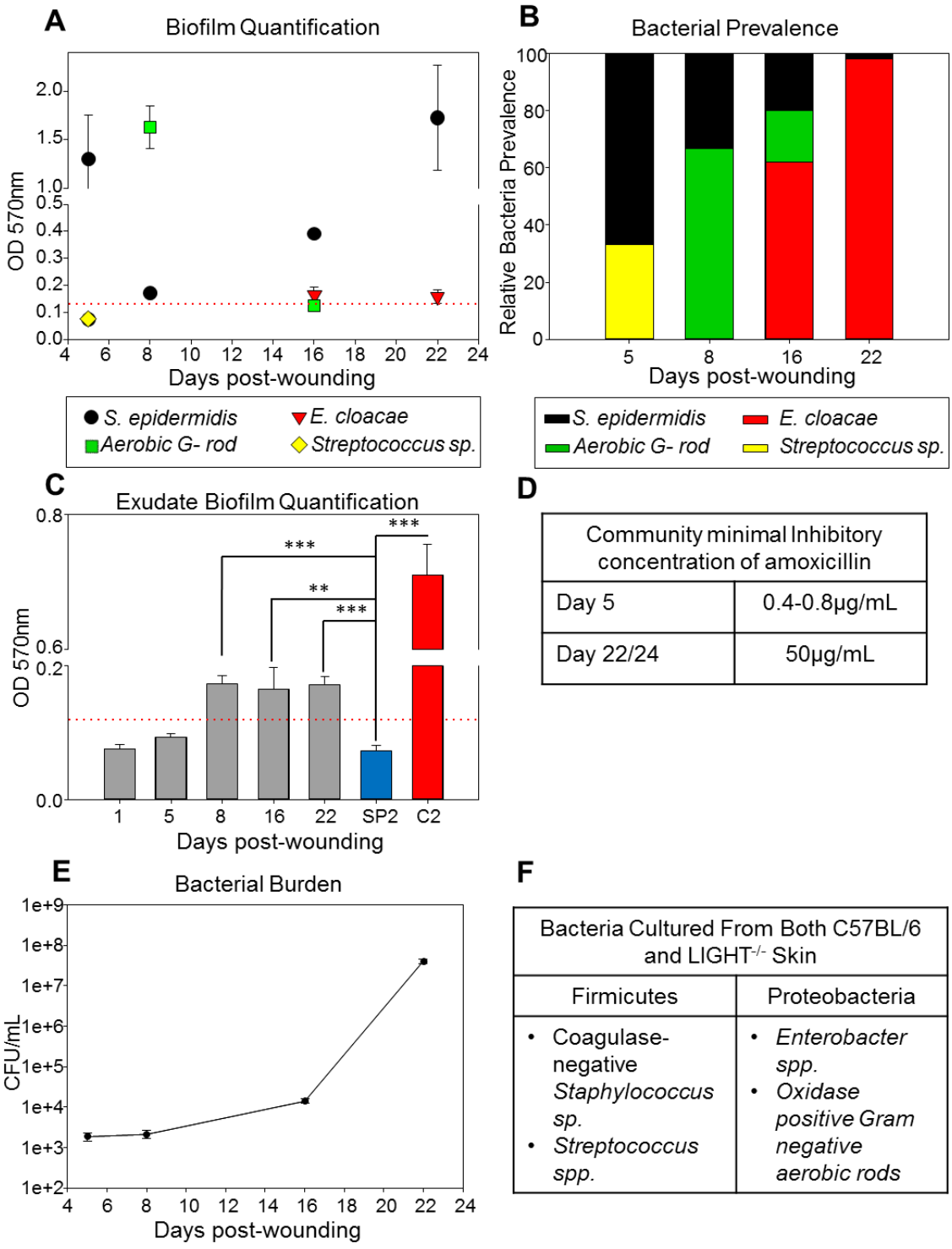

Community minimal Inhibitory concentration of amoxicillin	
Day 5	0.4-0.8µg/mL
Day 22/24	50µg/mL

Bacteria Cultured From Both C57BL/6 and LIGHT$^{-/-}$ Skin	
Firmicutes	Proteobacteria
• Coagulase-negative *Staphylococcus sp.* • *Streptococcus spp.*	• *Enterobacter spp.* • *Oxidase positive Gram negative aerobic rods*

Figure 2.11

Figure 2.12. Identification and characterization of the bioflora that colonized the old LIGHT$^{/-}$ chronic wounds. (A) Biofilm production/quantification of stained bacterial films adherent to plastic tissue culture plates was measured at OD570nm. Data are mean ± SD, *n= 4*. **(B)** Bacterial identification was done by growing them on tryptic soy agar and using an identification kit. Data are mean ± SD, *n= 4*. **(C)** Biofilm quantification of the exudates obtained from the wounds were performed at OD570nm. Biofilm quantification controls used were biofilm-negative (OD570nm < 0.125) *S. hominis* SP2 and biofilm-positive *S. epidermidis* C2. Data are mean ± SD, *n= 4.* **(D)** Bacterial burden was evaluated based on viable colony count and differentiation. Data are mean ± SD, *n= 4.* * $p<0.05$,** $p<0.01$,***$p<0.001$.

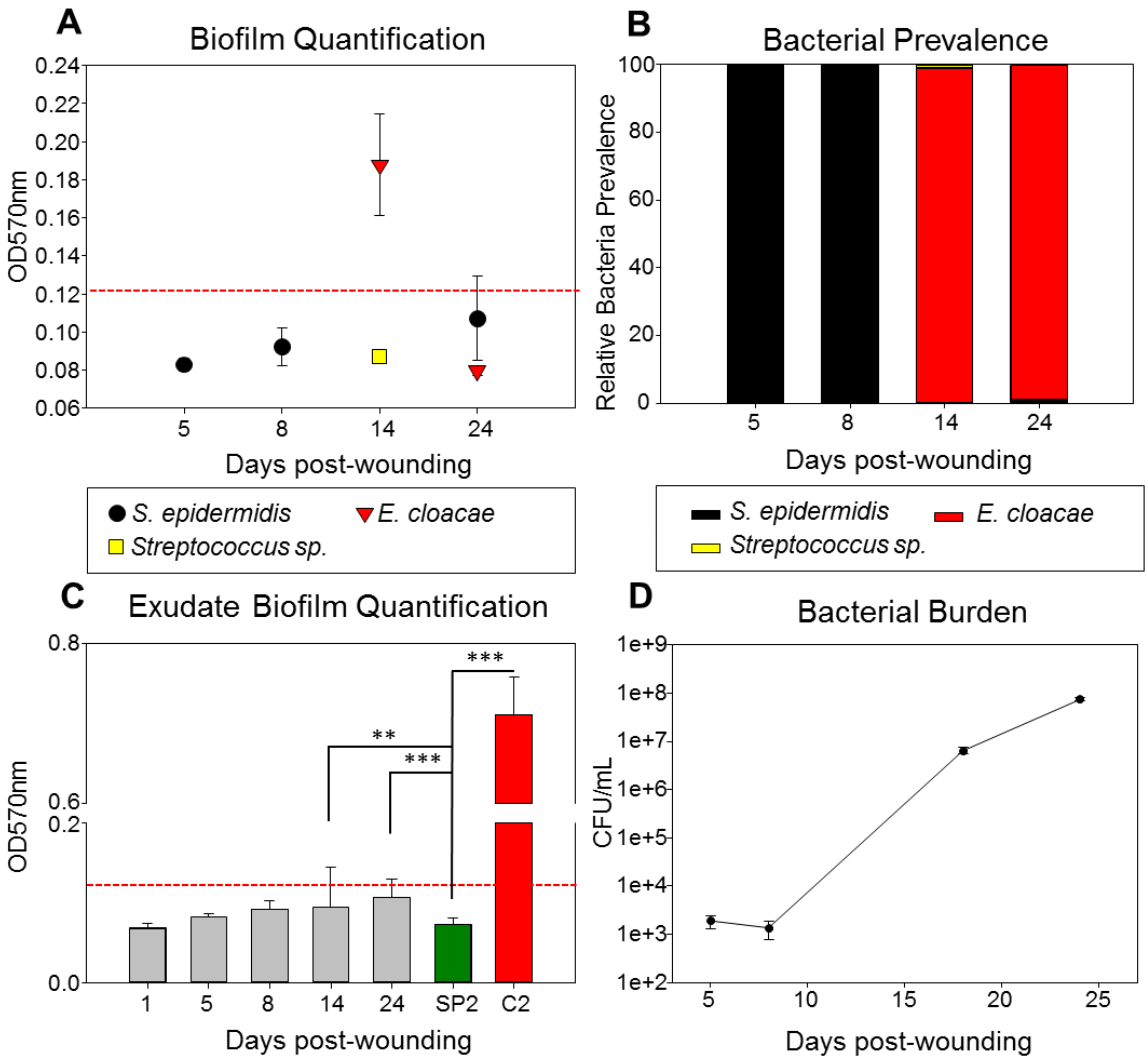
A
Biofilm Quantification
OD570nm
0.24
0.22
0.20
0.18
0.16
0.14
0.12
0.10
0.08
0.06
5
8
14
24
Days post-wounding
S. epidermidis
E. cloacae
Streptococcus sp.
B
Bacterial Prevalence
Relative Bacteria Prevalence
100
80
60
40
20
0
5
8
14
24
Days post-wounding
S. epidermidis
E. cloacae
Streptococcus sp.
C
Exudate Biofilm Quantification
OD570nm
0.8
0.6
0.2
0.0
**
***
***
1
5
8
14
24
SP2
C2
Days post-wounding
D
Bacterial Burden
CFU/mL
1e+9
1e+8
1e+7
1e+6
1e+5
1e+4
1e+3
1e+2
5
10
15
20
25
Days post-wounding

Figure 2.12

Figure 2.13. Morphological characterization of biofilm present in LIGHT$^{-/-}$ wounds. Scanning electron microscopy (SEM) images of the Au/Pd sputtered, fixed and dried, chronic wound samples were captured using an FEI XL30 FEG SEM. (**A**) Image shows the presence of bacterial rods (b) in the wound bed. (**B**) High magnification image of bacteria embedded in a biofilm-associated matrix (m) in a well-defined niche (n). (**C**) Matrix beneath the biofilm showing the presence of matrix (m) and of cocci bacteria (b). A Lymphocyte (L/arrow) was highlighted for size references. Scale bars 5μm (A,C) and 1μm (B).

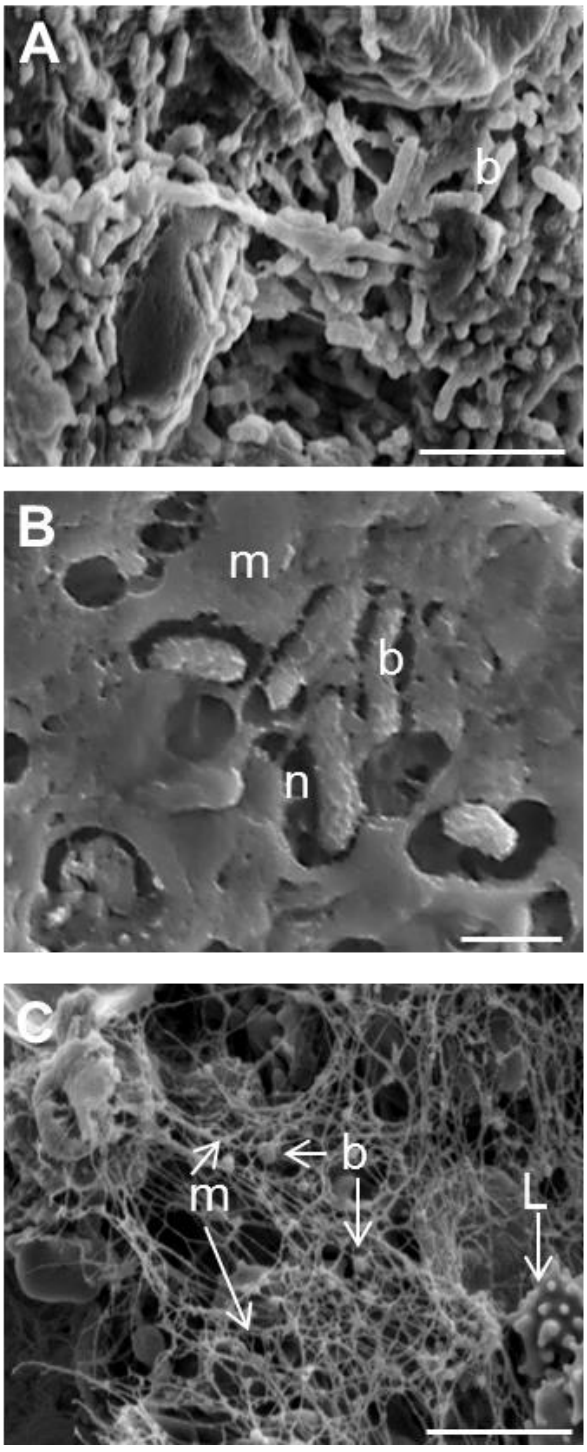

Figure 2.13

CHAPTER 3

ARACHIDONICACID-DERIVED SIGNALING LIPIDS AND FUNCTIONS IN IMPAIRED WOUND HEALING

ABSTRACT

Very little is known about lipid function during wound healing, and much less during impaired healing. Such understanding will help identify what roles lipid signaling plays in the development of impaired/chronic wounds. We took a lipidomics approach to study the alterations in lipid profile in our recently developed LIGHT$^{-/-}$ mouse model of impaired healing which has characteristics that resemble those of impaired/chronic wounds in humans, including high levels of oxidative stress, excess inflammation, increased extracellular matrix degradation and blood vessels with fibrin cuffs. The latter suggests excess coagulation and potentially increased platelet aggregation. We show here that in these impaired wounds there is an imbalance in the arachidonic acid (AA) derived eicosonoids that mediate or modulate inflammatory reactions and platelet aggregation. In the LIGHT$^{-/-}$ impaired wounds there is a significant increase in 8- and 5- isoprostanes, two signaling lipids derived from a non-enzymatic breakdown of AA. Of the enzymatically-derived breakdown products of AA, we found that early after injury there was a significant increase in the pro-inflammatory eicosanoids 11 and 15- HETE isomers, the leukotriene metabolites, LTD_4 and LTE_4 and the prostaglandins, PGE_2 and $PGF_{2\alpha}$. Some of these eicosanoids are not only pro-inflammatory but they are also pro-aggregatory. This led us to examine the levels of other eicosanoids known to be involved in this process. We found that the thromboxane (TXA_2/B_2), and the prostacyclin $6kPGF_{1\alpha}$ are elevated shortly after wounding and in some cases during healing. To determine whether they have an impact on platelet aggregation and hemostasis we tested LIGHT$^{-/-}$ mice wounds for these two parameters and found that, indeed, platelet

aggregation and hemostasis are enhanced in these mice when compared with the control mice. Understanding lipid signaling in impaired wounds can potentially lead to development of new therapeutics or in using existing non-steroidal anti-inflammatory agents to help correct the course of healing.

INTRODUCTION

Acute wounds that do not follow a concerted and overlapping set of repair processes, become impaired and may enter a state of chronicity (Lazarus et al., 1994). Deciphering the etiology of impaired and chronic wounds has remained one of the biggest challenges in addressing healing outcomes of problematic wounds. Hallmarks of impaired and chronic wounds include increased oxidative stress, deregulated levels of growth factors, imbalance in cytokines and chemokines, sustained inflammation, leaky blood vessels, and uncontrolled function of proteases (Mustoe et al., 2006a). Although therapies have been developed to correct the course of impaired healing and have been successful in varying degrees in animal models of impaired healing, their results in human clinical trials have been limited due to the multifactorial imbalance in the wound microenvironment (Demidova-Rice et al., 2012).

Lipids are an integral part of skin structure and functionality, and have been shown to mediate various roles in pathogenesis of several diseases including psoriasis, atopic dermatitis, and disorders arising from exposure to ultraviolet radiation (UVR) (Nicolaou, 2013). The study of lipid regulation and function in acute wound healing has only recently been described (Wijesinghe and Chalfant, 2013). Lipidomics is a branch of metabolomics dedicated to the systematic identification and quantification of an extensive assortment of lipids in cells, organs and extracellular fluids to correlate them to disease states (Wenk, 2005; Wijesinghe and Chalfant, 2013). The use of liquid chromatography mass spectrometry (LC-MS/MS) allows us to measure various lipids quantitatively at the same time. Not only does lipidomics hold promise to further our

knowledge of the underlying mechanisms to chronic wound development and progression, it also opens new avenues of risk assessment and evaluation of targeted therapeutics in a personalized and timely manner (Meikle et al., 2014).

Arachidonic acid (AA), precursor for a large number of signaling lipids, is a polyunsaturated fatty acid, generally found esterified to the sn-2 position of phospholipids in cell membranes. While there are several routes for liberation of AA, the primary mode of AA release involves its hydrolysis from the sn-2 position by phospholipase A2 (Balsinde et al., 2002). The release of AA initiates a cascade of events resulting in the generation of numerous lipid mediators (collectively termed eicosanoids) that trigger inflammation, increase vascular permeability and trigger platelet activation (Kuehl and Egan, 1980; Mruwat et al., 2013). These mediators are primarily be generated enzymatic pathways, although non-enzymatically generated eicosanoids are also quite common. The non-enzymatic pathway involves free radicals generated when there is excess oxidative stress that causes the production of isoprostanes (Montuschi et al., 2004; Ting and Khasawneh, 2010). Enzymatic metabolism of AA can occur either via the cytochrome P450's (Cyp450s), lipoxygenase and/or the cyclooxygenase pathways that give rise to inflammatory mediators (Schwab and Serhan, 2006; Spite et al., 2014). One of the metabolite classes generated by the metabolism of AA via the lipoxygenase pathway is the hydroxyeicosatetranoic acids (HETE's). These are involved in increasing inflammation and play roles in platelet activation. Another product of the action of lipoxygenase on AA is the leukotrienes, which are involved in inflammation and vascular permeability. Finally, cyclooxygenases act on AA to give prostanoids such as the

thromboxanes, prostacyclins, and prostaglandins that are crucial for skin physiology and homeostasis (Ricciotti and FitzGerald, 2011).

As described above, we have used the LIGHT$^{-/-}$ mice as a novel model to study impaired wounds (Petreaca et al., 2012). Because we observed excessive inflammation and fibrin "cuffs" in the blood vessels of the these mice, and it is known that many of the signaling lipids derived from AA metabolism can be involved in both processes, we hypothesized that AA metabolites may be major contributors to the underlying mechanism of impaired healing in these mice. We used a lipidomics approach in a single lipid analytical platform, to investigate their levels during the course of impaired healing. Here we show that AA-derived metabolites, both via the enzymatic and non-enzymatic pathways, are significantly elevated during the course of healing, but in particular in the first 48hrs after injury. This is the first study deciphering the elevated levels of lipid metabolites in impaired healing. This information may help in furthering our knowledge on how to develop better therapeutic interventions.

MATERIALS AND METHODS

Dermal excisional wound model: Animals were housed at the University of California, Riverside (UCR) vivarium. All experimental protocols were approved by the UCR Institutional Animal Care and Use Committee (IACUC). Experiments were performed using 4-5 month old mice. The procedure used was performed as previously described (Petreaca et al., 2012). Briefly, dorsal hair was removed using clippers and nair on both control and $LIGHT^{-/-}$. 24hrs later excisional wounds were performed on the dorsum of mice using a 7 mm biopsy punch (Acuderm, Inc, Fort Lauderdale, FL). Wound tissues were collected at various time points following injury using a 10-mm diameter biopsy punch.

Processing of tissues for lipid assay: 1ml of LCMS grade ethanol containing 0.05% BHT and 10ng of each internal standard ((d_4) 8-iso $PGF_{2\alpha,}$ (d_{11}) 5-iso $PGF_{2\alpha}$-VI, (d_4) 6k $PGF_{1\alpha}$, (d_4) $PGF_{2\alpha}$, (d_4) PGE_2, (d_4) PGD_2, (d_4) LTB_4, (d4) TXB_2, (d_4) LTC_4, (d_5) LTD_4, (d_5) LTE_4, (d_8) 5-hydroxyeicosatetranoic acid (5HETE), (d_8) 15-hydroxyeicosatetranoic acid (15HETE), (d_8) 14,15 epoxyeicosatrienoic acid, (d_8) arachidonic Acid, and (*d5*) eicosapentaenoic acid) was added to frozen wound tissues. Samples were mixed using a bath sonicator incubated overnight at -20^0C for lipid extraction. The insoluble fraction was precipitated by centrifuging at 12,000xg for 20min and the supernatant was transferred into a new glass tube.

Liquid chromatography mass spectrometry (LC-MS): For eicosanoid quantitation via UPLC ESI-MS/MS, the lipid extracts were dried under vacuum and reconstituted in

LCMS grade 50:50 EtOH:H_2O (100 µl). A 14min reversed-phase LC method utilizing a Kinetex C18 column (100 x 2.1mm, 1.7µm) and a Shimadzu UPLC was used to separate the eicosanoids at a flow rate of 500µl/min at 50°C. The column was first equilibrated with 100% Solvent A [acetonitrile:water:formic acid (20:80:0.02, v/v/v)] for two minutes and then 10µl of sample was injected. 100% Solvent A was used for the first two minutes of elution. Solvent B [acetonitrile:isopropanol (20:80, v/v)] was increased in a linear gradient to 25% Solvent B to 3min, to 30% by 6 minutes, to 55% by 6.1min, to 70% by 10min, and to 100% by 10.1min. 100% Solvent B was held until 13min, then decreased to 0% by 13.1min and held at 0% until 14min. The eluting eicosanoids were analyzed using a hybrid triple quadrupole linear ion trap mass analyzer (AB SCIEX 6500 QTRAP®,) via multiple-reaction monitoring in negative-ion mode. Eicosanoids were monitored using species specific precursor → product MRM pairs. The mass spectrometer parameters were: curtain gas: 30; CAD: High; ion spray voltage: -3500V; temperature: 300°C; Gas 1: 40; Gas 2: 60; declustering potential, collision energy, and cell exit potential were optimized per transition.

Elastase assay: Elastase activity of the wound samples at various time points after injury was done using a commercially available kit EnzChek Elastase Assay Kit (Life Technologies, Grand Island, NY). A fluorescence-labelled elastin substrate (*DQ elastin* from bovine neck filament; 4,4-difluoro-5,7-dimethyl-4-bora-3a,4a-diaza-*s*-indacene-3-propionic acid), was used as a substrate to be digested by the elastase in the samples to yield fluorescent products determined at Ex/Em of 480nm/530nm. Elastase from pig pancreas was used to create standard curve. Measurements were run in 96-well

microplates (black, flat bottomed, Nunc, Denmark). To 50 µL reaction buffer and 50 µL of DQ elastin substrate (100 µg/mL), 100 µL of the equilibrated sample solution was added and incubated for 2hrs while the fluorescence was measured every 15mins at 22^0 C, using the Victor plate reader.

Tail Bleeding Time: Hemostasis was measured using the tail transection technique, following previously established protocols (Lin et al., 2014; Paez Espinosa et al., 2012). Briefly, 5 months old mice were separated in two groups: $LIGHT^{-/-}$ (n=5) and C57BL/6 (n=5) were anesthetized by an intraperitoneal injection of ketamine (80 mg/kg) and xylazine (16 mg/kg). Mice were placed on a 37^oC heating blanket (Harvard Apparatus Limited, Edenbridge, KY, USA) before the tail was transected using a sterile scalpel to make a clean cut at a distance of 5 mm from the tip. After transection, the tail was immediately immersed in warmed saline (37^oC, constant temperature). The bleeding time was followed visually and determined as the time from the tail transection to the moment the blood flow stopped and did not resume within the next 60 sec. It is expected that less than 300µl of blood is lost even if the bleeding does not stop within 15 min. When bleeding did not stop within 15 min, pressure was applied to the tail to seal the wound, thus avoiding excessive loss of blood. A bleeding time beyond 15 min was considered as the cut-off time for the purpose of statistical analysis.

Platelet Aggregation: These studies were performed as described previously (Lin et al., 2014; Murad et al., 2012). Groups of five to six mice from each group were anesthetized by an intraperitoneal injection of ketamine (80 mg/kg) and xylazine (16 mg/kg) before

their blood was collected from the heart in 3.8% sodium citrate (1 part citrate to 9 parts blood) and pooled. Platelet rich plasma (PRP) was then isolated by differential centrifugation at 170g for 10min and platelet counts were adjusted to $3x10^8$ with Tyrode's buffer prior to each experiment. After establishing a baseline light transmission for 1min, platelets were stimulated with agonists. Aggregation of platelets was monitored using a Lumi-Aggregometer (Havertown, PA) at 37^oC under constant stirring at 1200 rpm. To calculate the % aggregation increase with respect to control mice, we used to following equation:

% increase in aggregation for LIGHT = [(B-A)/A]*100, where A% is the maximum aggregation for C57BL/6 mice and B% is the maximum aggregation for $LIGHT^{-/-}$ mice.

Statistical analysis: We used Graphpad Instat Software and Sigmaplot Software. Analysis of variance (ANOVA) was used to test significance of group differences between two or more groups. In experiments with only two groups, we used a Student's t-test.

RESULTS

To further understand the effects of the redox stress present in the wounds of the LIGHT$^{-/-}$ mouse model of impaired healing (Dhall et al., 2014; Petreaca et al., 2012), we took a lipidomics approach to evaluate the non-enzymatic and enzymatic breakdown of AA (**Fig. 3.1)**. The non-enzymatic breakdown of AA gives rise to isoprostanes whereas the enzymatic breakdown of AA can be accomplished via three major routes. Cyp450s that result in production of HETEs, lipoxygenases that cause increases in leukotrienes, and cyclooxygenases that lead to the generation of prostanoids. Prostanoids consist of three key groups namely thromboxane, prostacyclin, and prostaglandin. We will first describe our findings for pro-inflammatory lipids and then will show the results for those involved in platelet aggregation and hemostasis.

Pro-inflammatory AA-derive signaling lipids

Because the impaired wounds of the LIGHT$^{-/-}$ mice have high levels of oxidative stress, we investigated isoprostanes that are considered to be the golden markers of oxidative stress(Montuschi et al., 2004). We found that both 8-isoprostanes and 5-isoprostanes are greatly elevated shortly after wounding, reaching a peak at 24hrs post wounding and slowly declining to base levels by day 7 (**Fig 3.2A,B**).

The majority of the pro-inflammatory lipids derived from AA metabolism come from enzymatic reactions. We know that the impaired wounds in LIGHT$^{-/-}$ mice contain excess inflammation (Petreaca et al., 2012). Therefore, we looked for increases in pro-inflammatory lipids because it is known that they play an important role in the

chemotaxis of inflammatory cells, in particular neutrophils. These leukocytes produce elastase that is a broad-spectrum serine protease which causes extensive degradation of extracellular matrix and hence can result in poor development of the granulation tissue and lead to impaired healing.

Monooxygenation or epoxidation of AA can occur by cypP450 enzymes resulting in the production of hydroxyeicosatetranoic acids (HETEs). 15-HETE was significantly elevated in the LIGHT$^{-/-}$ mouse wounds throughout the first 7 days post wounding (**Fig. 3.3A**). Moreover, two substantial peaks were detected, at days 1 and 7 post wounding, in the LIGHT$^{-/-}$ mice when compared to the control C57BL/6 mice. We also show that the potent chemoattractant 11-HETE, was already significantly elevated at day 1 post wounding and remained elevated until beyond day 7 (**Fig. 3.3B**). This may explain the prolonged and sustained inflow of inflammatory cells in the wounds of these mice.

AA breakdown by lipoxygenases results in production of leukotrienes (LT) that further get metabolized by cysteinyl (cys) synthase to give rise to cys-LTD4. Inflammatory responses have been shown to be initiated in the presence of cystein leukotrienes (Samuelsson et al., 1987). We show that the level of cys-LTD$_4$ was significantly elevated during days 1 and 2 post wounding in the LIGHT$^{-/-}$ wounds (**Fig. 3.3C**). Further cleaving of cys-LTD$_4$ leads to cys-LTE$_4$ production, which is highly elevated during the first two days of wounding and remains higher than the control wounds until day 7 (**Fig. 3.3D**). The increases in these lipids indicate an early influx of inflammatory cells to the wound site.

Cyclooxygenase 2 (COX-2) gives rise to AA-derived prostaglandins (PGs). One of these PGs is PGE_2 which has a variety of biological functions, and is one of the most abundant of the inflammatory PGs (Ricciotti and FitzGerald, 2011). PGE_2 was increased at days 1-7 post wounding in the $LIGHT^{-/-}$ mice compared to the control wounds **(Fig. 3.3E**). This prolonged presence of PGE_2 most likely contributes to the presence of elevated inflammatory cells seen in the wounds of $LIGHT^{-/-}$ mice(Petreaca et al., 2012). Another pro-inflammatory PG is $PGF_{2\alpha}$ which is synthesized from PGH_2 via PGF synthase. $PGF_{2\alpha}$ peaked at day 1 post wounding declining to baseline by 7 days **(Fig. 3.3F**). This PG is a strong stimulator of neutrophil infiltration.

Because we found so many pro-inflammatory lipids elevated after wounding and several of them increase chemotaxis of neutrophils, and we know that neutrophils secrete elastase, we investigated whether elastase activity was elevated in the $LIGHT^{-/-}$ mouse wounds during the course of healing. We show that the elastase activity is already elevated in the unwounded skin but after wounding it becomes further elevated reaching a peak at day 1 and then decreasing to normal levels until day 7 when it rises again and by day 12 post wounding it is just as high as at day 1 **(Fig. 3.4**). These levels suggest a hostile proteolytic environment early after wounding which can put the healing process on an abnormal course and then again later when the wound tissue should begin to remodel. This course of events most likely will lead to impaired development of the healing tissue.

AA-derive signaling lipids that are important in platelet aggregation and hemostasis

During our analysis of the pro-inflammatory lipids, we observed that many of them were also involved in activating or enhancing platelet aggregation. In particular, 8-isoprostane, PGE_2, and 15-HETE are significantly involved in increasing platelet aggregation(Khasawneh et al., 2008; Vezza et al., 1993; Vijil et al., 2014). This observation and the fact that the $LIGHT^{-/-}$ mouse wound tissues contain blood vessels with fibrin "cuffs" (essentially clots) led us to examine the presence of additional lipids involved in platelet function. Indeed, AA metabolites generated via cyclooxygenase 1 (COX-1) are mediators of platelet aggregation and vascular constriction. We found that thromboxane A_2 (TXA_2), one such metabolite that is rapidly transformed into its stable product TXB_2, peaks at day 1 post wounding and is significantly increased at days 2 and 3 **(Fig. 3.5A**). Furthermore, COX-2 is the leading source for generation of $6kPGF_{1\alpha}$, the stable product of prostacyclin (PGI_2) (Libby et al., 1988). We show that the levels of 6kPGF1α are significantly elevated after day 1 reach a peak at day 3 and then decline to normal levels by day 9 post wounding (**Fig. 3.5B**). PGI_2/6kPGF1α is a powerful inhibitor of platelet aggregation. The complementary elevation of TXB_2 and 6kPGF1α suggests that upon elevation of platelet aggregation early after wounding by the various lipids described above, PGI_2/6kPGF1α comes in to reestablish equilibrium in platelet aggregation in the wounded tissue.

Given these results, we performed a series of experiments to evaluate platelet aggregation and hemostasis in the $LIGHT^{-/-}$ mice. We show that platelet aggregation in response to the agonist ADP (0.0625μM) is significantly increased 3 days after wounding

in the LIGHT$^{-/-}$ mice and that this enhancement is dose dependent when compared to the control C57BL/6 mice (**Fig. 3.6A**). Similar data are obtained when using the TXA2 mimetic U64419 (data not shown), another agonist for platelet aggregation. To capture the long-term effects of elevated levels of these pro-aggregation lipids, we examined the intensity of aggregation at Day 7 post wounding. We show that at this time the LIGHT$^{-/-}$ mice still display enhanced level of platelet aggregation (**Fig 3.6B**). However, the intensity of aggregation is less pronounced than at day 3. Because we observed that platelet aggregation is "highly" enhanced in the LIGHT$^{-/-}$ mice, we examined the tail bleeding time of non-wounded and wounded mice and observed that indeed the bleeding time in wounded LIGHT$^{-/-}$ mice (days 3 and 7) is significantly reduced in comparison to that seen in the C57BL/6 mice (**Fig 3.7A,B**).

DISCUSSION

Understanding the impairment in overlapping factors during the course of healing can help in finding targeted potential therapeutics (Mustoe et al., 2006b). Although lipid biology has been widely studied in artherosclerosis, cancer, platelet biology, oxidative stress and neurological settings (Hamberg et al., 1975; Montuschi et al., 2004; Samuelsson et al., 1987; Stevens and Yaksh, 1988), use of modern lipidomics approaches to study AA-derived signaling lipids in cutaneous injury has only caught momentum in recent years (Nicolaou, 2013; Wijesinghe and Chalfant, 2013). Here we present for the first time data on the lipid metabolite profile in a mouse model of impaired healing, the LIGHT$^{-/-}$ mouse. We show that the pro-inflammatory lipid metabolites in LIGHT$^{-/-}$ wounds, as a result of AA breakdown, both non-enzymatically and enzymatically, are increased very early during the course of healing and could potentially be involved in derailing proper healing. Also, we show that as a result of chemotaxis of inflammatory cells, especially neutrophils, there was an increased activity of elastase that can degrade the extracellular proteins and disrupt the formation and remodeling of the healing tissue. We also show significant increases in lipid metabolites that were involved in increased platelet aggregation; LIGHT$^{-/-}$ mice have significantly enhanced platelet aggregation and a shortened bleeding time.

Redox imbalance resulting from over production of ROS and/or a decrease in antioxidant capacity cause generalized tissue damage involving DNA, lipid peroxidation and protein modification (Schäfer and Werner, 2008). The significant increase in 8- and 5-isoprostanes is an important indicator of increase in oxidative stress, increase the

chemotaxis and adhesion of immune cells to the site of injury (Huber et al., 2003) and when 8-isoprotane interacts with receptor(s) for TXA2 they enhance platelet activation and aggregation (Khasawneh et al., 2008) leading to significant damage to the healing tissue early after wounding. In addition, 8-isoprotane has anti-angiogenic effect by increasing endothelial cell death and inhibiting micro vessel tube formation (Benndorf et al., 2008). This suggests that the increases in sustained inflammation and impaired healing due to increased ROS, and tissue damage seen in the wounds of LIGHT$^{-/-}$ mice can be attributed, at least in part, to the production of isoprostanes early post wounding.

The HETEs are products of AA metabolism that are derived from Cyp450s via the ω-oxidation of the carbon chain and/or from the lipoxygenase pathways (Spector et al., 1988). Particularly present in platelets and neutrophils, 11-HETE has been shown to be chemotactic for human neutrophils and hence its prolonged presence can lead to persistent inflammation (Goetzl et al., 1980). In addition to the increases in 11-HETE, we also show the elevated presence of 15-HETE in the LIGHT$^{-/-}$ wounds. 15-HETE is known to increase platelet aggregation and thrombin generation (Vijil et al., 2014), two major players in clot formation. Furthermore, levels of 15-HETE has been shown to increase with increases in monocytes and macrophages (Conrad et al., 1992). We have previously reported increases in macrophages in the LIGHT$^{-/-}$ wounds (Petreaca et al., 2012).

Application of cys-LTD$_4$ in human skin has been shown to cause infiltration of neutrophils (Soter et al., 1983). This LT can be secreted by macrophages, which are

increased in LIGHT$^{-/-}$ wounds (Petreaca et al., 2012), and prompt β-catenin translocation to the nucleus and activation of the target genes c-myc and cyclin D1 (Salim et al., 2014). Significant increase of expression of the latter two genes has been shown to be present in the non-healing wound edge of chronic ulcers and to inhibit epithelialization (Stojadinovic et al., 2005). Moreover, although the levels of cys-LTD_4 peak in the first 2 days post wounding and then go down to normal levels for the rest of the healing period, the levels of LTE_4, the stable metabolite of LTD_4, remain elevated during the first 7 days post wounding. Furthermore, LTE_4 can act as an agonist for mast cells that are prominently present in chronic ulcers and cause chronic inflammation and fibrosis (Abd-El-Aleem et al., 2005; Paruchuri et al., 2009). Both LTD_4 and LTE_4 can also elicit changes in microvasculature and reduce blood pressure. LTE_4 does so by stimulating endothelial cell contraction which opens gaps in the endothelium, leading to vascular leakage (Joris et al., 1987) The cumulative data of the leukotrienes suggests that they may be responsible for the increases in permeability and leaky vasculature seen in the LIGHT$^{-/-}$ wounds (Joris et al., 1987; Soter et al., 1983).

Elastase is a broad spectrum serine protease that degrades most extracellular and membrane proteins in addition to degrading elastin, and therefore plays an important role in the damage to the connective tissue during inflammatory processes (Söder, 1999). The presence of higher than normal levels of elastase later in the healing process may also be responsible for the impaired remodeling observed in the LIGHT$^{-/-}$ mice wounds.

Polyunsaturated fatty acid derived prostanoids are crucial for skin physiology and hemostasis. The two classes of compounds, PGs and TXA_2 are collectively termed prostanoids and are produced as a result of the cyclooxygenase enzymatic pathway (Ricciotti and FitzGerald, 2011). PGE_2, the most abundant of the prostaglandins, is produced by a diverse number of cells, including epidermal keratinocytes, dermal fibroblasts, and macrophages (in particular M1 macrophages) (Harris et al., 2002; Norris and Dennis, 2014). Increased levels of PGE_2 in the $LIGHT^{-/-}$ wounds has strong implications in generating a pro-inflammatory wound microenvironment with increased neutrophil infiltration, increased microvascular permeability and platelet aggregation (Ricciotti and FitzGerald, 2011). In addition, increased levels of prostaglandin $PGF_{2\alpha}$ also increased neutrophil infiltration (Nicolaou, 2013). TXA_2, a strong direct activator of platelet function leads to irreversible aggregation (Hamberg et al., 1975; Ting and Khasawneh, 2010) and has a very short half-life and hence converts to TXB_2. The significantly high levels of TXA_2 in the wounds of $LIGHT^{-/-}$ mice indicate complications in platelet behavior and hence improper healing outcomes. It is to note that along with TXA_2, many of the previously discussed inflammatory lipids, including 8 isoprostane, 15-HETE, and PGE_2, all increase platelet activation and aggregation.

The presence of several lipids known to activate platelets coupled with our previous findings that the $LIGHT^{-/-}$ mice have fibrin “cuffs” led us to examine platelet aggregation and hemostasis after wounding. Aggregation of platelets was significantly

enhanced in LIGHT$^{-/-}$ than C57BL/6 mice. This was observed regardless of the dose used of the agonist ADP both at days 3 and 7. Enhanced aggregation was more prominent in mice at 3 days post wounding when compared to day 7 post wounding. This could be attributed to the fact that PGI_2, measured via the secondary stable metabolite $6kPGF_{1\alpha}$, inhibits platelet aggregation (Needleman et al., 1979). This PG becomes elevated when the levels of the other lipids that induce platelet aggregation fall down; in fact, its levels remain significantly elevated even at 7 days post wounding. This observation may also derive from the finding that isoprostanes levels are more elevated at day 3 compared to day 7, and the fact that they are known to enhance platelet function (e.g., in response to the agonist ADP) (Khasawneh et al., 2008). Platelet activation is required for aggregation that is critical for clot formation during an episode of bleeding that may follow injury. Increases in lipids causing platelet aggregation reduce the time of bleeding due to a faster hemostasis response. The significant reduction in bleeding time in the LIGHT$^{-/-}$ mice, especially at day 3 post wounding, confirms the hyperactive platelet behavior.

CONCLUSION

The results presented here in the LIGHT$^{-/-}$ mouse model of impaired healing are the first to use lipidomics approaches to elucidate the lipid profile and behavior during the course of impaired healing. In particularly, platelet activating and pro-inflammatory lipids were elevated early after wounding resulting in increased platelet activation/aggregation, reduced time for bleeding and increased inflammation in the LIGHT$^{-/-}$ mice. These results have major implication for our understanding of impaired healing because they put into prospective a class of molecules that has so far been out of the conversation when trying to understand how impaired healing develops. We anticipate that further investigation of both pro- and anti-inflammatory lipid markers during impaired/chronic wounds will contribute to our understanding of the etiology of how these wounds develop which could lead to the use of existing therapeutics such as non-steroidal anti-inflammatory agents or to the development of new therapies to treat problematic wounds.

REFERENCES

Abd-El-Aleem, S. A., Morgan, C., Mccollum, C. N. and Ireland, G. W. (2005). Spatial distribution of mast cells in chronic venous leg ulcers. *Eur. J. Histochem.* **49**, 265–272.

Balsinde, J., Winstead, M. V and Dennis, E. a (2002). Phospholipase A2 regulation of arachidonic acid mobilization. *FEBS Lett.* **531**, 2–6.

Benndorf, R. a, Schwedhelm, E., Gnann, A., Taheri, R., Kom, G., Didié, M., Steenpass, A., Ergün, S. and Böger, R. H. (2008). Isoprostanes inhibit vascular endothelial growth factor-induced endothelial cell migration, tube formation, and cardiac vessel sprouting in vitro, as well as angiogenesis in vivo via activation of the thromboxane A(2) receptor: a potential link between ox. *Circ. Res.* **103**, 1037–46.

Conrad, D. J., Kuhn, H., Mulkins, M., Highland, E. and Sigal, E. (1992). Specific inflammatory cytokines regulate the expression of human monocyte 15-lipoxygenase. *Proc. Natl. Acad. Sci.* **89**, 217–221.

Demidova-Rice, T., Hamblin, M. R. and Herman, I. M. (2012). Acute and impaired wound healing: pathophysiology and current methods for drug delivery, part 2: role of growth factors in normal and pathological wound. *Adv. Ski. …* **25**, 349–370.

Dhall, S., Do, D., Garcia, M., Wijesinghe, D. S., Brandon, A., Kim, J., Sanchez, A., Lyubovitsky, J., Gallagher, S., Nothnagel, E. A., et al. (2014). A novel model of chronic wounds: importance of redox imbalance and biofilm-forming bacteria for establishment of chronicity. *PLoS One* **9**, e109848.

Goetzl, E. J., Brash, A. R., Tauber, A. I., Oates, J. A. and Howard, W. C. H. T. (1980). Modulation of human neutrophil function by monohydroxy-eicosatetraenoic acids. *Immunology* **30**, 491–497.

Hamberg, M., Svensson, J. and Samuelsson, B. (1975). Thromboxanes: a new group of biologically active compounds derived from prostaglandin endoperoxides. *Proc. Natl. Acad. Sci.* **72**, 2994–2998.

Harris, S. G., Padilla, J., Koumas, L., Ray, D. and Phipps, R. P. (2002). Prostaglandins as modulators of immunity. *Trends Immunol.* **23**, 144–150.

Huber, J., Bochkov, V. N., Binder, B. R. and Leitinger, N. (2003). The isoprostane 8-iso-PGE2 stimulates endothelial cells to bind monocytes via cyclic AMP- and p38 MAP kinase-dependent signaling pathways. *Antioxid. Redox Signal.* **5**, 163–9.

Joris, I., Majno, G., Corey, E. J. and Lewis, R. A. (1987). The mechanism of vascular leakage induced by leukotriene E4. Endothelial contraction. *Am. J. Pathol.* **126**, 19–24.

Khasawneh, F. T., Huang, J.-S., Mir, F., Srinivasan, S., Tiruppathi, C. and Le Breton, G. C. (2008). Characterization of isoprostane signaling: evidence for a unique coordination profile of 8-iso-PGF(2alpha) with the thromboxane A(2) receptor, and activation of a separate cAMP-dependent inhibitory pathway in human platelets. *Biochem. Pharmacol.* **75**, 2301–15.

Kuehl, F. and Egan, R. . (1980). Prostaglandins , Arachidonic Acid , and Inflammation. *Science (80-.).* **210**, 978–984.

Lazarus, G. S., Cooper, D. M., Knighton, D. R., Margolis, D. J., Percoraro, R. E., Rodeheaver, G. and Robson, M. C. (1994). Definitions and guidelines for assessment of wounds and evaluation of healing. *Wound Repair Regen.* 165–170.

Libby, P., Warner, S. and Friedman, G. (1988). Interleukin 1: a mitogen for human vascular smooth muscle cells that induces the release of growth-inhibitory prostanoids. *J. Clin. …* **81**, 487–498.

Lin, O. A., Karim, Z. A., Vemana, H. P., Espinosa, E. V. P. and Khasawneh, F. T. (2014). The antidepressant 5-HT2A receptor antagonists pizotifen and cyproheptadine inhibit serotonin-enhanced platelet function. *PLoS One* **9**, e87026.

Meikle, P. J., Wong, G., Barlow, C. K. and Kingwell, B. a (2014). Lipidomics: potential role in risk prediction and therapeutic monitoring for diabetes and cardiovascular disease. *Pharmacol. Ther.* **143**, 12–23.

Montuschi, P., Barnes, P. J. and Roberts, L. J. (2004). Isoprostanes: markers and mediators of oxidative stress. *FASEB J.* **18**, 1791–800.

Mruwat, R., Cohen, Y. and Yedgar, S. (2013). Phospholipase A 2 inhibition as potential therapy for inflammatory skin diseases. *Immunotherapy* **5**, 315–317.

Murad, J. P., Espinosa, E. V. P., Ting, H. J. and Khasawneh, F. T. (2012). The C-terminal segment of the second extracellular loop of the thromboxane A2 receptor plays an important role in platelet aggregation. *Biochem. Pharmacol.* **83**, 88–96.

Mustoe, T. a, O'Shaughnessy, K. and Kloeters, O. (2006a). Chronic wound pathogenesis and current treatment strategies: a unifying hypothesis. *Plast. Reconstr. Surg.* **117**, 35S–41S.

Mustoe, T. a, O'Shaughnessy, K. and Kloeters, O. (2006b). Chronic wound pathogenesis and current treatment strategies: a unifying hypothesis. *Plast. Reconstr. Surg.* **117**, 35S–41S.

Needleman, P., Wyche, A. and Raz, A. (1979). Platelet and Blood Vessel Arachidonate Metabolism and Interactions. *J. Clin. Invest.* **63**, 345–349.

Nicolaou, A. (2013). Eicosanoids in skin inflammation. *Prostaglandins. Leukot. Essent. Fatty Acids* **88**, 131–8.

Norris, P. C. and Dennis, E. a (2014). A lipidomic perspective on inflammatory macrophage eicosanoid signaling. *Adv. Biol. Regul.* **54**, 99–110.

Paez Espinosa, E. V, Murad, J. P., Ting, H. J. and Khasawneh, F. T. (2012). Mouse transient receptor potential channel 6: role in hemostasis and thrombogenesis. *Biochem. Biophys. Res. Commun.* **417**, 853–6.

Paruchuri, S., Tashimo, H., Feng, C., Maekawa, A., Xing, W., Jiang, Y., Kanaoka, Y., Conley, P. and Boyce, J. a (2009). Leukotriene E4-induced pulmonary inflammation is mediated by the P2Y12 receptor. *J. Exp. Med.* **206**, 2543–55.

Petreaca, M. L., Do, D., Dhall, S., McLelland, D., Serafino, A., Lyubovitsky, J., Schiller, N. and Martins-Green, M. M. (2012). Deletion of a tumor necrosis superfamily gene in mice leads to impaired healing that mimics chronic wounds in humans. *Wound Repair Regen.* **20**, 353–66.

Ricciotti, E. and FitzGerald, G. a (2011). Prostaglandins and inflammation. *Arterioscler. Thromb. Vasc. Biol.* **31**, 986–1000.

Salim, T., Sand-Dejmek, J. and Sjölander, A. (2014). The inflammatory mediator leukotriene D_4 induces subcellular β-catenin translocation and migration of colon cancer cells. *Exp. Cell Res.* **321**, 255–66.

Samuelsson, B., Dahlén, S., Lindgren, J., Rouzer, C. A., Serhan, C. N., Dahlen, S. and Lindgren, J. A. N. A. (1987). Leukiotrienes and Lipoxins: Structures, Biosynthesis, and Biological Effects. *Science (80-.).* **237**, 1171–1176.

Schäfer, M. and Werner, S. (2008). Oxidative stress in normal and impaired wound repair. *Pharmacol. Res.* **58**, 165–71.

Schwab, J. M. and Serhan, C. N. (2006). Lipoxins and new lipid mediators in the resolution of inflammation. *Curr. Opin. Pharmacol.* **6**, 414–20.

Söder, B. (1999). Neutrophil elastase activity, levels of prostaglandin E 2 , and matrix metalloproteinase-8 in refractory periodontitis sites in smokers and non-smokers. *Acta Odontol. Scand.* **57**, 77–82.

Soter, N. A., Lewis, R. A., Corey, E. J. and Austen, K. F. (1983). Local Effects of Synthetic Leukotrienes (LTC4,LTD4, and LTB4) in Human Skin. *J. Invest. Dermatol.* **80**, 115–119.

Spector, A. a., Gordon, J. a. and Moore, S. a. (1988). Hydroxyeicosatetraenoic acids (HETEs). *Prog. Lipid Res.* **27**, 271–323.

Spite, M., Clària, J. and Serhan, C. N. (2014). Resolvins, specialized proresolving lipid mediators, and their potential roles in metabolic diseases. *Cell Metab.* **19**, 21–36.

Stevens, M. K. and Yaksh, T. L. (1988). Time Course of Release In Vivo of PGE2 , PGF2a , 6-Keto PGF1a , and TxB2 into the Brain Extracellular Space after 15 Min of Complete Global Ischemia in the Presence and Absence of Cyclooxygenase Inhibition. *J. Cereb. Blood Flow Metab.* **8**, 790–798.

Stojadinovic, O., Brem, H., Vouthounis, C., Lee, B., Fallon, J., Stallcup, M., Merchant, A., Galiano, R. D. and Tomic-Canic, M. (2005). Molecular pathogenesis of chronic wounds: the role of beta-catenin and c-myc in the inhibition of epithelialization and wound healing. *Am. J. Pathol.* **167**, 59–69.

Ting, H. J. and Khasawneh, F. T. (2010). Platelet function and Isoprostane biology. Should isoprostanes be the newest member of the orphan-ligand family? *J. Biomed. Sci.* **17**, 24.

Vezza, R., Roberti, R., Nenci, G. G. and Gresele, P. (1993). Prostaglandin E2 potentiates platelet aggregation by priming protein kinase C. *Blood* **82**, 2704–13.

Vijil, C., Hermansson, C., Jeppsson, A., Bergström, G. and Hultén, L. M. (2014). Arachidonate 15-lipoxygenase enzyme products increase platelet aggregation and thrombin generation. *PLoS One* **9**, e88546.

Wenk, M. R. (2005). The emerging field of lipidomics. *Nat. Rev. Drug Discov.* **4**, 594–610.

Wijesinghe, D. S. and Chalfant, C. E. (2013). Systems-Level Lipid Analysis Methodologies for Qualitative and Quantitative Investigation of Lipid Signaling Events During Wound Healing. *Adv. wound care* **2**, 538–548.

FIGURE CAPTIONS

Figure 3.1. Schematic illustration of breakdown of AA by non-enzymatic and enzymatic pathways. Arachidonic acid (AA), via the non-enzymatic pathways breaks down in the presence of elevated levels of oxidative stress to give rise to 8- and 5-isoprostanes. The enzymatic pathway of AA metabolism can occur via three categories. Cytochrome P450 (Cyp450s) breaks down AA to result in Hydroxyeicosatetranoic acids (HETEs). The same metabolite can also be achieved via the Lipoxygenase pathways of AA breakdown. The Lipoxygenase metabolizes AA to the leukotrienes, in particular cystenyl leukotrienes, cys-LTD_4 and cys-LTE_4. The Cyclooxygenase (COX) pathway is subdivided to give AA breakdown products thromboxanes A2 (TXA_2) and stable metabolite TXB_2, prostacyclin (PGI_2) and stable metabolite $6kPGF_{1\alpha}$, prostaglandin E2 (PGE_2) and $PGF_{2\alpha}$.

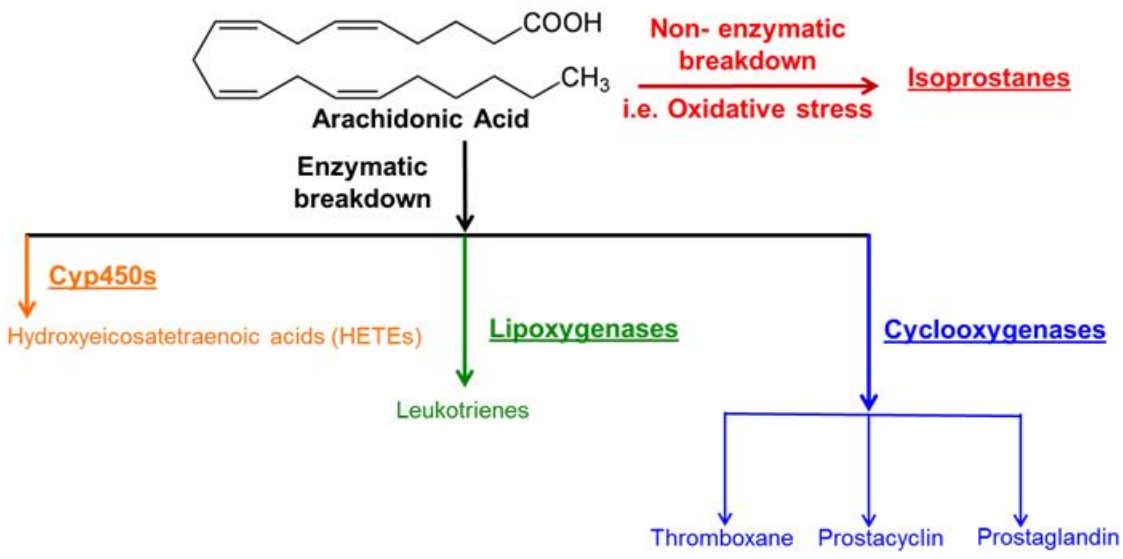
COOH
CH3
Arachidonic Acid
Non- enzymatic breakdown
i.e. Oxidative stress
Isoprostanes
Enzymatic breakdown
Cyp450s
Hydroxyeicosatetraenoic acids (HETEs)
Lipoxygenases
Leukotrienes
Cyclooxygenases
Thromboxane
Prostacyclin
Prostaglandin

Figure 3.1

Figure 3.2. Non-enzymatic breakdown of AA results in increased inflammatory lipids in impaired healing. Arachidonic acid derived isoprostanes, via reactive oxygen and nitrogen species non- enzymatic breakdown, are elevated **(A)** 8-isoprostanes **(B)** 5-isoprostanes .In LIGHT$^{-/-}$ mice, levels of both sharply increase in the first day. There is sustained presence of 8-isoprostanes for the first 7 days in LIGHT$^{-/-}$ mice whereas 5-isoprostanes gradually decrease to normal levels by 7 days.

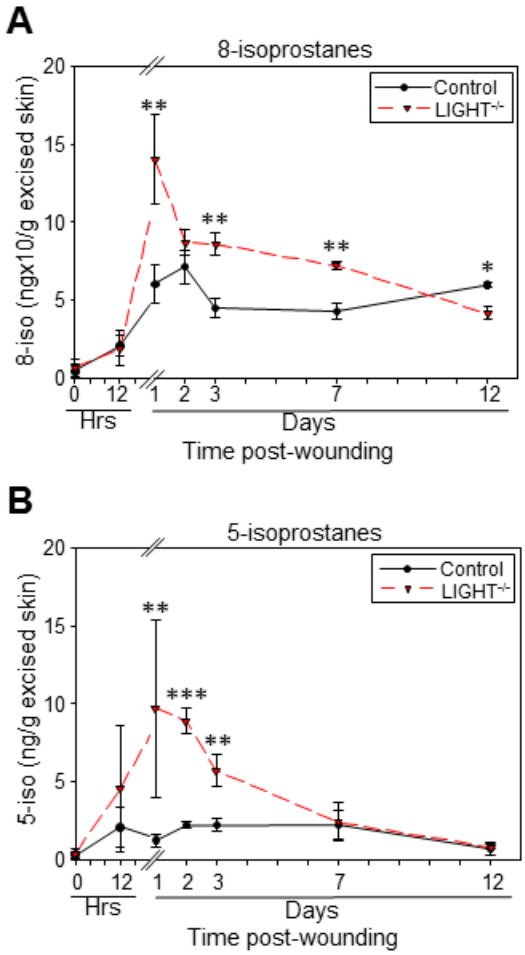
A
8-isoprostanes
Control
LIGHT-/-
8-iso (ngx10/g excised skin)
20
15
10
5
0
**
**
**
*
0
12
1
2
3
7
12
Hrs
Days
Time post-wounding
B
5-isoprostanes
Control
LIGHT-/-
5-iso (ng/g excised skin)
20
15
10
5
0
**
***
**
0
12
1
2
3
7
12
Hrs
Days
Time post-wounding

Figure 3.2

Figure 3.3. Enzymatically derived pro-inflammatory AA metabolites are elevated in impaired healing. Cytochrome P450 mediated enzymatic breakdown of AA-derived results in significant elevation of HETEs shortly after wounding of the $LIGHT^{-/-}$ mice. $LIGHT^{-/-}$ tissues collected at multiple time points after wounding were assayed for **(A)** 15- HETE which showed two peaks, one at day 1 and the other at day 7 post wounding and **(B)** 11-HETE which was overall elevated throughout the period of healing with respect to control mice. **(C)** Lipoxygenase-mediated enzymatic breakdown product Cystenyl Leukotriene D_4 (cys-LTD_4) was significantly prominent during the first 2 days of healing in $LIGHT^{-/-}$ mice, suggesting a substantial influx of inflammatory cells. **(D)** Cystenyl Leukotriene E_4 (LTE_4) is involved in increasing inflammation and was found to be elevated when compared to C57BL/6 mice throughout the course of healing. **(E)** Cyclooxygenase (COX)-mediated breakdown of AA gives rise to exacerbated levels of prostaglandin E2 (PGE_2), which is involved in increased inflammation and neutrophil aggregation, was significantly elevated throughout the course of healing when compared to controls. **(F)** Prostaglandin F2α ($PGF_{2\alpha}$) levels had two significantly elevated peaks at days 1 and 3 post wounding.

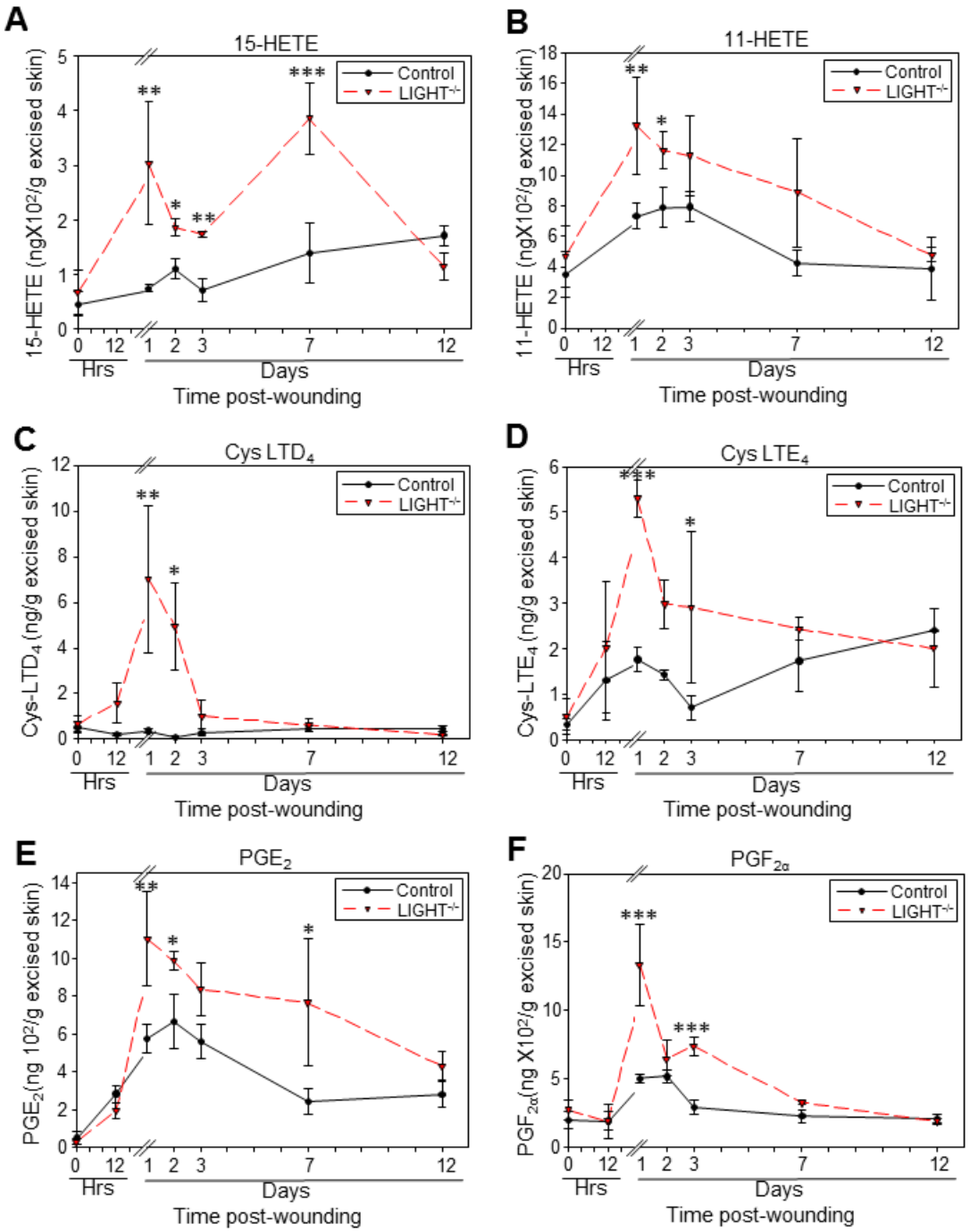
A
15-HETE
15-HETE (ngX10²/g excised skin)
Control
LIGHT-/-
Hrs
Days
Time post-wounding
B
11-HETE
11-HETE (ngX10²/g excised skin)
C
Cys LTD4
Cys-LTD4 (ng/g excised skin)
D
Cys LTE4
Cys-LTE4 (ng/g excised skin)
E
PGE2
PGE2(ng 10²/g excised skin)
F
PGF2α
PGF2α(ng X10²/g excised skin)

Figure 3.3

Figure 3.4. Elastase activity is elevated during the course of healing in impaired healing. Elastase activity was significantly elevated in the skin of LIGHT$^{-/-}$ mice when compared to C57BL/6 mice. This activity was exacerbated 1 day post wounding, potentially putting the healing on a course that leads to impaired healing. Moreover, the elastase activity was also significantly increased during the remodeling phase of healing contributing to impaired healing by interfering with the remodeling process.

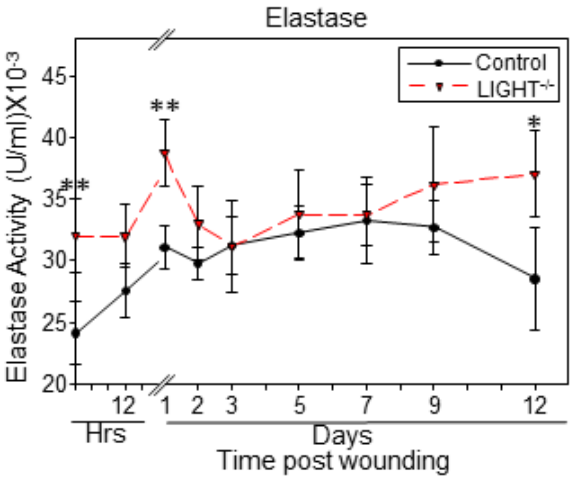
Elastase
Control
LIGHT-/-
Elastase Activity (U/ml)X10-3
45
40
35
30
25
20
**
**
*
12
1
2
3
5
7
9
12
Hrs
Days
Time post wounding

Figure 3.4

Figure 3.5. Signaling lipids that increase platelet aggregation are increased in impaired healing. (A) Cyclooxygenase (COX)-mediated AA metabolite thromboxane A2, measured by thromboxane B2 (TXB_2) levels, are significant increased during the first 3 days of healing suggesting enhanced platelet activity and increases in platelet aggregation. **(B)** $6kPGF_{1\alpha}$ is stable metabolite of prostaglandin I_2 (PGI_2), was significantly increased from day three to day 7 post wounding as a response to the enhanced platelet aggregation.

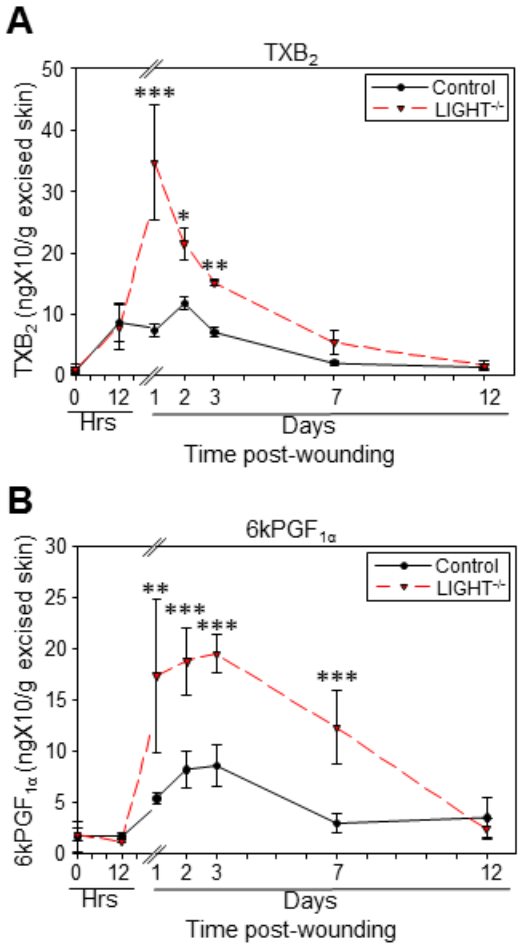
A
TXB2
Control
LIGHT-/-
TXB2 (ngX10/g excised skin)
50
40
30
20
10
0
***
*
**
0
12
1
2
3
7
12
Hrs
Days
Time post-wounding
B
6kPGF1α
Control
LIGHT-/-
6kPGF1α (ngX10/g excised skin)
30
25
20
15
10
5
0
**
***
***
***
0
12
1
2
3
7
12
Hrs
Days
Time post-wounding

Figure 3.5

Figure 3.6. Platelet aggregation is increased during impaired healing. Platelet aggregation was estimated using aggregometer and the agonist adenosine diphosphate (ADP). **(A)** Platelet aggregation 3 days post wounding was significantly enhanced in the LIGHT$^{-/-}$ mice and the aggregation occurred in a ADP dose-dependent manner. There was a 50% enhanced aggregation observed in LIGHT$^{-/-}$ mice when compared to control mice for 0.25 µM ADP. **(C)** At day 7 post wounding there was a 40.7% enhanced aggregation observed in LIGHT$^{-/-}$ mice when compared to control mice when 0.25 µM ADP was used. The enhanced aggregation seen in LIGHT$^{-/-}$ mice was reduced from day 3 to day 7.

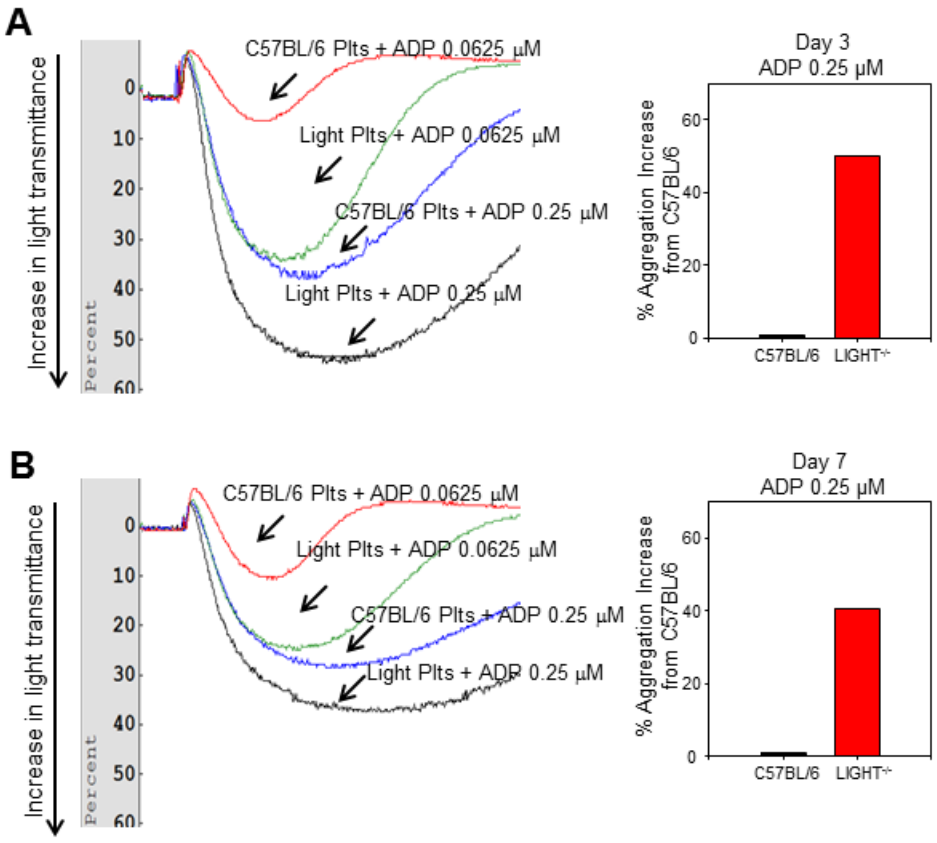
A
Increase in light transmittance
Percent
0
10
20
30
40
50
60
C57BL/6 Plts + ADP 0.0625 µM
Light Plts + ADP 0.0625 µM
C57BL/6 Plts + ADP 0.25 µM
Light Plts + ADP 0.25 µM
Day 3
ADP 0.25 µM
% Aggregation Increase from C57BL/6
0
20
40
60
C57BL/6
LIGHT-/-
B
Increase in light transmittance
Percent
0
10
20
30
40
50
60
C57BL/6 Plts + ADP 0.0625 µM
Light Plts + ADP 0.0625 µM
C57BL/6 Plts + ADP 0.25 µM
Light Plts + ADP 0.25 µM
Day 7
ADP 0.25 µM
% Aggregation Increase from C57BL/6
0
20
40
60
C57BL/6
LIGHT-/-

Figure 3.6

Figure 3.7. Coagulation time is faster in impaired healing. Tail vein bleeding time in LIGHT$^{-/-}$ mice suggested faster clotting and reduced coagulation time when compared to C57BL/6 control mice. **(A)** Bleeding time was significantly reduced in LIGHT$^{-/-}$ mice at 3 days post wounding. **(B)** Bleeding time is significantly faster in LIGHT$^{-/-}$ mice than in the control mice but is increased from that seen at day 3 post wounding.

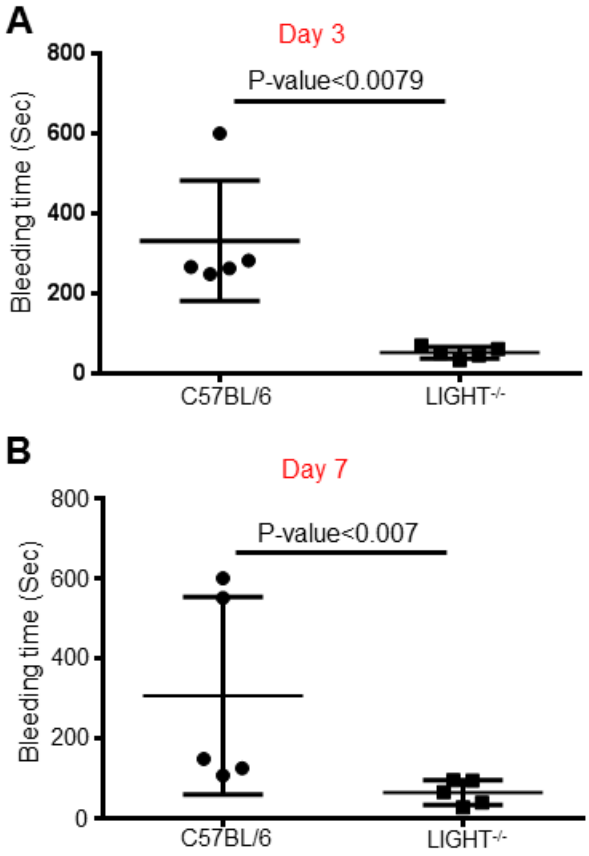
A
Day 3
P-value<0.0079
Bleeding time (Sec)
800
600
400
200
0
C57BL/6
LIGHT-/-
B
Day 7
P-value<0.007
Bleeding time (Sec)
800
600
400
200
0
C57BL/6
LIGHT-/-

Figure 3.7

SECTION 2

CHRONIC WOUNDS

CHAPTER 4

GENERATING AND REVERSING CHRONIC WOUNDS IN DIABETIC MICE

ABSTRACT

By 2025, more than 500M people worldwide will suffer from diabetes; 125M will develop foot ulcer(s) and 20M will undergo an amputation, creating a major health problem. Understanding how these wounds become chronic will provide insights to reverse chronicity. We hypothesized that oxidative stress (OS) in wounds is a critical component for generation of chronicity. We used the db/db mouse model of impaired healing and inhibited, at time of injury, two major antioxidant enzymes, catalase and glutathione peroxidase, creating high OS in the wounds. This was necessary and sufficient to trigger wounds to become chronic. The wounds initially contained a polymicrobial community that with time selected for specific biofilm-forming bacteria. To reverse chronicity we treated the wounds with the antioxidants α-tocopherol and N-acetylcysteine, and found that OS was highly reduced, biofilms had increased sensitivity to antibiotics, and granulation tissue was formed with proper collagen deposition and remodeling. We show for the first time generation of chronic wounds in which biofilm develops spontaneously, illustrating importance of early and continued redox imbalance coupled with the presence of biofilm in development of wound chronicity. This model will help decipher additional mechanisms and potentially better diagnosis of chronicity and treatment of human chronic wounds.

INTRODUCTION

Wound healing is a dynamic process involving many factors and cell types including soluble mediators, blood cells, fibroblasts, endothelial cells and extracellular matrix. Normal wound healing is divided into several sequential phases that overlap in space and time: homeostasis, inflammation, granulation tissue formation, and tissue remodeling. Chronic wounds develop as a result of defective regulation of one or more of the complex molecular and biological events involved in proper healing (Galiano et al., 2004; Lobmann et al., 2002; Maruyama et al., 2007). Diabetic foot ulcers and other similar chronic wounds impact approximately 6.5M people and cost approximately $25B/year in the US alone (Sen et al., 2009). The critical need for a cure of chronic wounds is underlined by the continuous increase in type II diabetes which accounts for 90-95% of all diabetes (CDC, 2014). Challenges in understanding these problematic events result from varying disease etiologies, existing co-morbidities and, importantly, lack of animal models that mimic the characteristics of chronic wounds in humans. The importance of developing such models has been recognized by the National Institute of General Medical Sciences call for proposals in this field. Furthermore, difficulties with human tissue collection complicate chronic wound research; for the most part, a clinician sees the patient when the wound is already at an advanced stage of chronicity and critical evidence of causality is already lost.

Although the series of events leading to development of chronic wounds remains unclear, toxic concentrations of reactive oxygen species (ROS) and presence of biofilm-

producing bacterial colonies are considered as key players (Bjarnsholt et al., 2008; James et al., 2003; James et al., 2007; Petreaca et al., 2012; Wlaschek and Scharffetter-Kochanek, 2005). The db/db mouse model of type II diabetes has impaired healing (Greenhalgh et al., 1990) with decreased levels of reduced glutathione (GSH) (Mudge et al., 2002), which results in reduction of glutathione peroxidase (GPx) activity and an increase in ROS. The latter promote leukocyte adhesion, thereby increasing immigration of inflammatory cells into the wound tissue (Kishimoto et al., 1989). It has also been suggested that ROS impair keratinocyte migration *in vitro*, potentially inhibiting re-epithelialization (Ponugoti et al., 2013). High levels of ROS also lead to DNA damage, gene dysregulation, cell death and a hostile proteolytic environment (Sen and Roy, 2008). Moreover, chronic wounds in humans are rich in microbiota, including anaerobic bacteria not revealed by culture that can form biofilms and cause excessive bioburden in these wounds (Bjarnsholt et al., 2008; James et al., 2007). *Staphylococcus aureus, Enterococcus faecalis, Pseudomonas aeruginosa,* coagulase-negative staphylococci and *Proteus* species are among the most commonly cultured species in human chronic wounds (Gjødsbøl et al., 2006).

We hypothesize that manipulating specific redox parameters immediately post-wounding will lead to development of chronic wounds in db/db mice and that restoring the antioxidant status will reverse chronicity and lead to proper healing. Here we show that inhibition of the activity of GPx and catalase, two antioxidant enzymes, immediately after wounding generates chronic wounds containing spontaneously-formed antibiotic-resistant polymicrobic bacterial biofilms. Moreover, chronicity can be reversed by

treatment with the antioxidants N-acetyl cysteine (NAC) and α-tocopherol (α-toc). This novel model for chronic wounds provides insight into the mechanisms involved in chronic wound development and may contribute to development of new therapeutics.

MATERIALS AND METHODS

Animals: C57BL/6 and db/db mice (Jackson Laboratories; Bar Harbor, ME) were housed in the UCR vivarium and used following protocols approved by the Institutional Animal Care and Use Committee (IACUC).

Dermal excision wound model, preparation of tissue for extracts and for histology: The procedures used were previously described by us (Petreaca et al., 2012). Briefly, mice were anesthetized with a single intraperitoneal injection of ketamine (80 mg/kg body weight)/ xylazine (16 mg/kg body weight). Full-thickness 7 mm punch wounds (excision of the skin and the underlying panniculus carnosus) were made on the back of the mice. The animals were euthanized using carbon-dioxide at various time points and the wound tissue was collected for histology and protein analysis using a 10mm punch (wound bed + surrounding tissue). For protein analysis, zirconium oxide beads weighing approximately the same as the wound tissue were added to tissue in safe lock tubes, followed by addition of 10ml of RIPA buffer per mg of tissue. The tissues were bullet blended for homogenization. The extracts were then centrifuged at 14000rpm for 15 minutes at 4^{o}C. The supernatants were used fresh or aliquots prepared and stored at -80^{o}C for later use. The samples were normalized to protein levels.

Superoxide dismutase activity assay: Total tissue superoxide dismutase (SOD) activity was measured by using a commercially available kit (Cayman Chemical, Catalog# 706002, Ann Arbor, USA) that measures all three types of SOD (Cu/Zn-, Mn-, and EC-SOD). One unit of SOD is defined as the amount of enzyme needed to cause 50%

dismutation of the superoxide radical. Briefly, xanthine oxidase and hypoxanthine generate superoxide radicals that are dismutated by SOD and in the process tetrazolium salt are converted to a formazan dye that is read at 450 nm. The SOD activity of the samples was calculated from the linear regression of a standard curve that was determined using the SOD activity of bovine erythrocytes at various concentrations run under the same conditions. The SOD activity was expressed as U/ml of tissue extract.

Hydrogen peroxide activity assay: Tissue hydrogen peroxide (H_2O_2) levels were measured by using a commercially available kit (Cell Technology Inc., Catalog# FLOH 100-3, Mountain View, USA) that utilizes a non-fluorescent detection reagent. The assay is based on the peroxidase-catalyzed oxidation by H_2O_2 of the non-fluorescent substrate 10-acetyl-3,7-dihydroxyphenoxazine to a fluorescent resorufin. 50µl of tissue extracts collected at different time points post-wounding and normalized to protein concentration were mixed with 50µl of the reaction cocktail in an opaque 96-well assay plate. Fluorescent intensities were measured at 530 nm (excitation)/590 nm (emission) using a Victor 2 (fluorescence and absorbance) microplate reader. The amounts of H_2O_2 in the supernatants were derived from a seven-point standard curve generated with known concentrations of H_2O_2.

Catalase activity assay: Tissue catalase activity was measured by using a commercially available kit (Cayman Chemical, Catalog# 707002, Ann Arbor, USA). The enzyme assay for catalase is based on the peroxidatic function of catalase with methanol to produce formaldehyde in the presence of an optimal concentration of H_2O_2. The formaldehyde

produced was measured spectrophotometrically, with 4-amino-3-hydrazino-5-mercapto-1,2,4-triazole (purpald) as the chromogen, at 540 nm in a 96-well place. The catalase activity was expressed as nmol/min/ml of tissue extract.

Glutathione peroxidase activity assay: A commercially available kit (Cayman Chemical, Catalog# 703102, Ann Arbor, USA) was used to measure tissue glutathione peroxidase (GPx) activity. The activity was measured indirectly by a coupled reaction with glutathione reductase (GR). GPx reduces H_2O_2 to H_2O and in the process oxidized glutathione (GSSG) is produced that in turn is recycled to its reduced state by GR and NADPH. Oxidation of NADPH to NADP+ is accompanied by a decrease in absorbance at 340nm. Under conditions in which GPx activity is rate limiting, the rate of decrease in the absorbance measured at 340nm, in a 96-well plate at 1-min interval for a total of 5min using a Victor 2 microplate reader, is directly proportional to the GPx activity of the sample. GPx activity was expressed as nmol/min/ml of tissue extract.

Chronic wound model: To generate chronic wounds in db/db mice we performed full thickness 7mm diameter excision wounds on the dorsum of 6-7 months old mice. Twenty minutes prior to wounding, mice were treated *once* intraperitoneally (IP) with 3-amino-1,2,4-triazole (ATZ) (Aldrich Chemistry; St.Louis, MO) at 1g/kg body weight, an inhibitor for catalase. Immediately after wounding, they were treated *once* topically with the inhibitor for GPx, mercaptosuccinic acid (MSA), (Sigma Lifesciences; St.Louis, MO) at 150mg/kg body weight. Immediately after wounding, the wounds were covered with tegaderm (3M; St. Paul, MN) to prevent contamination and were kept covered for the

duration of the experiments. In these mice it is easy to fully remove the hair from the back and hair grows very slowly hence we had no problems keeping the tegaderm in place. The tegaderm was removed periodically to take pictures of the wound and then immediately replaced. The wounds were fully-chronic 20 days after wounding and remained open sometimes for more than 3 months, depending on the experiment. *Control db/db mice* were treated exactly the same way but instead of inhibitors of the antioxidant enzymes they were treated with the vehicle (PBS). To reverse chronicity, at 20 days, the antioxidant NAC (Aldrich Chemistry (St.Louis, MO) was topically applied to the wound at 200mg/kg and the tegaderm replaced. Simultaneously, the mice were injected intraperitoneally with α-toc, Sigma Lifesciences (St.Louis, MO) at 50mg/kg. This treatment continued with NAC applied to the wound topically every day using an insulin syringe to deposit the solution under the Tegarderm and over the wound and with α-toc IP every-other-day for 20 days (40days post-wounding). At this point, the antioxidant treatment was stopped and the wounds went on to heal around 30 days after initiation of treatment with antioxidants (50days post-wounding). For the antioxidant controls, the mice were treated exactly the same but with vehicle rather than antioxidants. In some experiments, tissues were collected at various time points for detailed histological/histochemical, biochemical, and cellular/molecular evaluation, and in some cases the tissues, were analyzed for type and level of bacterial infection/biofilm production. Chronic wounds were successfully created in over 100 animals.

Bacteria isolation and characterization: To obtain the wound microbiome samples we used sterile cotton Q-tips to swab the wound bed, including the surface of the wound, but

yet minimizing disruption of the wound microenvironment to allow for longitudinal studies of the microbiome. The content of each swab was suspended in 1.0% w/v protease peptone and 20.0% v/v glycerol solution. Wounded tissue for bacteria analysis was obtained using sterile scissors and suspended in 1.0% w/v protease peptone and 20.0% v/v glycerol solution. Tissues were homogenized in the presence of zirconium oxide beads using a bullet blender at 4^{o}C. Bacteria were cultured for 16-18h at 37^{o}C on tryptic soy agar plates (BD Difco, Sparks, MD), containing 5.0% v/v defibrinated sheep blood (Colorado Serum Company, Denver, CO), and 0.08% w/v Congo red dye (Aldrich Chemistry, St.Louis, MO). Colonies were differentiated and isolated based on size, hemolytic pattern, and Congo red uptake. Resulting cultures were examined using Gram stain and visualized with optical microscopy. Gram-negative rods were characterized using the API20E identification kit (Biomerieux, Durham, NC), and oxidase test (Fluka Analytical, St. Louis, MO). When required, the *Pseudomonas* Isolation Agar culture test, 42^{o}C growth test in tryptic soy broth (TSB) (BD Difco, Sparks, MD), and motility test were used. Gram positive cocci cultures were differentiated based on catalase activity and coagulation activity (Fluka Analytical, St. Louis, MO), 6.5% w/v NaCl tolerance test, and hemolytic activity. Biofilm production was quantified using methods described previously (Christensen et al., 1985) with minor modifications. Briefly, 3-5µL of the wound swabbed sample was seeded in 100uL of TSB and grown in humidified incubator at 37^{o}C in a 96-well polystyrene flat-bottomed tissue culture plate under static condition. Bacterial content was removed by inverting and gently flicking the plate. The plate was washed three times by slowly submerging the plate and gently flicking the inverted plate

to remove the water. The wells were dried by tapping onto absorbent paper and then air dried at 65^{o}C for 30minutes. The plate was cooled and stained with Hucker crystal violet (Kolodkin-Gal et al., 2012) for 5minutes. Excessive stain was removed by rinsing the plate with water and then air dried overnight. The optical density at 570nm was then taken using the SpectraMax M2e microplate reader (Molecular Device, Sunnyvale, CA). Samples that give an OD of or above 0.125 were considered biofilm-positive else were considered biofilm-negative.

Viable bacteria cells count*:* Wound swab samples were resuspended in sterile Luria broth (LB) to yield a 1:4 v/v ratio of sample-to-TSB solution. Bacterial colonies were visually counted on typticase soy agar plates containing 5% sheep red blood cells incubated at 37^{o}C overnight in a humidified incubator.

Community minimal inhibitory concentrations assay: Wound swab samples (containing bacteria), were seeded on flat bottomed tissue culture plates for 3-4hr at 37^{o}C in a humidified incubator were challenged with antibiotic for 12hr at various concentrations in TSB. Optical density at 595nm (OD595nm) was used to quantify bacterial growth. The community minimal inhibitory concentration (CMIC) is defined as the lowest concentration of antibiotic that resulted in ≤50% increase in OD595nm compared to before introduction of antibiotic.

Bacterial staining: Frozen sections of chronic wound tissues were stained using ViaGram Red + Bacterial Gram-Stain and Viability Kit (Life Technologies, Carlsbad, CA) with modifications to the manufacturer's protocol. Briefly, the frozen tissue sections

were washed in 1X PBS for 5 minutes at room temperature to remove the OCT. Sections were then incubated in wheat germ agglutinin (WGA) conjugate stock solution for 5 minutes. The WGA solution was drained off the slide followed by the addition of 2.5µl of the DAPI/SYTOX Green working solution for 10 minutes at room temperature. The excess working solution was then removed from the section. Sections were mounted and visualized using a Nikon Microphot-FXA microscope with a Nikon DS-Fi1 digital camera.

Scanning Electron Microscopy: Tissues collected were fixed in 4% paraformaldehyde for 4hrs at room temperature and then processed as described in (Dhall et al., 2014). Briefly, samples were dehydrated in a series of ethanol for 20min each followed by critical point drying of the tissues, using Balzers CPD0202 and Au/Pd sputtering in the Sputter coater Cressington 108 auto. The samples were imaged using an XL30 FEG scanning electron microscope.

Biofilm carbohydrate composition: Chronic wound swab samples were washed with 80% and 100% ethanol to eliminate low molecular weight components and then with 2:1 (v/v) chloroform:methanol to remove lipids and acetone in preparation for drying. Samples were desiccated under vacuum in the presence of P_2O_5. Total protein content of the dried swab sample was estimated by the Lowry protein assay. Total carbohydrate content of dried swab sample was estimated by colorimetric phenol-sulfuric acid assay (Gilbert, 1962), using gum arabic as the standard. For glycosyl composition analysis, dried swab sample was cleaved by trifluoroacetic acid hydrolysis and the resulting

monosaccharides were derivatized by methanolysis, N-acetylation and trimethylsilylation as described (Chambers and Clamp, 1971; Chaplin, 1982) with minor modifications. Gas chromatography-flame ionization detection and gas chromatography-mass spectrometry were performed as previously described (Fu et al., 2007). DNA was extracted using the DNeasy Blood and Tissue kit (Qiagen, Chatsworth, CA) according to the manufacturer's instructions. DNA concentration was measured and purity confirmed by calculating the OD_{260}/OD_{280} absorption ratio.

Second Harmonic Generation (SHG) imaging: SHG imaging was done as previously described (Petreaca et al., 2012). Equipped with an NLO interface for a femtosecond Titanium-Sapphire laser excitation source (Chameleon-Ultra, Coherent, Incorporated, Santa Clara, CA) for multiphoton excitation, an inverted Zeiss LSM 510 NLO META laser scanning microscope (Carl Zeiss Microscopy, LLC, Thornwood, NY) for transmitted light and epifluorescence was used. The Chameleon laser provided femtosecond pulses at a repetition rate of about 80 MHz, with the center frequency tunable from 690 to 1040 nm. A long working distance objective (Zeiss, 40X water, N.A. 0.8) was used to acquire images. The sample two-photon signals were epicollected and discriminated by the short pass 650 nm dichroic beam splitter. A META detection module with signals sampled in a 394–405 nm detection range (lex = 800 nm) was used to collect the SHG images. Each image presented in this work is 12 bit, 512 X 512 pixels representing 225 mm X 225 mm field of view.

Statistical analysis: We used Graphpad Instat Software and Sigmaplot Software. Analysis of variance (ANOVA) was used to test significance of group differences between two or more groups. In experiments with only two groups, we used a Student's t-test. Because the differences we observe are not small, we perform experiments in groups of three mice and then repeat the experiment in groups of three as many times as needed to be confident of the results. For the majority of the cases, 2 sets of experiments to a total of 6 animals were sufficient to achieve significant results.

RESULTS

Impaired healing and redox imbalance early post-wounding in db/db mouse wounds

Both db/db and C57BL/6 mice were wounded as described in the Methods section. Wounds were imaged periodically to record wound closure. The C57BL/6 wounds closed in about 11 days whereas the db/db mouse wounds took up to 32 days to close, with flaky and crusty appearance (**Fig. 4.1A,B**). We examined levels of oxidative stress in these wounds by measuring the detoxifying capacity of SOD. SOD activity was significantly elevated in db/db mice compared to C57BL/6 mice (**Fig. 4.1C**), as was the product of this detoxification process, H_2O_2 (**Fig. 4.1D**). However, catalase activity was significantly lower in db/db mice than that of the C57BL/6 (**Fig. 1E**) whereas GPx activity was slightly lower very early and more so at 48hrs (**Fig. 4.1F**). These results show an increase in oxidative stress very early post-wounding in the db/db mouse wounds. The non-wounded skin of the db/db mice (t=0) already has exacerbated levels of oxidative stress (**Fig. 4.1C,D**) which correlates well with the impaired healing these mice exhibit. This led us to *hypothesize* that high oxidative stress levels in the wound tissue critically contribute to impaired healing and that exacerbated oxidative stress contributes to chronic wound development.

Manipulating the redox microenvironment leads to chronicity

A chronic wound is one that "has failed to proceed through an orderly and timely reparative process to produce anatomic and functional integrity or that has proceeded through the repair process without establishing a sustained anatomic and functional result" (Arnold and Barbul, 2006; Mustoe et al., 2006). In humans these wounds stay non-healing for at least 3 months (Mustoe et al., 2006) whereas in animals it has been difficult to establish how long wounds need to be impaired to be considered chronic. However, in general, wounds that do not close by the normative period of time and show minimalistic healing by 26 days have been considered chronic (Bonomo et al., 2000). To test our hypothesis we significantly increased oxidative stress in the db/db wounds by further inhibiting, at the time of wounding, both catalase and GPx activity, two potent antioxidant enzymes. The mice were wounded and treated as described in the Methods section under *Chronic wound model.* 3-amino-1,2,4-triazole (ATZ) was chosen to inhibit catalase because this inhibitor binds specifically and covalently to the active center of the enzyme and inactivates it (Feinstein et al., 1957). Mercaptosuccinic acid (MSA) was chosen to inhibit GPx because the thiol moiety binds to the selenocysteine active site of this enzyme and inactivates it (Chaudiere et al., 1984). ATZ has been shown to reduce catalase activity when injected intraperitoneally in rats and mice (Heim et al., 1956; Legg and Wood, 1970; Neurobiology, 1994). In rats, the inhibition of catalase activity in liver and kidney was shown to return to normal levels by day 7 after one IP dose of inhibitors (Heim et al., 1956; Legg and Wood, 1970). MSA, also known as thiomalate, is the most potent of all mercaptans for inhibiting GPx. It has been shown to clear from the plasma in

a matter of a few hours to a couple of days (Chaudiere et al., 1984). The specific doses described in the Methods section were chosen after an extensive literature search to determine what has worked in mice for effective inhibition of these enzymes without causing major side effects (Amantea et al., 2009; Guidet and Shah, 1989; Kingma et al., 1996; Welker et al., 2012). Moreover, the treatment with inhibitors affects the breakdown of H_2O_2, a product of the oxidative burst generated by neutrophils that are present early after wounding. As a consequence, inhibition of the two antioxidant enzymes increases the strength of oxidative burst without affecting neutrophil activity.

Control C57BL6 mice treated with either PBS or the inhibitors for the two antioxidant enzymes (IAE) closed by day 12 and 20 respectively (**Fig. 4.2A,B**). The wounds in the IAE treated mice took longer to close and initially appeared to be ulcerous but did not form exudate. db/db mice treated with PBS healed by 30 days and did not form exudate or become ulcerous (**Fig. 4.2C**). The wounds of the db/db treated with IAE, however, became ulcerous, developed exudate and remained open as long as a 100 days and sometimes more (**Fig. 4.2D,E**). The areas of the wounds were measured by removing the tegaderm, lightly cleaning the wound and taking a picture before covering the wound again with tegaderm (inset in **Fig 4.2E** shows a picture of such wounds). As is observed in humans with chronic wounds (Himes, 1999), the weight of db/db mice with chronic wounds steadily decreased by as much as 40% by day 40 post-wounding (**Fig. 4.2F**). This was not primarily due to treatment with the inhibitors because db/db mice treated with the IAE without wounding lost only weight until day 15 and then began to recover whereas the mice with chronic wounds continue to dramatically lose weight (**Fig. 4.2F**).

Chronic wounds in db/db mice sustain complex microbiota in the presence of redox imbalance

Microbial infection of wounds in db/db mice was first observed about 4 days after treatment with IAE and persisted for at least 56 days in most animals (**Fig. 4.3A**); the presence of biofilm-associated microbial infection was first seen about 15 days post-wounding. Bacterial isolation and characterization showed that the samples collected from the wounds are comprised of many bacterial species and contains both biofilm- and non-biofilm-producing species (**Fig. 4.3B**). Interestingly, monospecies cultures revealed that S. epidermidis isolated from day 4 samples produces biofilm when grown independently from the community, suggesting that communal interactions may be an important regulator of biofilm production. As the infection progresses, the bacterial composition evolves from several species of non-biofilm producers (day 4) to progressively fewer species at day 15 that are biofilm producers. By day 30 only 2 species remained (Enterococcus sp. and E. cloacae) and by day 56 the only bacterium remaining was E. cloacae which by that time had become biofilm producing (**Fig. 4.3B,C**). Furthermore, evaluation of chronic wound tissues to obtain the bacterial profile in the wound bed, showed that the profile was closely similar to the bacterial species in the wound bed collected in the swab sample, with only minor differences (e.g., relative abundance among bacterial species).

Impaired healing has been shown to be associated with high bacterial burden (Siddiqui and Bernstein, 2010). Counts of Colony Forming Units (CFU) from wound

swab samples revealed that bacterial burden was at its highest at 20 days post-wounding ($1.4\pm0.1x10^5$ CFU), thereby pushing the wound into a state of chronicity. At day 30, there was a reproducible dramatic decrease in bacterial burden (approximately 28X) compared to day 20 that coincided with the disappearance of *S. epidermidis* and of *Pseudomonas sp*. However, by day 40, wound bioburden was dominated by *E cloacae* and bioburden had recovered to a level comparable to day 20, and remained relatively unchanged thereafter (**Fig. 4.3D**).

Chronic wound microbiota is resistant to antibiotic challenge

Microbial communities living within biofilms are often resistant to antibiotics (Percival et al., 2010). Quantifying the microbial community minimal inhibitory concentration (CMIC) of amoxicillin required to inhibit the growth of the microbial community demonstrated that biofilm-positive bacterial communities appearing at 15days and after are more resistant to antibiotic killing, and this resistance increased with time (**Fig 4.3E**). Biofilm negative bacterial communities collected at 4 days post-wounding showed CMIC of less than15μg/ml and by day 56, these communities were more than 200μg/ml and the biofilm-forming bacteria.

To determine whether normal skin microbiota can be the source for infection, we took skin swabs from unwounded C57BL/6 and db/db mice and cultured the skin microbial flora (**Fig. 4.3F**). The majority of the bacteria found on both C57BL/6 and db/db skins belonged to the Firmicutes phylum, specifically *Staphylococcus sp. and*

Streptococcus sp. We were also able to isolate bacteria from the Proteobacteria phylum (specifically *Bacillus Pseudomonas,* and *Enterobacter*) (**Fig. 4.3F**). The bacterial species that colonized C57BL/6 and db/db wounds were similar but the db/db skin on average has higher bacterial density than C57BL/6 (not shown). Furthermore, these bacteria are known to be similar to normal human skin microbiota (Cho and Blaser, 2012). Thus, skin microbiota of non-wounded skin in our model is very similar to that of humans and is a contributor to the biofilm found in chronic wounds. It is notable that the bacterial profile isolated from the skin of db/db mice was similar to that observed using near-full-length 16S rRNA sequencing for bacterial species that colonized db/+ and db/db unwounded skin (Grice et al., 2010).

Treatment with antioxidant agents reverses chronicity

In this model system, the wounds are chronic by 20 days post-wounding and post-treatment with IAE. To reverse chronicity, we treated the animals with the antioxidant agents (AOA) NAC and α-toc. NAC is produced by most cells in the body; hence we applied it locally to the wound every day. This approach has been shown to be effective in diabetic mice (Khanna et al., 2010). α-toc, on the other hand, is produced primarily by the liver and circulates throughout the body. Therefore, we applied it IP (Daisuke et al., 1997; Diego-Otero, 2009), simulating systemic delivery in humans. The doses we used are described in Materials and Methods. The treatment doses for α-toc and NAC were chosen after extensive literature searches (Ikeda et al., 2003; Ivanovski et al., 2005;

Senoglu et al., 2008)

We found that healing improved dramatically by 30 days post-AOA treatment (50 days post wounding) as compared to the wounds treated with vehicle that can take up to 100 days to close **(**compare **Figs. 4.4A,B with Figs 4.2A-E)**. Moreover, the weights of the db/db mice treated with AOA began to stabilize starting at 20 days after the initiation of treatment (40 days post wounding) **(Fig. 4.4C).** These results, coupled with our finding that when the mice are treated only with inhibitors without wounding they do not lose weight past day 15 or so, indicate that the great loss of weight is due to the wounds and not to the treatment with IAE (compare **Fig. 4.4C with Fig. 4.2F**). The AOAs were also able to restore the detoxifying capability of catalase and GPx to reduce oxidative stress. SOD increased within 10 days post-treatment with AOAs (30 days post wounding) **(Fig. 4.4D)**. Also, H_2O_2 levels decreased by day 10 post treatment compared to increasing H_2O_2 levels in chronic wounds **(Fig. 4.4E)** and both catalase and GPx enzyme activity increased following treatment whereas they were approximately constant in chronic wounds **(Fig. 4.4F,G)**.

To test whether the two AOAs are needed together to reverse chronicity, we treated the chronic wounds individually with NAC (**Fig. 4.5A**) or α-toc (**Fig. 4.5B**). Visual examination of the wounds treated with single antioxidants shows little difference from those treated with both together (compare **Figs. 4.5A,B** with **Fig. 4.4A**). Quantitatively, α-toc was a close approximation to the two agents together for wound closure; NAC was slightly less effective (**Fig. 4.5C)**. Similarly, for weight loss, α-toc

closely matched combined agents and NAC was slightly less efficient (**Fig. 4.5D**). These findings suggest that either of the AOAs is able to reverse the chronic state. However, these measurements of macroscopic parameters are insufficient to adequately characterize reversal of chronicity. As shown in Figure 6, the structure of the wound tissue is immature when the mice are treated with the individual AOAs but not when treated with both.

Histological examination of db/db chronic wounds shows a complete loss of tissue structure; there is no epidermis and all that is present of the granulation tissue is a very thin band of undifferentiated tissue (**Fig. 4.6A; shown between the arrows**). Therefore, this tissue cannot be analyzed further. Db/db non-chronic wounds after closure showed that the granulation tissue is poorly developed (**Fig. 4.6B, first panel**). Chronic wounds treated with NAC or α-toc individually (**Fig. 4.6B, panels 4.2&3**) are much improved but their epidermis and granulation tissue are immature. In contrast, chronic wounds treated with both antioxidants (**Fig. 4.6B, panel 4**) show a well-developed granulation tissue and with thinner epidermis containing rets. Moreover, Masson trichrome (MT) stain and Second Harmonic Imaging Microscopy (SHIM) for collagen deposition and structure revealed a similar pattern (**Fig. 4.6C**); the overall deposition of fibrillar collagen in the wounds treated with both AOAs was better than those of db/db non-chronic wounds and chronic wounds treated with either AOA alone (**Fig. 4.6C compare panel 4 with 1-3**). As shown by keratin 10 staining (**Fig. 4.6D**), the epidermis was well organized and thinner in the animals treated with both AOAs (**panel 4**) than in the non-chronic db/db and those treated with the AOAs individually (**panels 1-3**).

Controlling redox stress leads to decrease in biofilm-production and increased sensitivity to antibiotic

After 10 days of AOA treatment (day 30 post wounding), biofilm-producing capacity of the chronic wound microbial flora is reduced by approximately 30% (**Fig. 4.7A**). By day 50 post-wounding the microbial flora was considered to be negative for biofilm production (OD570nm < 0.125). Similarly, microbial profiling showed that by day 50 the overall biofilm-producing capacity of the individual bacterial species was reduced markedly (**Fig. 4.7B**). This is most noticeable by the drastic decrease in biofilm-production by *S. epidermidis* at day 50 compared to day 20 and the loss of biofilm-production by *Pseudomonas sp.* at day 60 compared to day 30. The use of AOA treatment affected the bacterial composition of the wounds, most notably by the reduction and then elimination of *Enterococcus sp.*, the increasing prevalence of non-biofilm producing *E. cloacae*, and the colonization by *Pseudomonas sp.* (**Fig. 4.7C**). CFU counts (**Fig. 4.7D**) revealed a marked decrease in bacterial burden at 10 days of AOA treatment that, in contrast to non-AOA-treated wounds, remained relatively unchanged thereafter.

To determine whether the reduction in biofilm production resulting from AOA treatment enhances the antimicrobial effect of amoxicillin, CMICs of wounds treated with NAC and α-toc were evaluated (**Fig. 4.7E**). After 10 days of antioxidant treatment, the CMIC for amoxicillin was reduced significantly. Similar reduction was observed with other antibiotics, such as carbenicillin and gentamicin (**Fig. 4.7E**). These observations confirm that abating redox stress with NAC+α-toc alters the wound environment

resulting in a bacterial phenotype that produces less biofilm and is more sensitive to antibiotics.

To further confirm the presence of biofilm-forming bacteria in chronic wounds and the decrease in colonization upon AOA treatment, we performed both light microscopy with fluorescent staining and scanning electron microscopy (SEM). For the light microscopy we stained frozen sections of chronic wound tissue (IAE treated) at 20 days post wounding with a combination of Sytox green, which has high affinity for nucleic acids, and wheat germ agglutinin (WGA) conjugated with Texas Red which labels ECM molecules including biofilm. Both Gram-negative and Gram-positive bacteria in the tissue appear as very small green specks because their nuclei are stained with the Sytox green. They are associated and embedded in the red matrix stained by WGA (**Fig. 4.8A,B**). As previously reported, although SYTOX Green and WGA stain both host and bacteria, the size and morphology of the cells enabled distinguishing the presence of bacteria from host cells (Han et al., 2011). This technique is now considered as one of the staining techniques for biofilms in tissue specimens (James et al., 2014). The SEM pictures of chronic wounds (IAE treated) show an abundance of bacteria at 20 days post-wounding *when compared to a normal db/db wound at 10 days* (**Fig. 4.8C,D**). We used 10 days for the db/db non-chronic wounds as control because biofilm is already seen by day 10 in wounds treated with IAE. Bacteria were embedded in a biofilm-like matrix (stars) covering the wound (**Fig. 4.8C**). Upon treatment with AOA for 10 days (30 days post wounding), there was a reduction in the biofilm matrix seen in the wound (**compare Fig. 4.8E with 4.8F**). Furthermore, by 20 days of AOA treatment, there was

further decrease in the presence of matrix and bacteria when compared to the increase in biofilm formation observed in the chronic wound (**compare Fig. 4.8G with 4.8H**). Following bacterial species identification and confirmation of presence of biofilms in the chronic wound, we evaluated the composition of the biofilm (**Fig. 4.8I**). Carbohydrate analysis using gas chromatography shows the various carbohydrates forming the biofilm. Total protein content of the dried biofilm in swab sample was 44.6% ± 15.1% (w/w) and total DNA content was 1.55% ± 0.19074% (w/w). Total carbohydrate content of the dried biofilm in the swab sample was analyzed by colorimetric phenol-sulfuric acid assay was 1.98% ± 0.45% (w/w) and by gas chromatography analyzing glycosyl composition was 2.74% ± 1.46% (w/w). The latter showed that N-acetylglucosaminyl (GlcNAc), galactosyl, mannosyl, galacturonosyl, and glucuronosyl were the major glycosyl residues in the dried biofilm. Neither iduronosyl nor N-acetylgalactosaminyl residues were detected in the biofilm. Among the glycosyl residues, the relatively high amounts of N-acetylglucosaminyl and mannosyl residues were consistent with the presence of N-glycan type glycoproteins. Other glycosyl residues, particularly galacturonosyl residues, seemed to be of other origin.

DISCUSSION

We show here that we can generate chronic wounds in a diabetic mouse model of impaired healing by creating high levels of oxidative stress in the wound tissue using IAE at wounding. The wounds remain open for 80-100 days or longer. We also show that chronicity of these wounds can be reversed by application of appropriate AOAs, leading to healing. These findings are summarized schematically in **Fig. 4.9**. Briefly, we find that H_2O_2 is elevated very early after wounding of these mice and that the antioxidant enzyme activity is significantly lower than in wounds of normal mice, suggesting an increase in oxidative stress in the wound tissue. Accordingly, we developed a protocol in which the oxidative stress environment in these impaired wounds is further increased by inhibition of the two critical antioxidant enzymes, catalase and GPx, and therefore increasing the levels of H_2O_2. These wounds go on to form chronic ulcers within 20 days of this treatment. The ulcers remain open for months and develop a complex microbiota of biofilm-forming bacteria that are also found in chronic wounds in humans. Chronicity was reversed by treatment of the chronic wounds with the antioxidant agents NAC and α-toc.

NAC has been studied as a cysteine donor, a precursor for GSH (glutathione) (Aydin et al., 2002; Kamboj et al., 2006; Lavoie et al., 2008). The increase in GSH, in presence of NAC, has proven to combat the effects due to increases in H_2O_2, hence mitigating oxidative stress (Li et al., 1994; Maheshwari et al., 2011). Furthermore, NAC has been shown to reduce the production of $O_2^{\cdot -}$ and $ONOO^-$ (Failli et al., 2002; Luo et

al., 2009; Nakagami, 2003). Also, when introduced to bacterial biofilms, the inhibitory action on biofilm formation and adhesion in *Staphylococcus epidermidis and Pseudomonas aeruginosa* had a dose-dependent effect (Pérez-Giraldo et al., 1997; Zhao and Liu, 2010). The effects of NAC on biofilms, already proven to work in biofilms from respiratory tract infections, are attributed to the mucolytic property that disrupts disulphide bonds in mucus and reduces the viscosity of biofilms (Pérez-Giraldo et al., 1997; Pintucci et al., 2010). In addition, we used the antioxidant α-tocopherol that incorporates into the lipid bilayer (Liebler et al., 1986). α-tocopherol has been shown to reduce oxidative stress by scavenging H_2O_2 and specifically decreasing lipid peroxidation (Gülçin et al., 2005). Furthermore, the efficacy of α-tocopherol to reduce $O_2^{\cdot -}$ in hyperglycemic conditions hold importance for its use in diabetic patients (Venugopal et al., 2002). Under these conditions, the oxidative stress falls rapidly, the biofilm dismantles and the wound heals. This, to the best of our knowledge, is the first chronic wound model in which biofilm develops spontaneously allowing for longitudinal assessment of the wound microbiome in its natural environment. These findings define a unique relationship between redox imbalance and complex biofilm development in wound chronicity, providing an opportunity to understand the mechanisms of action of both and potentially for the development of new therapies for humans.

There are many similarities between the development of chronicity in these mice and similar chronic wounds in humans, especially non-pressure diabetic ulcers. For example, mice with chronic wounds lose considerable weight, as also occurs in many humans suffering from chronic wounds (Gilmore A.Shirley, Robinson Gretchen,

Posthauer Ellen Mary, 1995). Also, a very complex microbiota spontaneously develops in these mice wounds, as it does in humans wounds (Scales and Huffnagle, 2013). *Staphylococcus epidermidis* and other coagulase-negative staphylococci exist as harmless or even beneficial commensal bacteria of the skin. However, in diabetic, elderly, and immobile individuals, these commensal bacteria can cause diseases and are responsible for a large percentage of infection in wounds that do not heal (Grice and Segre, 2011). In our animal model, microbial flora that colonize the db/db mouse wounds are identified as *S. epidermidis*, *Enterococcus sp.*, *Enterobacter cloacae*, and *Pseudomonas sp.*, and they exist as a complex and dynamic community. Although commensal gram-negative bacteria *E. cloacae* are not reported from normal human skin, their presence in human wounds comes from gastrointestinal contamination of the skin (Grice and Segre, 2011; Roth and James, 1988). Others have shown that microbial flora cultured from patients with venous leg ulcers with or without clinical symptoms are polymicrobic (Gjødsbøl et al., 2006; Hansson et al., 1995). Furthermore, similar microbiota are found in combat wounds, chronic necrotizing skin diseases, and other chronic wounds (Be et al., 2014; Dowd et al., 2008; Sebeny et al., 2008).

The establishment of selective microbial populations toward chronicity is probably due to both bacterial competition and cooperation in concert with the unique clinical and immunological phenotype and pathophysiology of the host wound tissue. In the diabetic mice of our study, chronic wounds evolve into essentially a monospecific infection dominated by biofilm-producing *E. cloacae*. In other species (including humans), the specific biofilm producers may differ but the overall result is likely to be the

same. From our observations, the bacterial ecology in our mouse model is polymicrobic and dynamic. The molecular factors and parameters that resulted in the dynamics observed in our mouse model are yet to be defined and require further investigation. Our hypothesis is that due to competition and fitness, certain species will outcompete to predominate in the wounds and establish chronic infection. Therefore, there are differences in the bacterial species that colonize the wound at day 20 and 30. For reasons that we cannot yet explain, the microbial ecology tends to change dramatically around day 30, transitioning from a polymicrobic infection to a monospecific infection.

It is clear from our histological sections that the granulation tissue of the chronic wounds is virtually non-existent, making it essentially impossible to perform studies to identify inflammatory cells and/or blood vessels. In addition, we observed that the epidermis does not progress to close the wound and, in fact, the wound size increases. This is in agreement with our previously published findings in which cornea excision wounds in mice exposed to second-hand cigarette smoke increased in size (Ma and Martins-Green, 2009). In that case, the smoke exposure created increased stress in the wound that led to inhibition of cornea epithelial migration to cover the wound. Furthermore, the leading edge to the epithelium did not adhere to the underlying cornea stroma. We speculate that similar processes are occurring in the chronic wounds and we are currently investigating these possibilities.

ROS is known to play a critical role in wound healing (D'Autréaux and Toledano, 2007; Sen and Roy, 2008). Under normal physiological conditions, generation of H_2O_2 is

seen very early after injury. This occurs in the presence of nicotinamide-adenine-dinucleotide (NADH)-dependent oxidases (NOXs) produced by resident endothelial cells and fibroblasts, followed by neutrophils and macrophages (Roy et al., 2006). For proper healing, a delicate balance needs to exist between their good and deleterious effects in the wound tissue. A balanced ROS response will clean and inhibit infection while simultaneously triggering signaling mechanisms that stimulate healthy healing (Klyubin et al., 1996; Loo et al., 2012; Sen and Roy, 2008). However, elevated levels of ROS can cause a wide variety of tissue damage and lead to impaired healing (Dröge, 2002). Therefore, for a positive role in healing, ROS needs to be in balance to be an effective antimicrobial and signaling agent but yet not to cause destructive effects to the tissue. If not, the high levels of ROS or the reduced levels of antioxidant scavenger molecules such as the antioxidant enzymes catalase and GPx and antioxidant vitamins such as VitE, C and D, will lead to chronic wounds (Schäfer and Werner, 2008). The data presented here show that exacerbation of the levels of ROS immediately after wounding by inhibiting catalase and GPx, causes the wound to become populated with a polybacterial infection that then leads to selection for bacteria that form biofilm, causing wounds with impaired healing to become chronic. The question now is: How does the increase in ROS levels lead to development of biofilm that puts the wound in a state that leads to chronicity? To that end, we currently are investigating the differences in gene expression levels in the presence or absence of IAE in both C57BL/6 and db/db mice (unpublished data). The observed pattern of gene expression, coupled with the fact that some of them are related to changes in oxidative stress, inflammation, apoptosis, and mitochondrial functions that

regulate oxidative stress, suggests that these processes are critical for development of biofilm-induced chronicity. We speculate that a variety of genes that are altered when ROS is significantly increased favor the ability of the bacteria to produce virulence factors that allow them to form biofilm.

CONCLUSION

We have been successful in creating the first chronic wound model in which biofilm forms naturally without the need of introducing bacteria grown *ex-vivo*. In this model, excessive increase in ROS at the time of wounding provides the skin microbiota with favorable conditions to grow and be able to form biofilms (**Fig. 9**). The restoration of the redox balance by application of AOA causes biofilm to disappear from the wounds, resulting in significant improvement in wound healing. Others have proposed that the pathogenesis of chronic wounds is dependent on factors such as tissue hypoxia, bacterial colonization, ischemia-reperfusion injury and an altered cellular and systemic stress response. We propose that the critical parameter for development of chronic wounds in diabetic humans, and perhaps others, is an excessively high level of reactive oxygen species in the local microenvironment of the wound very early after injury. In this microenvironment, normal skin bacteria that otherwise would not form biofilm colonize the wound and become biofilm-producers.

REFERENCES

Amantea, D., Marrone, M. C., Nisticò, R., Federici, M., Bagetta, G., Bernardi, G. and Mercuri, N. B. (2009). Oxidative stress in stroke pathophysiology validation of hydrogen peroxide metabolism as a pharmacological target to afford neuroprotection. In *International review of neurobiology*, pp. 363–74.

Arnold, M. and Barbul, A. (2006). Nutrition and wound healing. *Plast. Reconstr. Surg.* **117**, 42S–58S.

Aydin, S., Ozaras, R., Uzun, H., Belce, A., Uslu, E., Tahan, V., Altug, T. and Dumen, E. (2002). N-Acetylcysteine Reduced the Effect of Ethanol on Antioxidant System in Rat Plasma and Brain Tissue. *Tohoku J. Exp. Med.* **198**, 71–77.

Be, N. a, Allen, J. E., Brown, T. S., Gardner, S. N., McLoughlin, K. S., Forsberg, J. a, Kirkup, B. C., Chromy, B. a, Luciw, P. a, Elster, E. a, et al. (2014). Microbial profiling of combat wound infection through detection microarray and next-generation sequencing. *J. Clin. Microbiol.*

Bjarnsholt, T., Kirketerp-Møller, K., Jensen, P. Ø., Madsen, K. G., Phipps, R., Krogfelt, K., Høiby, N. and Givskov, M. (2008). Why chronic wounds will not heal: a novel hypothesis. *Wound Repair Regen.* **16**, 2–10.

Bonomo, S. R., Davidson, J. D., Tyrone, J. W., Lin, X. and Mustoe, T. a (2000). Enhancement of wound healing by hyperbaric oxygen and transforming growth factor beta3 in a new chronic wound model in aged rabbits. *Arch. Surg.* **135**, 1148–53.

CDC (2014). National Diabetes Statistics Report: Estimates of Diabetes and Its Burden in the United States. *US Dep. Heal. Hum. Serv.*

Chambers, R. E. and Clamp, J. R. (1971). An assessment of methanolysis and other factors used in the analysis of carbohydrate-containing materials. *Biochem. J.* **125**, 1009–18.

Chaplin, M. F. (1982). A rapid and sensitive method for the analysis of carbohydrate components in glycoproteins using gas-liquid chromatography. *Anal. Biochem.* **123**, 336–341.

Chaudiere, J., Wilhelmsen, E. C. and Tappel, a L. (1984). Mechanism of selenium-glutathione peroxidase and its inhibition by mercaptocarboxylic acids and other mercaptans. *J. Biol. Chem.* **259**, 1043–50.

Cho, I. and Blaser, M. J. (2012). The human microbiome: at the interface of health and disease. *Nat. Rev. Genet.* **13**, 260–70.

Christensen, G. D., Simpson, W. a, Younger, J. J., Baddour, L. M., Barrett, F. F., Melton, D. M. and Beachey, E. H. (1985). Adherence of coagulase-negative staphylococci to plastic tissue culture plates: a quantitative model for the adherence of staphylococci to medical devices. *J. Clin. Microbiol.* **22**, 996–1006.

D'Autréaux, B. and Toledano, M. B. (2007). ROS as signalling molecules: mechanisms that generate specificity in ROS homeostasis. *Nat. Rev. Mol. Cell Biol.* **8**, 813–24.

Daisuke, K., Lee, I. K., Ishii, H., Kanoh, H. and King, G. L. (1997). Prevention Treatment of Glomerular Dysfunction with d-a-Tocopherol in Diabetic Rats by. *J. Am. Soc. Nephrol.* **8**, 426–435.

Dhall, S., Do, D., Garcia, M., Wijesinghe, D. S., Brandon, A., Kim, J., Sanchez, A., Lyubovitsky, J., Gallagher, S., Nothnagel, E. A., et al. (2014). A novel model of chronic wounds: importance of redox imbalance and biofilm-forming bacteria for establishment of chronicity. *PLoS One* **9**, e109848.

Diego-Otero, Y. de (2009). α-Tocopherol Protects Against Oxidative Stress in the Fragile X Knockout Mouse an Experimental Therapeutic Approach for the Fmr1 Deficiency.pdf. 1011–1026.

Dowd, S. E., Sun, Y., Secor, P. R., Rhoads, D. D., Wolcott, B. M., James, G. a and Wolcott, R. D. (2008). Survey of bacterial diversity in chronic wounds using pyrosequencing, DGGE, and full ribosome shotgun sequencing. *BMC Microbiol.* **8**, 43.

Dröge, W. (2002). Free radicals in the physiological control of cell function. *Physiol. Rev.* **82**, 47–95.

Failli, P., Palmieri, L., D'Alfonso, C., Giovannelli, L., Generini, S., Rosso, A. Del, Pignone, A., Stanflin, N., Orsi, S., Zilletti, L., et al. (2002). Effect of N-acetyl-l-cysteine on peroxynitrite and superoxide anion production of lung alveolar macrophages in systemic sclerosis. *Nitric Oxide* **7**, 277–282.

Feinstein, R. N., Berliner, S. and Green, F. (1957). Mechanism of Inhibition of Catalase By 3-Amino-1,2,4-triazole. *Arch. Biochem. Biophys.* **76**, 32–44.

Fu, H., Yadav, M. P. and Nothnagel, E. A. (2007). Physcomitrella patens arabinogalactan proteins contain abundant terminal 3-O-methyl-L: -rhamnosyl residues not found in angiosperms. *Planta* **226**, 1511–24.

Galiano, R. D., Tepper, O. M., Pelo, C. R., Bhatt, K. a, Callaghan, M., Bastidas, N., Bunting, S., Steinmetz, H. G. and Gurtner, G. C. (2004). Topical vascular endothelial growth factor accelerates diabetic wound healing through increased angiogenesis and by mobilizing and recruiting bone marrow-derived cells. *Am. J. Pathol.* **164**, 1935–47.

Gilbert, A. (1962). New Colorimetric Methods of Sugar Analysis. *Methods Enzymol.* **184**, 85–95.

Gilmore A.Shirley, Robinson Gretchen, Posthauer Ellen Mary, R. J. (1995). Clinical Indicators Associated with Unintentional Weight loss and Pressure Ulcers in Elderly Residents of Nursing Facilities.pdf. 984–992.

Gjødsbøl, K., Christensen, J. J., Karlsmark, T., Jørgensen, B., Klein, B. M. and Krogfelt, K. A. (2006). Multiple bacterial species reside in chronic wounds: a longitudinal study. *Int. Wound J.* **3**, 225–31.

Greenhalgh, D. G., Sprugel, K. H., Murray, M. J. and Ross, R. (1990). PDGF and FGF stimulate wound healing in the genetically diabetic mouse. *Am. J. Pathol.* **136**, 1235–46.

Grice, E. A. and Segre, J. A. (2011). The skin microbiome. *Nat. Rev. Microbiol.* **9**, 244–53.

Grice, E. a, Snitkin, E. S., Yockey, L. J., Bermudez, D. M., Liechty, K. W. and Segre, J. a (2010). Longitudinal shift in diabetic wound microbiota correlates with prolonged skin defense response. *Proc. Natl. Acad. Sci. U. S. A.* **107**, 14799–804.

Guidet, B. R. and Shah, S. V (1989). In vivo generation of hydrogen peroxide by rat kidney cortex and glomeruli. *Am. J. Physiol.* **256**, F158–64.

Gülçin, İ., Alici, H. A. and Cesur, M. (2005). Determination of in Vitro Antioxidant and Radical Scavenging Activities of Propofol. *Chem. Pharm. Bull. (Tokyo).* **53**, 281–285.

Han, A., Zenilman, J. M., Melendez, J. H., Shirtliff, M. E., Agostinho, A., James, G., Stewart, P. S., Mongodin, E. F., Rao, D., Rickard, A. H., et al. (2011). The importance of a multifaceted approach to characterizing the microbial flora of chronic wounds. *Wound Repair Regen.* **19**, 532–41.

Hansson, C., Hoborn, J., Möller, A. and Swanbeck, G. (1995). The microbial flora in venous leg ulcers without clinical signs of infection. Repeated culture using a validated standardised microbiological technique. *Acta Derm. Venereol.* **75**, 24–30.

Heim, W. G., Appleman, D. and Pyfrom, H. T. (1956). Effects of 3-Amino-l, 2,4-Triazole (AT) on Catalase and Other Compounds. *Am. J. Physiol.* **186**, 19–23.

Himes, D. (1999). Protein-calorie malnutrition and involuntary weight loss: the role of aggressive nutritional intervention in wound healing. *Ostomy. Wound. Manage.* **45**, 46–51, 54–5.

Ikeda, S., Tohyama, T., Yoshimura, H., Hamamura, K., Abe, K. and Yamashita, K. (2003). Dietary alpha-tocopherol decreases alpha-tocotrienol but not gamma-tocotrienol concentration in rats. *J. Nutr.* **133**, 428–34.

Ivanovski, O., Szumilak, D., Nguyen-Khoa, T., Ruellan, N., Phan, O., Lacour, B., Descamps-Latscha, B., Drüeke, T. B. and Massy, Z. a (2005). The antioxidant N-acetylcysteine prevents accelerated atherosclerosis in uremic apolipoprotein E knockout mice. *Kidney Int.* **67**, 2288–94.

James, T. J., Hughes, M. a, Cherry, G. W. and Taylor, R. P. (2003). Evidence of oxidative stress in chronic venous ulcers. *Wound Repair Regen.* **11**, 172–6.

James, G. a, Swogger, E., Wolcott, R., Pulcini, E. deLancey, Secor, P., Sestrich, J., Costerton, J. W. and Stewart, P. S. (2007). Biofilms in chronic wounds. *Wound Repair Regen.* **16**, 37–44.

James, G., Marc, A. and Hunt, A. (2014). Imaging Biofilms in Tissue Specimens. In *Antibiofilm Agents* (ed. Rumbaugh, K. P. and Ahmad, I.), pp. 31–44. Berlin, Heidelberg: Springer Berlin Heidelberg.

Kamboj, A., Kiran, R. and Sandhir, R. (2006). Carbofuran-induced neurochemical and neurobehavioral alterations in rats: attenuation by N-acetylcysteine. *Exp. brain Res.* **170**, 567–75.

Khanna, S., Biswas, S., Shang, Y., Collard, E., Azad, A., Kauh, C., Bhasker, V., Gordillo, G. M., Sen, C. K. and Roy, S. (2010). Macrophage dysfunction impairs resolution of inflammation in the wounds of diabetic mice. *PLoS One* **5**, e9539.

Kingma, J. G., Simard, D., Rouleau, J. R., Tanguay, R. M. and Currie, R. W. (1996). Effect of 3-aminotriazole on hyperthermia-mediated cardioprotection in rabbits. *Am. J. Physiol.* **270**, H1165–71.

Kishimoto, T. K., Jutila, M. A., Berg, E. L. and Butcher, E. C. (1989). Neutrophil Mac-1 and MEL-14 adhesion proteins inversely regulated by chemotactic factors. *Science* **245**, 1238–41.

Klyubin, I. V, Kirpichnikova, K. M. and Gamaley, I. A. (1996). Hydrogen peroxide-induced chemotaxis of mouse peritoneal neutrophils. *Eur. J. Cell Biol.* **70**, 347–51.

Kolodkin-Gal, I., Cao, S., Chai, L., Böttcher, T., Kolter, R., Clardy, J. and Losick, R. (2012). A self-produced trigger for biofilm disassembly that targets exopolysaccharide. *Cell* **149**, 684–92.

Lavoie, S., Murray, M. M., Deppen, P., Knyazeva, M. G., Berk, M., Boulat, O., Bovet, P., Bush, A. I., Conus, P., Copolov, D., et al. (2008). Glutathione precursor, N-acetyl-cysteine, improves mismatch negativity in schizophrenia patients. *Neuropsychopharmacology* **33**, 2187–99.

Legg, P. G. and Wood, R. L. (1970). Effects of catalase inhibitors on the ultrastructure and peroxidase activity of proliferating microbodies. *Histochemie.* **22**, 262–76.

Li, W.-C., Wang, G.-M., Wang, R.-R. and Spector, A. (1994). The Redox Active Components H202 and N-AcetyI-L-Cysteine Regulate Expression of c-jun and c-fos in Lens Systems. *Exp. Eye Res.* **59**, 179–190.

Liebler, D. C., Kling, D. S. and Reed, D. J. (1986). Antioxidant protection of phospholipid bilayers by alpha-tocopherol. Control of alpha-tocopherol status and lipid peroxidation by ascorbic acid and glutathione. *J. Biol. Chem.* **261**, 12114–9.

Lobmann, R., Ambrosch, a, Schultz, G., Waldmann, K., Schiweck, S. and Lehnert, H. (2002). Expression of matrix-metalloproteinases and their inhibitors in the wounds of diabetic and non-diabetic patients. *Diabetologia* **45**, 1011–6.

Loo, A. E. K., Wong, Y. T., Ho, R., Wasser, M., Du, T., Ng, W. T. and Halliwell, B. (2012). Effects of hydrogen peroxide on wound healing in mice in relation to oxidative damage. *PLoS One* **7**, e49215.

Luo, Z., Chen, Y., Chen, S., Welch, W. J., Andresen, B. T., Jose, P. A. and Wilcox, C. S. (2009). Comparison of inhibitors of superoxide generation in vascular smooth muscle cells. *Br. J. Pharmacol.* **157**, 935–43.

Ma, C. and Martins-Green, M. (2009). Second-hand cigarette smoke inhibits wound healing of the cornea by stimulating inflammation that delays corneal reepithelialization. *Wound Repair Regen.* **17**, 387–96.

Maheshwari, A., Misro, M. M., Aggarwal, A., Sharma, R. K. and Nandan, D. (2011). N-acetyl-L-cysteine counteracts oxidative stress and prevents H2O2 induced germ cell apoptosis through down-regulation of caspase-9 and JNK/c-Jun. *Mol. Reprod. Dev.* **78**, 69–79.

Maruyama, K., Asai, J., Ii, M., Thorne, T., Losordo, D. W. and D'Amore, P. a (2007). Decreased macrophage number and activation lead to reduced lymphatic vessel formation and contribute to impaired diabetic wound healing. *Am. J. Pathol.* **170**, 1178–91.

Mudge, B. P., Harris, C., Gilmont, R. R., Adamson, B. S. and Rees, R. S. (2002). Role of glutathione redox dysfunction in diabetic wounds. *Wound Repair Regen.* **10**, 52–8.

Mustoe, T. a, O'Shaughnessy, K. and Kloeters, O. (2006). Chronic wound pathogenesis and current treatment strategies: a unifying hypothesis. *Plast. Reconstr. Surg.* **117**, 35S–41S.

Nakagami, H. (2003). NADPH oxidase-derived superoxide anion mediates angiotensin II-induced cardiac hypertrophy. *J. Mol. Cell. Cardiol.* **35**, 851–859.

Neurobiology, B. (1994). Pergamon Effects of 3-Amino-l , 2 , 4-Triazole on Brain Catalase in the Mediation of Ethanol Consumption in Mice. **11**, 235–239.

Percival, S. L., Hill, K. E., Malic, S., Thomas, D. W. and Williams, D. W. (2010). Antimicrobial tolerance and the significance of persister cells in recalcitrant chronic wound biofilms. *Wound Repair Regen.* **19**, 1–9.

Pérez-Giraldo, C., Rodríguez-Benito, A., F. J. Morán, C. H., Blanco, M. T. and Gómez-García*, A. C. (1997). Influence of N-acetylcysteine on the formation of biofilm by Staphylococcus epidermidis. *J. Antimicrob. Chemother.* **39**, 643–646.

Petreaca, M. L., Do, D., Dhall, S., McLelland, D., Serafino, A., Lyubovitsky, J., Schiller, N. and Martins-Green, M. M. (2012). Deletion of a tumor necrosis superfamily gene in mice leads to impaired healing that mimics chronic wounds in humans. *Wound Repair Regen.* **20**, 353–66.

Pintucci, J. P., Corno, S. and Garotta, M. (2010). Biofilms and infections of the upper respiratory tract. *Eur. Rev. Med. Pharmacol. Sci.* **14**, 683–90.

Ponugoti, B., Xu, F., Zhang, C., Tian, C., Pacios, S. and Graves, D. T. (2013). FOXO1 promotes wound healing through the up-regulation of TGF-β1 and prevention of oxidative stress. *J. Cell Biol.* **203**, 327–43.

Roth, R. R. and James, W. D. (1988). Microbial ecology of the skin. *Annu. Rev. Microbiol.* **42**, 441–64.

Roy, S., Khanna, S., Nallu, K., Hunt, T. K. and Sen, C. K. (2006). Dermal wound healing is subject to redox control. *Mol. Ther.* **13**, 211–20.

Scales, B. S. and Huffnagle, G. B. (2013). The microbiome in wound repair and tissue fibrosis. *J. Pathol.* **229**, 323–31.

Schäfer, M. and Werner, S. (2008). Oxidative stress in normal and impaired wound repair. *Pharmacol. Res.* **58**, 165–71.

Sebeny, P. J., Riddle, M. S. and Petersen, K. (2008). Acinetobacter baumannii skin and soft-tissue infection associated with war trauma. *Clin. Infect. Dis.* **47**, 444–9.

Sen, C. K. and Roy, S. (2008). Redox signals in wound healing. *Biochim. Biophys. Acta* **1780**, 1348–61.

Sen, C. K., Gordillo, G. M., Roy, S., Kirsner, R., Lambert, L., Hunt, T. K., Gottrup, F., Gurtner, G. C. and Longaker, M. T. (2009). Human skin wounds: a major and snowballing threat to public health and the economy. *Wound Repair Regen.* **17**, 763–71.

Senoglu, N., Yuzbasioglu, M. F., Aral, M., Ezberci, M., Kurutas, E. B., Bulbuloglu, E., Ezberci, F., Oksuz, H. and Ciragil, P. (2008). Protective effects of N-acetylcysteine and beta-glucan pretreatment on oxidative stress in cecal ligation and puncture model of sepsis. *J. Invest. Surg.* **21**, 237–43.

Siddiqui, A. R. and Bernstein, J. M. (2010). Chronic wound infection: facts and controversies. *Clin. Dermatol.* **28**, 519–26.

Venugopal, S. K., Devaraj, S., Yang, T. and Jialal, I. (2002). -Tocopherol Decreases Superoxide Anion Release in Human Monocytes Under Hyperglycemic Conditions Via Inhibition of Protein Kinase C- . *Diabetes* **51**, 3049–3054.

Welker, A. F., Campos, É. G., Cardoso, L. A. and Hermes-lima, M. (2012). Role of catalase on the hypoxia / reoxygenation stress in the hypoxia-tolerant Nile tilapia.

Wlaschek, M. and Scharffetter-Kochanek, K. (2005). Oxidative stress in chronic venous leg ulcers. *Wound Repair Regen.* **13**, 452–61.

Zhao, T. and Liu, Y. (2010). N-acetylcysteine inhibit biofilms produced by Pseudomonas aeruginosa. *BMC Microbiol.* **10**, 140.

FIGURE LEGENDS

Figure 4.1. db/db mouse wounds have increased oxidative stress and delayed healing. Time course of wound closure in C57BL/6 mice **(A)** and in db/db mice **(B)**. Wound areas were traced and analyzed using Image J and show delayed closure as compared to C57BL/6. **(C)** SOD activity was measured using tetrazolium salt that converts into a formazan dye detectable at 450nm. SOD activity was significantly elevated in the db/db wounds. **(D)** H_2O_2 measurements were based on the peroxidase-catalyzed oxidation by H_2O_2 and fluorescent product resorufin read fluorometrically at 530nm/605nm. H_2O_2 levels were significantly higher in the db/db wounds, confirming the elevated SOD activity in the early hours post wounding. **(E)** Catalase activity was measured by an enzymatic reaction spectrophotometrically detected with the chromogen purpald at 540nm and showed reduced activity in the db/db wounds, suggesting a buildup in H_2O_2. **(F)** GPx activity was measured by a coupled reaction with glutathione reductase where GPx activity was rate-limiting and absorbance was read at 340nm per 1 min intervals. GPx activity showed significantly lower levels at 4hrs and 48hrs post wounding. These levels confirm improper detoxification of H_2O_2 leading to redox stress. *Time zero represents unwounded skin. n=6. All data are Mean ± SD. *p<0.05,**p<0.01,***p<0.001. n=6 for each of the studies unless indicated differently.*

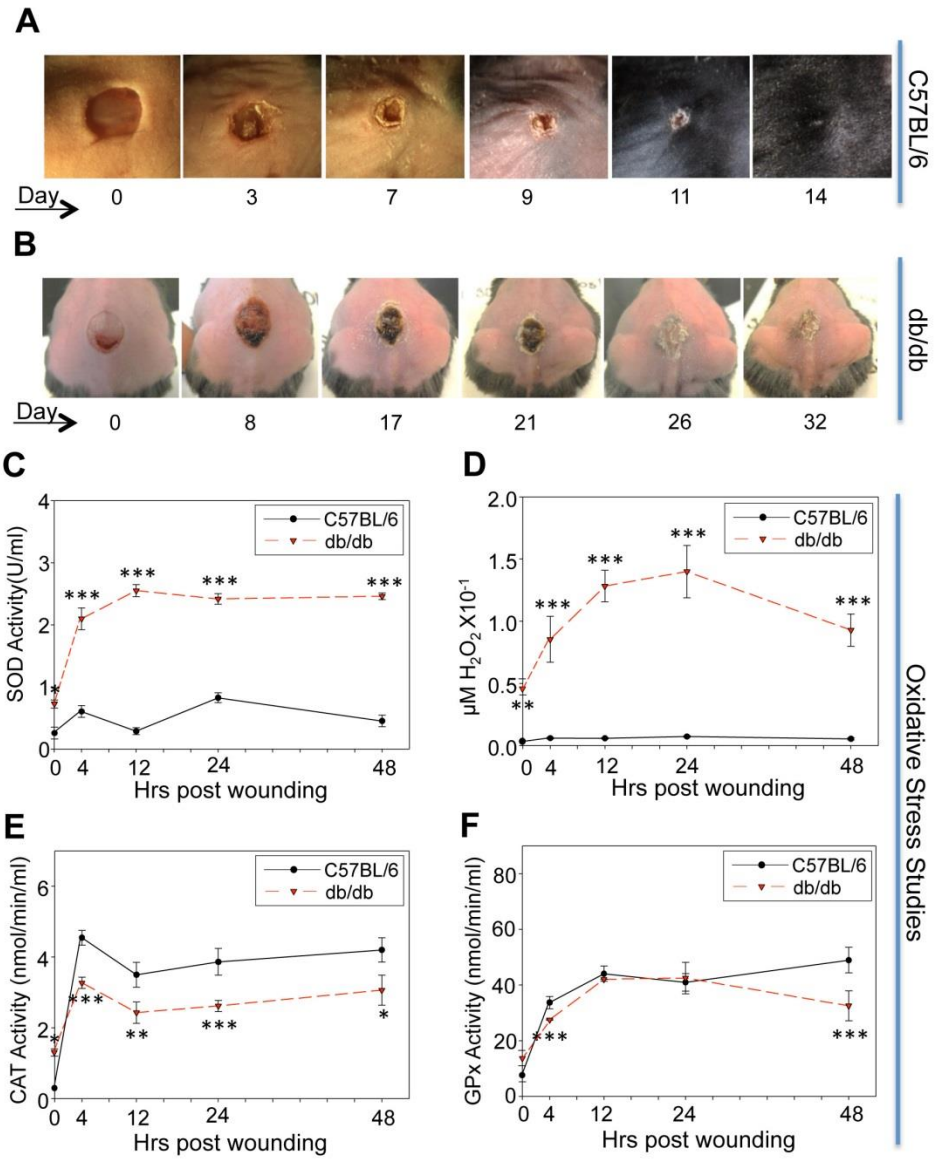
A
C57BL/6
Day
0
3
7
9
11
14
B
db/db
Day
0
8
17
21
26
32
C
SOD Activity(U/ml)
C57BL/6
db/db
Hrs post wounding
D
μM H_2O_2 X10^{-1}
C57BL/6
db/db
Hrs post wounding
E
CAT Activity (nmol/min/ml)
C57BL/6
db/db
Hrs post wounding
F
GPx Activity (nmol/min/ml)
C57BL/6
db/db
Hrs post wounding
Oxidative Stress Studies

Figure 4.1

Figure 4.2. Redox imbalance leads to chronic wound development. (A) Wound closure in C57BL/6 mice treated with PBS occurs by 15 days post wounding. **(B)** C57BL/6 mice treated with inhibitors heal by 20 days post wounding. **(C)** Db/db mice treated with PBS heal completely by 30days. **(D)** Db/db mice treated with inhibitors become chronic and do not heal for as long as 100 days. **(E)** Percent open wound area over time in wounds of C57BL/6 and db/db mice after treatment with PBS or IAE. **(F)** Weight loss in C57BL/6 and db/db mice after PBS and IAE treatment. n=7 for each treatment except for db/db mice treated with IAE; we have now treated well over 100 mice. *All data are Mean ± SD. *p<0.05,**p<0.01,***p<0.001.*

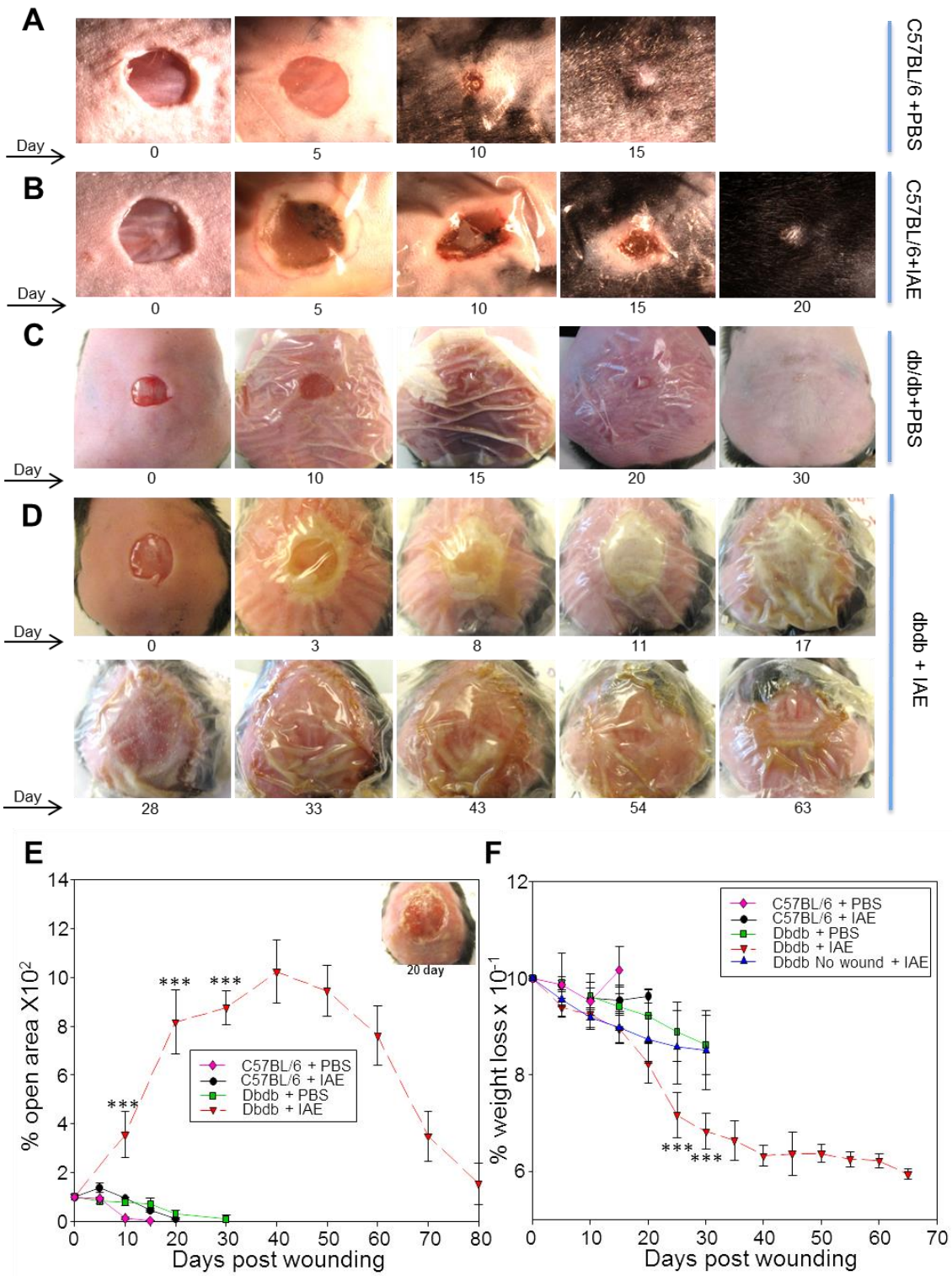
A
Day
0
5
10
15
C57BL/6 +PBS
B
Day
0
5
10
15
20
C57BL/6+IAE
C
Day
0
10
15
20
30
db/db+PBS
D
Day
0
3
8
11
17
Day
28
33
43
54
63
dbdb + IAE
E
% open area X10^2
Days post wounding
20 day
C57BL/6 + PBS
C57BL/6 + IAE
Dbdb + PBS
Dbdb + IAE
***
F
% weight loss x 10^-1
Days post wounding
C57BL/6 + PBS
C57BL/6 + IAE
Dbdb + PBS
Dbdb + IAE
Dbdb No wound + IAE

Figure 4.2

Figure 4.3. Chronic wounds contain complex antimicrobial-resistant wound microbiota. (A) Bacterial content of in the swab sample were quantified by measuring the optical densities of stained bacterial films at OD570nm ($\geq$0.125 is considered to be biofilm positive – dashed red line). **(B)** Specific bacterial strain identification shows a dynamic presence of different species with biofilm-forming-capacity. **(C)** Bacterial prevalence of individual species shows the changing dynamics of the wound microbiota. Quantifying the relative percentage of individual bacterial species demonstrated that *Enterococcus sp.* and *S. epidermidis* made a up large majority of the microbial mass with traces of *Pseudomonas* and *E. cloacae* at 4 days post IAE treatment. At day 20, the majority of the biomass was composed of biofilm-producing *Enterococcus sp.* (~40%) and non-biofilm-producing *E. cloacae* (50%). By day 30, biofilm-producing *S. epidermidis* disappeared. At day 40, the wounds progressively advanced toward a monospecies infection dominated by *E. cloacae* and to lesser extent by biofilm-producing *Pseudomonas.* By day 56, the wounds are exclusively colonized by biofilm-producing *E. cloacae*. **(D)** Bacterial burden was evaluated by colony forming unit counts in db/db wounds treated with IAE. **(E)** The community minimum inhibitory concentration (CMIC) on wound the wound swab samples was examined using the antibiotic amoxicillin. With time, the resistance increased. **(F)** Skin swabs were collected from C57BL/6 and db/db mice to evaluate their normal skin microbiota. Very similar bacteria where found in the skin of both mouse strains. *All data are Mean ± SD. n=6 for each of the studies unless indicated differently*.

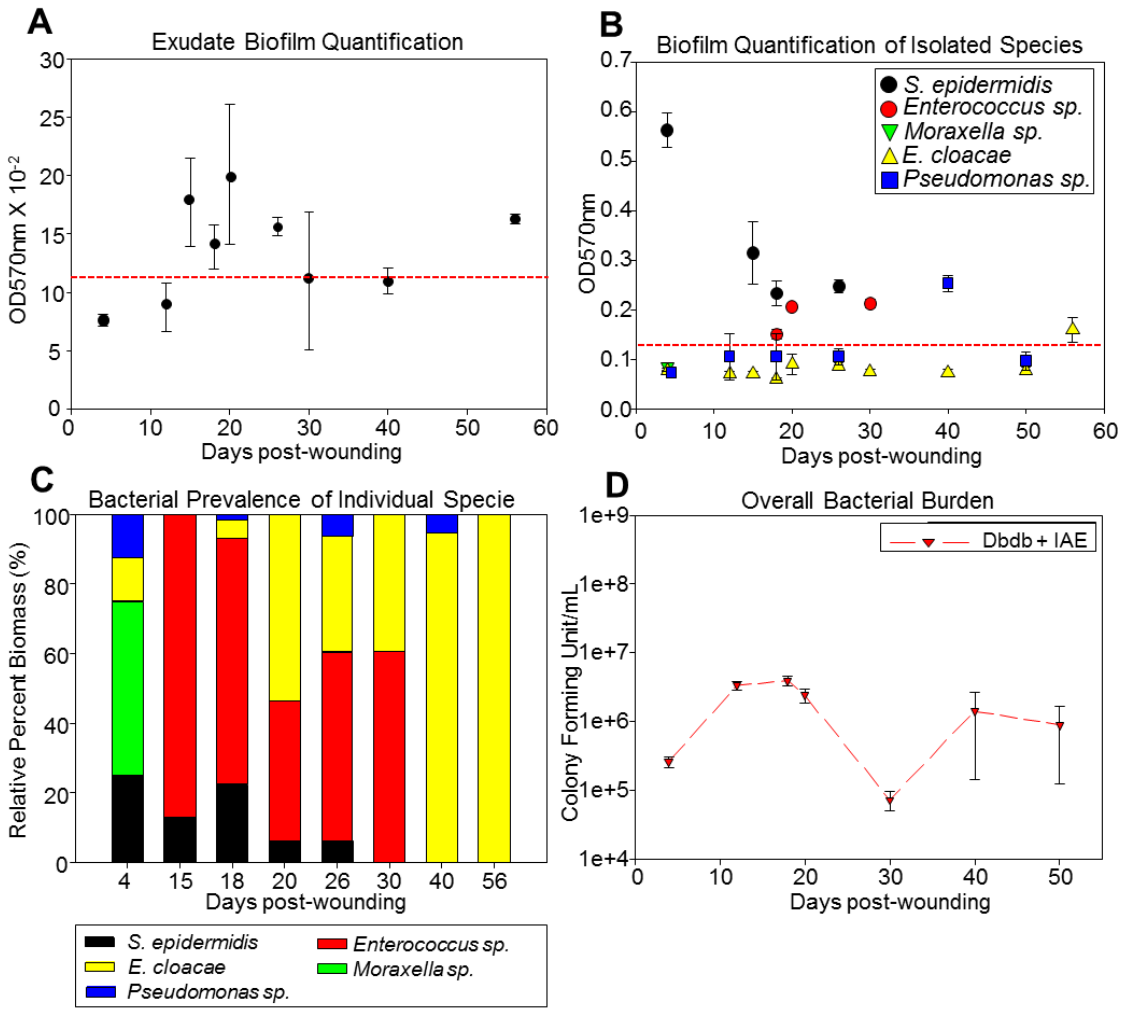

E

CMIC of GPx/CAT inhibitor treated wounds	
	Amoxicillin (µg/mL)
Day 4	6-13
Day 18	13-25
Day 26	50-100
Day 56	>200

F

Normal Skin Microbiota

C57BL/6	*db/db*
• Coagulase-negative *Staphylococcus sp.* • *Streptococcus sp.* • *E. cloacae* • Presumptively *Pseudomonas sp.*	• Coagulase-negative *Staphylococcus sp.* • Hemolytic *Streptococci sp.* • *E. cloacae* • Presumptively *Bacillus sp*

Figure 4.3

Figure 4.4. Treating chronic wounds with AOA leads to proper healing and reduced oxidative stress. (A) Chronic wounds of db/db mice treated with IAE and then AOA, NAC and α-toc, show a faster rate of wound closure. Wound areas were traced and analyzed using Image J. **(B)** Percent open wound area in db/db wounds treated with IAE and then AOA compared to db/db wounds treated with IAE alone. AOA significantly accelerated wound closure. **(C)** Weight loss was significantly higher in db/db mice treated with IAE alone than when treated with IAE and then AOA. **(D)** The levels of SOD in db/db wounds treated with PBS were significantly higher than db/db wounds treated with IAE suggesting that the latter have reduced dismutation of $O_2^{\cdot-}$ radicals and accumulation of reactive radicals. AOA treatment of chronic wounds significantly increased SOD activity 10 days post-treatment suggesting increased dismutation of $O_2^{\cdot-}$ radicals. **(E)** Increases in H_2O_2 levels (examined as described in Fig. 1), in db/db wounds treated with AOA were stabilized in comparison to the increasing stress in the non-AOA treated wound. **(F)** Catalase activity was significantly increased in PBS treated wounds in the first 15days as compared to the IAE treated wounds. AOA treatment of chronic db/db wounds significantly increased catalase activity by 20days of treatment. **(G)** GPx in the db/db mice treated with PBS was significantly higher than the db/db mice treated with IAE. Enzyme activity in the db/db chronic wounds treated with AOA was significantly higher than db/db mice with only IAE. The overall effect was stabilized levels in H_2O_2. *All data are Mean ± SD. *p<0.05,**p<0.01. n=6 or 7 for each of the studies unless indicated differently.*

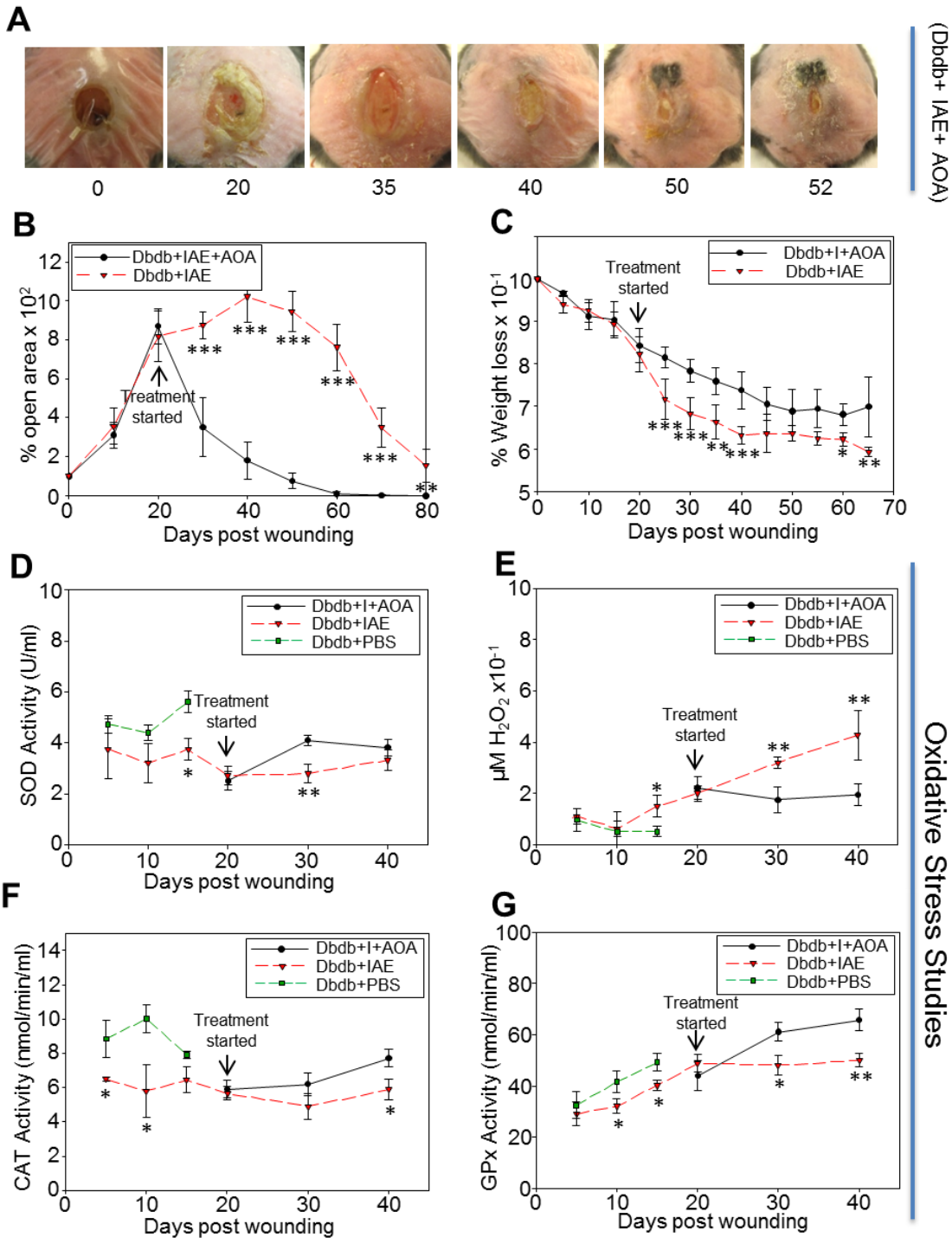
A
0
20
35
40
50
52
(Dbdb+ IAE+ AOA)
B
Dbdb+IAE+AOA
Dbdb+IAE
% open area x 10²
Treatment started
Days post wounding
C
Dbdb+I+AOA
Dbdb+IAE
% Weight loss x 10⁻¹
Treatment started
Days post wounding
D
Dbdb+I+AOA
Dbdb+IAE
Dbdb+PBS
SOD Activity (U/ml)
Treatment started
Days post wounding
E
Dbdb+I+AOA
Dbdb+IAE
Dbdb+PBS
μM H2O2 x10⁻¹
Treatment started
F
Dbdb+I+AOA
Dbdb+IAE
Dbdb+PBS
CAT Activity (nmol/min/ml)
Treatment started
Days post wounding
G
Dbdb+I+AOA
Dbdb+IAE
Dbdb+PBS
GPx Activity (nmol/min/ml)
Treatment started
Days post wounding
Oxidative Stress Studies

Figure 4.4

Figure 4.5. Chronic wounds treated with individual antioxidants. (A) Wound closure in db/db chronic wounds treated with AOA α-toc was observed by day 53 post wounding. **(B)** Wound closure in db/db chronic wounds treated with AOA NAC was observed by day 53 post-wounding. **(C)** Percent open wound area was calculated using Image J. Open area was significantly decreased in db/db wounds treated with IAE and then AOA. **(D)** Mouse weight loss was significantly higher in animals with no AOA treatment. *n=5. All data are Mean ± SD. *p<0.05,**p<0.01,***p<0.001.*

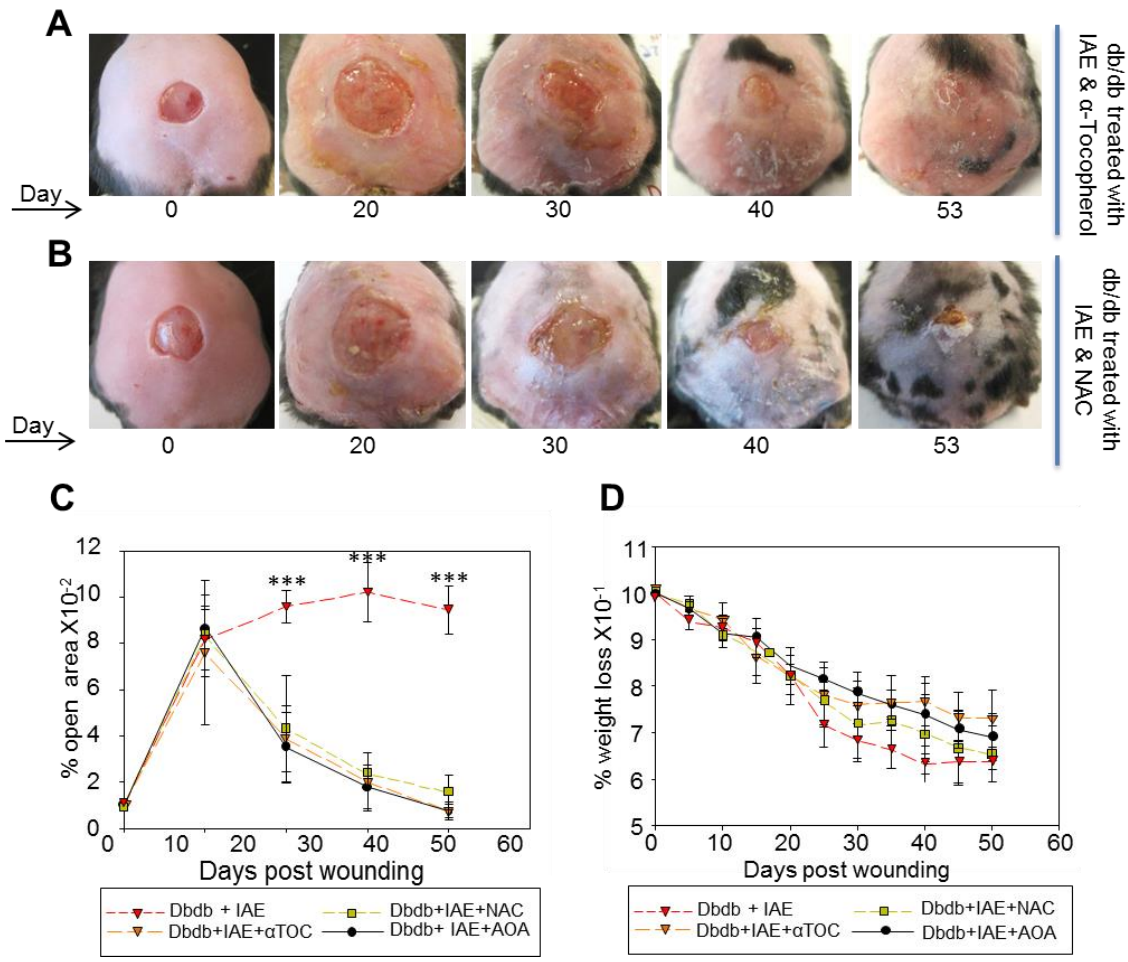
A
Day
0
20
30
40
53
db/db treated with IAE & α-Tocopherol
B
Day
0
20
30
40
53
db/db treated with IAE & NAC
C
% open area X10-2
Days post wounding
***
***
***
Dbdb + IAE
Dbdb+IAE+αTOC
Dbdb+IAE+NAC
Dbdb+ IAE+AOA
D
% weight loss X10-1
Days post wounding
Dbdb + IAE
Dbdb+IAE+αTOC
Dbdb+IAE+NAC
Dbdb+IAE+AOA

Figure 4.5

Figure 4.6. Histological evaluation of normal, chronic and treated wounds. (**A**) H&E-stained section of day 64 chronic wound in db/db mice treated with IAE. (**B**) H&E-stained sections of representative animals to illustrate the histology at wound closure of db/db wounds from a non-treated animal (panel 1), an animal treated with IAE and then with AOA α-toc (panel 2), an animal treated with IAE and then with AOA NAC (panel 3) and an animal treated with IAE and then both AOA (panel 4). Scale bar 100μm. **(C)** Representative Masson-trichrome staining (blue color) illustrating loss of collagen deposition in non-treated db/db mice (panel 1). A decrease in collagen deposition was seen in chronic wounds treated with AOA individually (panels 2&3). Chronic wounds treated with both AOA had a significant increase in collagen deposition and fibril formation (panel 4). Second Harmonic Generated Imaging (SHIM) shows abnormalities in collagen bundles in the non-treated db/db wounds whereas no clear fibers are seen in individual AOA treated wounds. In wounds with both AOA, fibers are well formed and appear more mature. For SHIM the scale bar is 10μm. **(D)** Keratin 10 illustrates the presence of the epithelial cytoskeleton in the terminally differentiating epithelial cells found in the suprabasal layer. The epithelium is much more mature in the wounds treated with both AOA. Scale bar is 100μm.

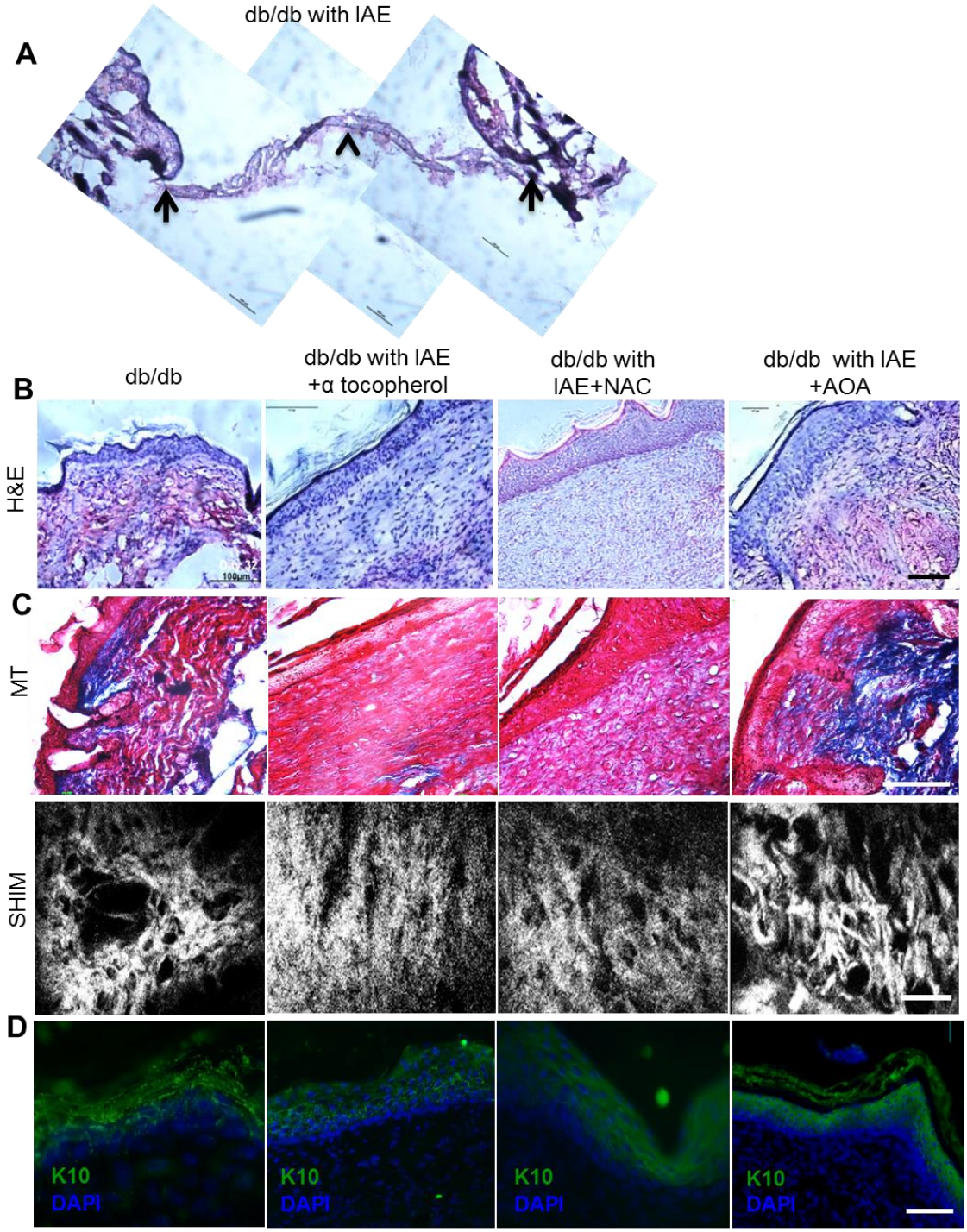
db/db with lAE
A
B
db/db
db/db with lAE
+α tocopherol
db/db with
lAE+NAC
db/db with lAE
+AOA
H&E
C
MT
SHIM
D
K10
DAPI
K10
DAPI
K10
DAPI
K10
DAPI

Figure 4.6

Figure 4.7. AOA treatment reduces biofilm forming microbiota and increases bacterial antibiotic susceptibility. (A) The bacterial content of the swab samples were evaluated by measuring optical densities at OD570nm. AOA treatment reduced biofilm formation. **(B)** Individual bacterial colonies with biofilm-forming-capacity were quantified by measuring the optical densities and were also reduced with AOA treatment. **(C)** Bacterial prevalence of individual species was again reduced with AOA treatment. **(D)** Bacterial burden measured by colony forming unit counts was significantly reduced in AOA treated db/db wounds. **(E)** Community minimum inhibitory concentration (CMIC) of bacteria present in wounds treated with AOA was performed using Gentamicin (Gm), Carbenicillin (Cb), and Amoxicillin (Amox). CMIC degreased significantly with time of AOA treatment. *n= 5. All data are Mean ± SD. **p<0.01,***p<0.001. NS = non-significant.*

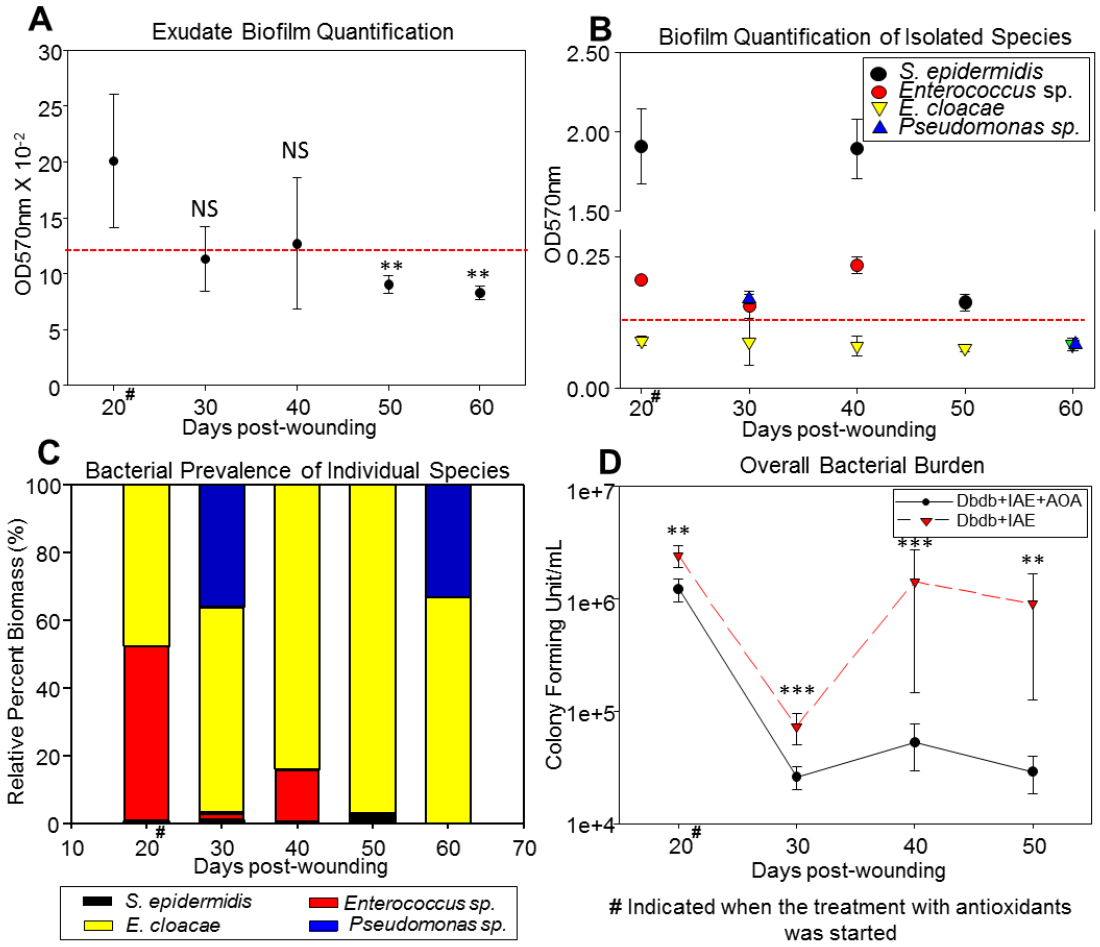

CMIC of NAC/αToc Treated Wounds			
	Amox (μg/mL)	Cb (μg/mL)	Gm (μg/mL)
Day 20#	25	25-50	13-25
Day 30	13-25	13	3-6
Day 40	6-13	6-13	3-6
Day 50	6-13	6-13	3-6

Figure 4.7

Figure 4.8. Morphological characterization of biofilm in chronic and AOA treated wounds. (**A,B**) Fluorescent microscopy of frozen sections of chronic wounds IAE treated at 20days post-wounding, stained by Sytox green for bacterial DNA and wheat germ agglutinin conjugated with Texas Red for the tissue and biofilm matrix, shows presence of biofilm. (**C**) SEM shows bacteria embedded in a biofilm-associated matrix (stars) with presence of bacteria [B] in chronic wounds at day 20 after wounding and treatment with IAE. (**D**) Day 10 db/db wounds without inhibitors to illustrate how the tissue looks like in non-IAE treated wounds. (**E**) Chronic wounds treated with IAE at day 30 after wounding show more biofilm than at day 20 (C) and much more than the day 30 wounds that were treated with AOA for 10 days **(F)**. (**G**) Chronic wounds treated with IAE at day 40 after wounding show more biofilm than at day 30 (E) and much more than the day 40 wounds that were treated with AOA for 20 days **(H).** Scale bars for (C-H) is 5μm. **(I)** Biochemical analysis of the biofilm obtained from chronic wounds.

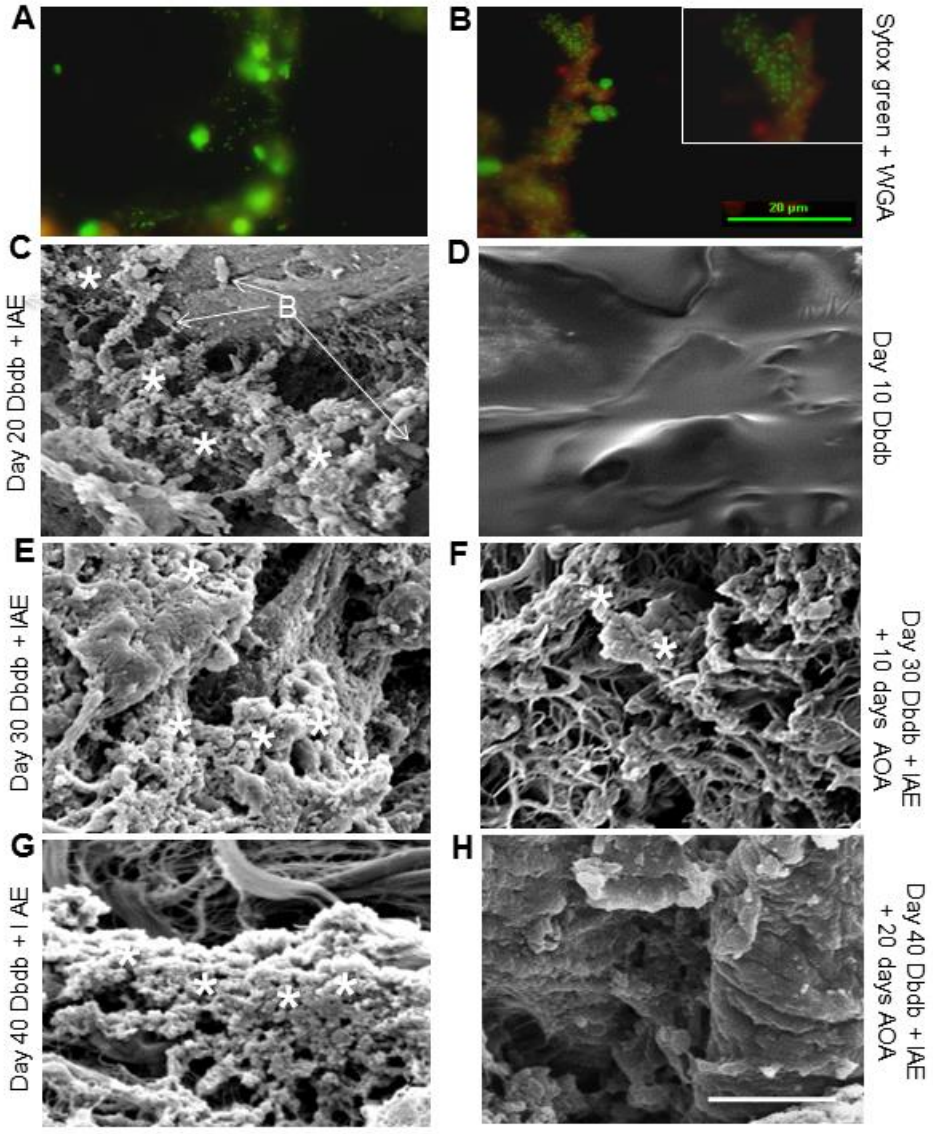

I

Glycosyl Residue	Mol% ± Std Dev
Arabinose (Ara)	0.86 ± 0.35
Rhamnose (Rha)	2.56 ± 1.17
Fucose (Fuc)	1.78 ± 0.55
Xylose (Xyl)	2.89 ± 1.17
Glucuronic Acid (GlcU)	6.14 ± 2.34
Galacturonic Acid (GalU)	8.89 ± 3.17

Glycosyl Residue	Mol% ± Std Dev
N-Acetylglucosamine (GlcNAc)	20.08 ± 6.53
Iduronic Acid (IduA)	-
N-Acetylgalactosamine (GalNAc)	-
Mannose (Man)	16.53 ± 4.39
Galactose (Gal)	17.01 ± 4.17
Glucose (Glc)	23.24 ± 13.09

Figure 4.8

Figure 4.9. Schematic illustration of our chronic wound development model and how chronicity is reversed. A wound is created in the presence of excessive levels of reactive oxygen species by inhibiting key antioxidant enzyme (IAE) activity. These wounds become chronic and produce wound exudate that contains bacterial biofilms. Reversal of chronicity towards normal healing was achieved by application of antioxidant agents (AOA) α-toc and N- acetyl cysteine (NAC).

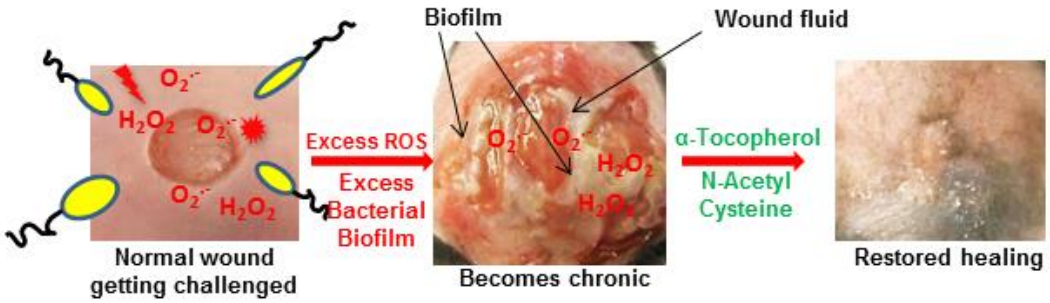
Biofilm
Wound fluid
$O_2^{\cdot-}$
H_2O_2
$O_2^{\cdot-}$
$O_2^{\cdot-}$
H_2O_2
Excess ROS
Excess
Bacterial
Biofilm
$O_2^{\cdot-}$
$O_2^{\cdot-}$
H_2O_2
H_2O_2
α-Tocopherol
N-Acetyl
Cysteine
Normal wound
getting challenged
Becomes chronic
Restored healing

Figure 4.9

SUMMARY AND CONCLUSION

In this work, the role of oxidative stress and the presence of biofilm forming bacteria in causing chronic wounds was studied and a novel model of chronic wounds has been developed. I first showed that reactive oxygen species (ROS), increases in H_2O_2 due to decreased antioxidant activity, was observed in adult LIGHT$^{-/-}$ mice and the effects are exacerbated in old mice. Furthermore the antioxidant capacity in adult LIGHT$^{-/-}$ mice was comparable to C57BL/6 but decreased in old mice. The real time generation of ROS after wounding, shown for the first time using luminol, is much higher in LIGHT$^{-/-}$ mice than in the control. Nitrosative stress was also significantly increased very early post wounding in LIGHT$^{-/-}$ adult and old mice. Levels of nitrate and nitrite (metabolites of nitric oxide) were significantly elevated post wounding. Early phosphorylation of eNOS and increases in iNOS suggests increases in NO production. Moreover, lipid peroxidation, protein modification and DNA damage were all increased due to stress in wound tissue. In addition, cell death by necrosis and apoptosis are high in LIGHT$^{-/-}$ wounds. Manipulation of wounds with antioxidant enzyme inhibitors and introduction of biofilm-forming bacteria resulted in chronic wound development.

To advance our understanding of the course of wounds in the LIGHT$^{-/-}$ impaired model of healing, I took a systems approach, by using lipidomics and find that impaired wounds have increases in AA metabolites: isoprostanes (8- and 5- isoprostanes), leukotrienes (cys-LTD_4 and cys-LTE_4), prostanoids (thromboxane, prostacyclins, and prostaglandins), and increases in hydroxyeicosatetraenoic acids (11-HETE and 15-HETE). All of these lipids are inflammatory mediators and have roles in platelet aggregation and vascular function. Furthermore, I showed that upon wounding LIGHT$^{-/-}$

mice have increases in platelet aggregation and decreases in coagulation time. These encouraging results of increases in platelet aggregation and reduced time in clotting upon wounding suggest that the increases in lipids involved in platelets may also have effects on vascular permeability that lead to extravasation and hence formation of fibrin 'cuffs'.

To confirm the studies in the LIGHT$^{-/-}$ mouse model I used the preclinical *in vivo* mouse model that has been widely accepted to mimic type II diabetes in humans to show that db/db mice have increased oxidative stress very early in the wound microenvironment. Treatment of the wounds with one dose of the inhibitors for antioxidants catalase and glutathione peroxidase (GPx) resulted in formation of chronic wounds with biofilm forming bacteria that were also resistant to antibiotics. Antioxidant treatment significantly increased both catalase and GPx activity. Because GPx measurements consisted of assessing the activity of the antioxidant enzyme, deciphering whether there was an increase in generation of GPx, or there were increases in the intracellular pool of cysteine and hence glutathione in increasing the activity will be of importance to understand the mechanism to combat increases in H_2O_2 levels, especially in diabetics.

Very few studies have been done to show the reduction in biofilm formation in presence of NAC treatment and even to a lesser extent using α-tocopherol. Both the antioxidants incorporated in this work have not been used to treat chronic wounds in humans. NAC and α-tocopherol used to treat chronic wounds individually or in

combination showed significant reduction in biofilm formation and improvement in tissue healing.

An important finding in the antioxidant treated, individually and in combination, chronic wounds was the observed difference in the collagen deposition and maturation. Because collagen deposition, maturation and buddle formation was enhanced when chronic wounds were treated with both the antioxidants, unlike individually treated wounds, there is a need to understand the mechanism of action of the combination of NAC and α-tocopherol. NAC increases intracellular glutathione levels to increase GPx activity and acts as a mucolytic agent, whereas α-tocopherol is not involved in GPx metabolism or biofilm reduction.

In conclusion, LIGHT$^{-/-}$ mice have imbalanced redox levels in the wound tissue that are exacerbated with age. This causes tissue damage by alteration of lipids, proteins and DNA and by increasing cell death, all creating an environment conducive to impaired healing. Furthermore, manipulation of the wound microenvironment to increase the oxidative stress in the presence of biofilm-forming bacteria leads to the development of chronic wounds 100% of the time, identifying oxidative stress levels in wound tissue as a critical factor to control in human chronic wounds and reverse the course to healthy healing. Furthermore, elucidating lipid signaling in impaired and chronic wound models could lead to the discovery of lipid biomarkers involved in the genesis of problematic wounds and the development of therapeutics to correct/modulate lipid signaling that aids in improved/regenerative healing.

Finally, while others have proposed that the pathogenesis of chronic wounds is dependent on factors such as tissue hypoxia, bacterial colonization, ischemia-reperfusion injury and an altered cellular and systemic stress response, I propose that the critical parameter for development of chronic wounds in diabetic humans and perhaps others is an excessively high level of reactive oxygen species in the local microenvironment of the wound very early after injury. In this db/db wound microenvironment, normal skin bacteria that otherwise would not form biofilm, colonize the wound and become biofilm-producers, that upon restoration of the redox balance causes biofilms to disappear from wounds, resulting in significantly improved wound healing. These results validate the importance of our novel *in vivo* model of chronic wounds and will help advance our understanding (of both host and microbe) of the path to chronicity.